INVESTIGATION OF SERIOUS–FATAL INJURIES

USING BIOMECHANICAL FINITE ELEMENT MODELS

_____

HIDEYUKI   KIMPARA

INVESTIGATION OF SERIOUS–FATAL INJURIES
USING BIOMECHANICAL FINITE ELEMENT MODELS

by

HIDEYUKI KIMPARA

DOCTORAL THESIS

Submitted to the Graduate School of Engineering,

Nagoya University,

Nagoya, JAPAN

**in partial fulfillment of the requirements
for the degree of**

DOCTOR OF ENGINEERING

March 25$^{\text{th}}$ 2015

Thesis Screening Committee

Main Examiner

Professor Eiichi Tanaka

Committee Members

Professor   Koji Mizuno
Professor   Eisuke Kita
Associated Professor   Kohei Murase

To My Wife, Tamaki,
and Our Families

ABSTRACT

In Japan, traffic accident data suggest an increase in the number of disabled persons associated with a moderate increase in the number of injured persons and a greatly reduced number of fatalities. Previous studies of traffic accident data in the US have suggested that the head and chest were the primary or secondary body regions observed to suffer serious injuries. Spinal cord injuries were also important in terms of serious–fatal injuries. In the last few decades, basic theories and hypotheses have been established from analyses of real-world accidents and Post Mortem Human Subject (PMHS) tests. Anthropomorphic test devices (ATDs) and multibody-based models have also shown good predictions of the whole body kinematics during impacts. However, it is difficult to obtain detailed information about a crash from field data as well as about the internal injury mechanisms of the human body from PMHS or ATD test data owing to the limited number of test cases. Therefore, this study employed finite element (FE) modeling techniques to investigate the mechanisms of serious–fatal injuries during impact.

First, a head-neck complex FE model with the brain and spinal cord was applied to a parametric study of a simplified frontal crash scenario to investigate the effects of restraint conditions on central nervous system (CNS) injuries. This study led to better configurations of head and torso restraints during anteroposterior head-neck responses. In addition, concussive and nonconcussive football head impacts were analyzed using a detailed head/brain FE model to elucidate the mechanisms of traumatic brain injuries (TBIs) and the threshold for sustaining injuries. The analysis results provided new mild traumatic brain injury (MTBI) criteria based on angular head motions.

Second, a retrospective review of published PMHS test data of frontal and lateral blunt impacts to the chest and isolated rib bending tests were conducted for assessing chest injury biomechanics. Chest stiffness was found to be significantly higher in males than in females for frontal impact; furthermore, male ribs showed significantly higher cross-sectional area and bending stiffness than female ribs. To elucidate the roles of biomechanical parameters such as the human subject's size, mass density, Young's modulus of bone and internal organs, and thickness of bony structure, two series of parametric studies were conducted using Total HUman Model for Safety (THUMS), a commercially available human body FE model. The maximum chest compression ratio, the best predictor of the number of rib fractures, was found to be correlated with the area moment of inertia of the ribcage. Then, the findings of biomechanical parameters relevant to chest injuries were used for developing a three-dimensional FE model of the 5th percentile female chest. As the results predicted by the model showed good agreement with experimental data for females for two sets of frontal impacts, one set of lateral impact, two sets of oblique impacts, and a series of ballistic impacts, the effects of the rib's size and area moment of inertia on the impact responses were confirmed.

Accordingly, human body FE models are concluded to be useful for investigating the mechanisms of serious–fatal injuries and assessing injury severities during automotive crashes.

*Keywords***:**   Safety, Injury biomechanics, Human body modeling, Computational biomechanics, Traumatic brain injury, and Injury criteria.

ACKNOWLEDGMENTS

TABLE OF CONTENTS

ABBREVIATIONS

AAAM	Association for the Advancement of Automotive Medicine
AIS	Abbreviated Injury Scale
AF05	American Female 5th percentile
ALL	Anterior Longitudinal Ligaments
AM50	American Male 50th percentile
AM95	American Male 95th percentile
ATD	Anthropomorphic Test Device
BRIC	Brain Injury Criterion
CAE	Computer-Aided Engineering
CCIS	Cooperative Crash Injury Study
CEM	Combined Evaluation Method
CG	Center of Gravity
CL	Capsular Ligament
C_{max}	Maximum Chest Compression Ratio
CNS	Central Nervous System
CSDM	Cumulative Strain Damage Measure
CSF	Cerebrospinal Fluid
D_{max}	Maximum Chest Deflection
DAI	Diffuse Axonal Injury
DOF	Degrees of Freedom
E	Young's Modulus
E_t	Tangent Modulus
FE	Finite Element
F_{max}	Maximum Chest Force
FMVSS	Federal Motor Vehicle Safety Standard
FPS	First principal strain
Fxed Ribs	Number of Fractured Ribs
G	Shear Modulus
G_0	Short Term Shear Modulus
G_∞	Long Term Shear Modulus
GIAJ	General Insurance Association of Japan
H	Height
HIC	Head Injury Criterion
HIP	Head Injury Power
I_{Rc}	Area Moment of Inertia of the Rib Cage
I_{rib}	Area Moment of Inertia of the Ribs Alone

ISL	Interspinous Ligament
ITARDA	Institute for Traffic Accident Research and Data Analysis
K	Bulk Modulus
K_a	Initial Chest Apparent Stiffness
KLC	Kleiven's linear combination
λ	Basic Scaling Factor
LN	Ligamentum Nuchae
MAacc	Maximum angular acceleration
MADYMO	Mathematical Dynamic Model
MAIS	Maximum AIS
MAvel	Maximum angular velocity
MLacc	Maximum linear acceleration
MLIT	Ministry of Land, Infrastructure, Transport and Tourism
MLvel	Maximum linear velocity
MMLM	Modified Maximum Likelihood Method
MOI	Moment of Inertia
MPS	Maximum principal strain
MPSS	Maximum product of strain and strain rate
MSR	Maximum strain rate
MSS	Maximum shear strain
MTBI	Mild Traumatic Brain Injury
NPA	National Police Agency of Japan
NASS	National Automotive Sampling System
NFL	National Football League
NHTSA	National Highway Traffic Safety Administration
NLIRO	Non-Life Insurance Rating Organization of Japan
PLL	Posterior Longitudinal Ligaments
PMHS	Post Mortem Human Subject
PRHIC	Power Rotational Head Injury Criterion
Rib Fxs	Number of Rib Fractures
RIC	Rotational Injury Criterion
ρ	Mass Density
SAE	Society of Automotive Engineers
SCI	Spinal Cord Injury
SI	Severity Index
SIMon	Simulated Injury Monitor
σ_y	Yield Stress
SSL	Supraspinous Ligament

TBI	Traumatic Brain Injury
THUMS	Total HUman Model for Safety
TL	Transverse Ligament
VC$_{max}$	Maximum Viscous Criterion
W	Body weight
WSUBIM	Wayne State University Brain Injury Model
WSUHTM	Wayne State University Human Thoracic Model
WSUTC	Wayne State University Tolerance Curve

NOTATIONS

Chapter 3

A	Effective values of linear acceleration
$a(t)$	Resultant linear acceleration
$\alpha(t)$	Resultant angular acceleration
I_{ii}	Moment of inertia (MOI)
n	Weighting factor
T	Time duration
ω_r	Maximum resultant angular velocity

LIST OF TABLES

LIST OF FIGURES

Chapter 1   Introduction

1.1. Traffic Accident Data in Japan

Traffic accident analyses can be used to reveal current problems pertaining to automotive crashes in the field.   Some key findings may indicate significant accident pattern and injury mechanisms that might become essential factors to reduce fatalities and injury severities.

Figure 1.1 shows general trends in automotive accident data from 1970 to 2005 based on police data in Japan (Institute for Traffic Accident Research and Data Analysis [ITARDA], 2006[57]).   The vertical axis represents the numbers of traffic accidents, fatalities, and injured persons in this period.   The data show that all of these numbers decreased in the early 1970s and then increased slightly in the 1980s.   However, from 1992, only fatalities started to decrease.   In 2005, the number of fatalities was 6,871, which was 60% lower than that in 1992.   On the other hand, until the early 2000s, the numbers of accidents and injured persons kept increasing.
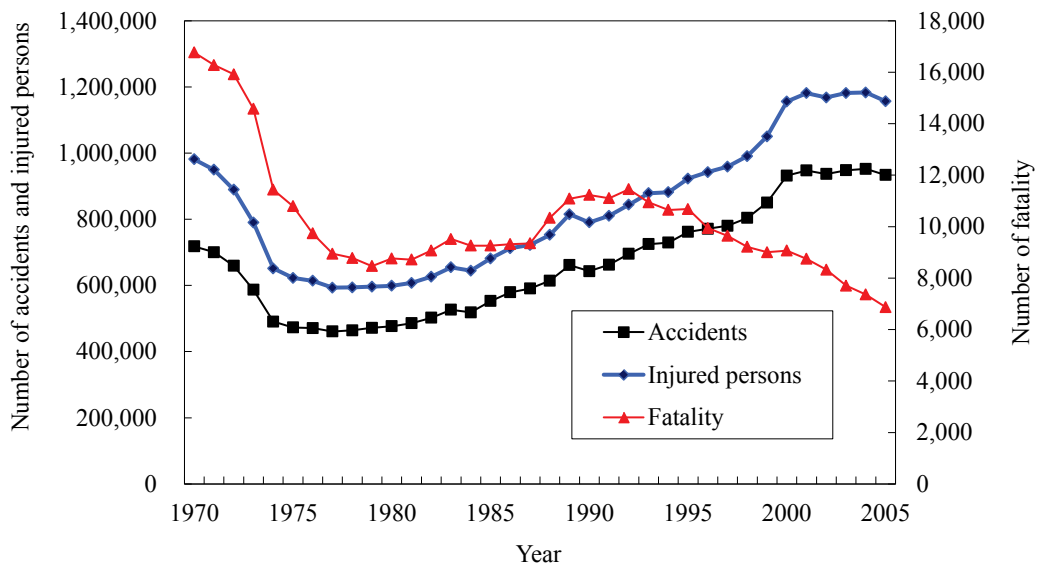
Figure 1.1:   Trends of traffic accidents in Japan (1970–2005) [ITARDA, 2006]

The National Police Agency of Japan (NPA); Ministry of Land, Infrastructure, Transport and Tourism (MLIT); and Non-Life Insurance Rating Organization of Japan (NLIRO) annually report the total numbers of fatalities, injured persons, and disabled persons in Japan.   Figure 1.2 shows the trends of the same from 1989 to 2003 (National Agency for Automotive Safety & Victims' Aid in Japan, 2006[101]).   The vertical axis represents the rates of fatalities, injured persons, and disabled persons assuming that these numbers are 100 in 1989.   Although the data show that fatalities decreased continuously, the numbers of

injured and disabled persons increased.   In 2003, the number of disabled and injured persons was almost 2.3 and 1.4 times that in 1989, respectively.

In Japan, men and women are widely considered to have equal status, and this is reflected by the increase in the number of licensed female drivers between 1970 and 2005.   Figure 1.3 shows the percentages of licensed male and female drivers in Japan as reported by the Institute for Traffic Accident Research and Data Analysis (ITARDA, 2006[57]).   In 1970, only 12% of females had a driver's license, compared to 58% of males.   By 2005, 60% of females had a driver's license, and this constituted 43% of all licensed drivers in Japan.   Considering the increased number of female drivers on the road today, there is great concern about how often they will sustain injuries in automotive crashes.
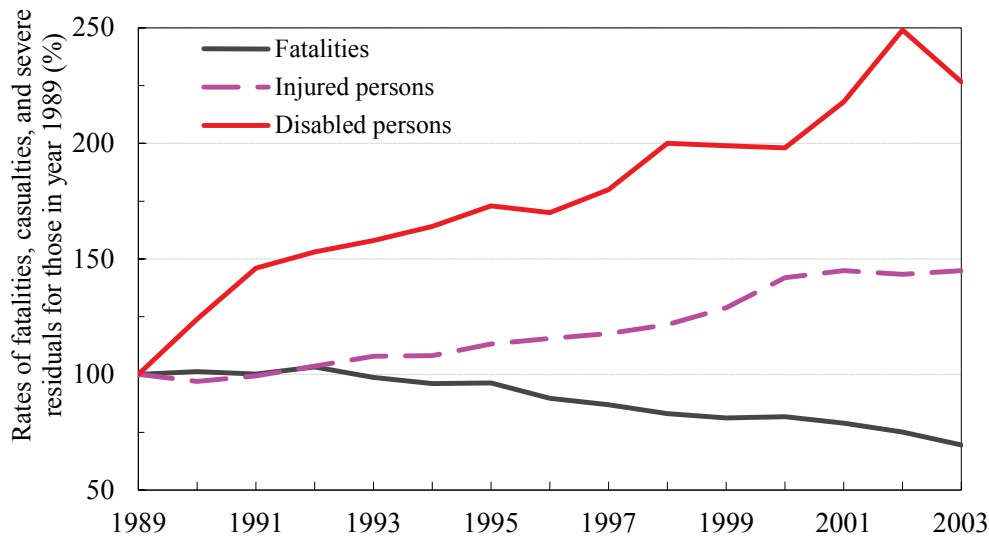
Figure 1.2:   Changes in numbers of fatalities and injured and disabled persons due to automotive crashes in Japan (1989-2003) [National Agency for Automotive Safety & Victims' Aid in Japan, 2006]
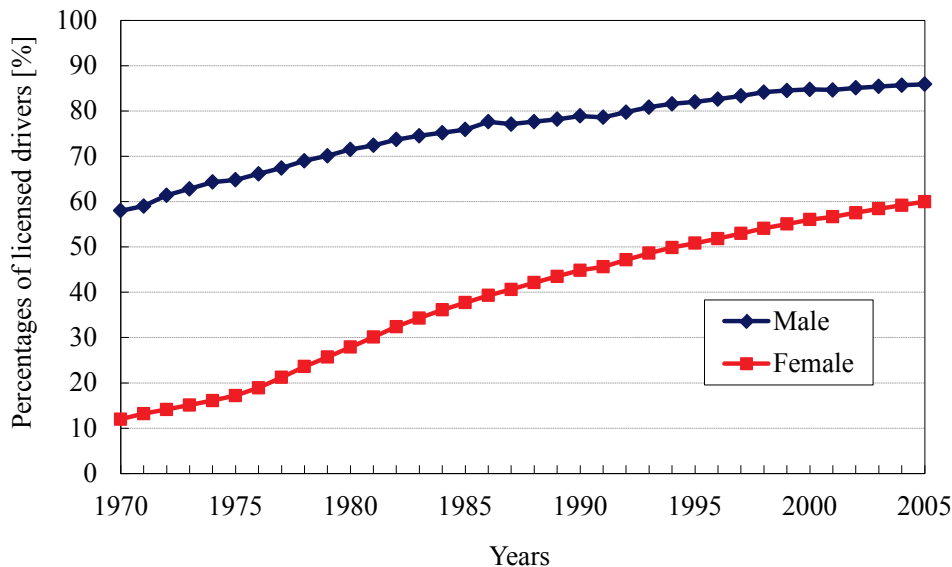
Figure 1.3:   Percentages of licensed drivers in Japan (1989–2003) [ITARDA, 2006]

In the US, for example, the National Highway Traffic Safety Administration (NHTSA, 2001[102]) reported that fatalities among female drivers increased by ~16% from 1991 to 2001 compared to a 2% increase in male drivers during the same period.   Figure 1.4 shows the distributions of fatalities and injured persons in terms of gender and role of occupants in Japan.   In Japan, the number of female occupant fatalities was only 23% of all occupant fatalities.   However, the number of injured female occupants was 47% of all injured occupants.

The General Insurance Association of Japan (GIAJ) (2006[37]) counted the number of victims and personal costs of traffic accidents based on insurance payment records.   Figure 1.5 shows pie charts of the
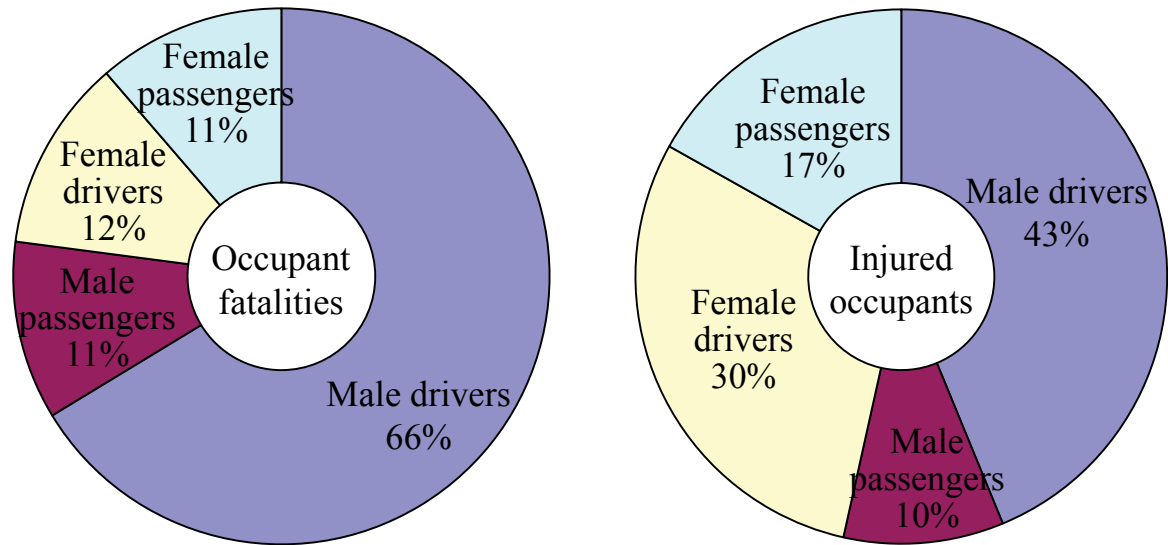
Figure 1.4:   Distributions of fatalities and injured persons in terms of gender and role of occupants in Japan [ITARDA, 2006]
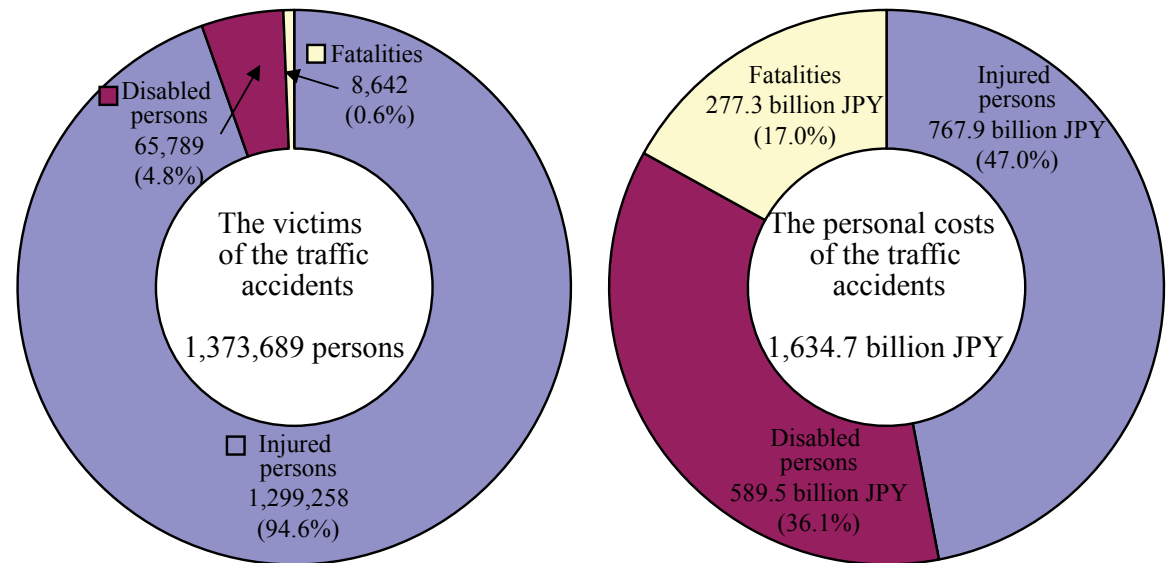
Figure 1.5:   Rates and total amounts of victims and personal costs of traffic accidents in Japan (Apr. 2003–Mar. 2004) [GIAJ, 2006]

distributions of victims and personal costs of traffic accidents in Japan from April 2003 to March 2004. Fatalities and disabled persons accounted for only ~5% of all victims of traffic accidents; however, the total personal costs for the same were more than 53% of all personal costs.   Therefore, serious vehicular accidents that cause fatalities or disabilities have a strong influence on society.

Information about the principal injured body parts should provide important insights for investigating injury mechanisms during automotive crashes.   Figure 1.6 shows the distributions of primary damaged body parts sustained by vehicular occupants involved in traffic accidents in Japan as reported by ITARDA (2006)[57].   Among minor injuries, neck injury was ranked the most frequently damaged body part (79%).   Among serious injuries, too, neck injury was ranked the most frequent injury, but with a reduced rate (22%).   In addition, among serious injuries, chest and lower extremity injuries were ranked the second and third most frequently injured body parts (21% and 20%, respectively).   In fatal cases, head and chest injuries accounted for 38% and 29% of all cases, and neck injury were ranked 4th (6%).
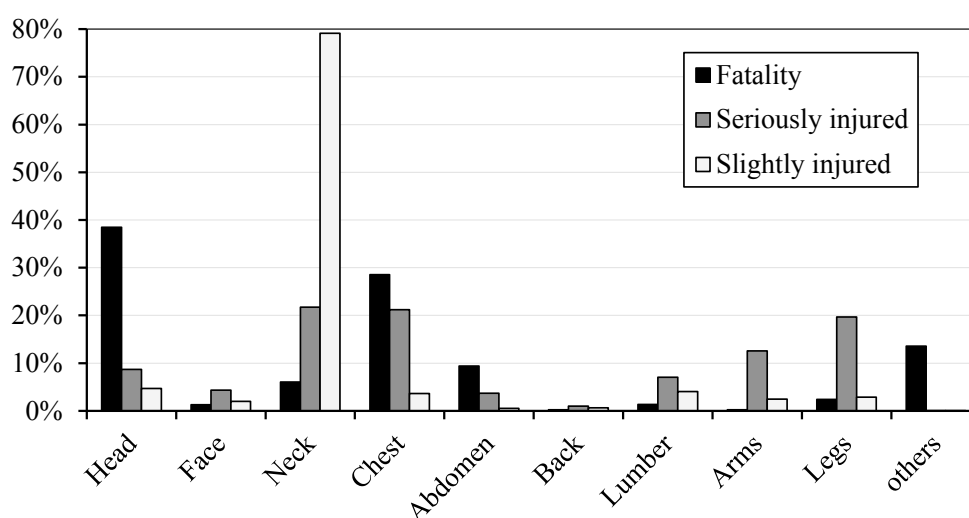
Figure 1.6:   Percentages of primary damaged body parts sustained by occupants in traffic accidents in Japan (2005) [ITARDA, 2006]

These Japanese traffic data suggest the following: the number of injured and disabled persons increased, while the number of fatalities gradually decreased.   Although the total number of fatalities and disabled persons was small, their personal costs were significantly higher than those of injured persons. Head and chest injuries were recognized as significant injuries in fatal crashes.   A further detailed analysis of traffic data in Japan is necessary to understand these differences and injury mechanisms during crashes. For example, the word "injured" in records covers injury severities ranging from minor to critical.   In addition, the reasons for female fatalities being much lesser than male fatalities remain unknown, while the total number of injured males and females has become similar (Figure 1.4).   To elucidate the injury mechanisms through biomechanical analyses, the records of gender difference, injury severity, and primary injured body regions must be related to each other.

1.2. Injuries and Classifications

1.2.1. Abbreviated Injury Scale

The Abbreviated Injury Scale (AIS) was the first widely implemented injury severity scale. The AIS is monitored by a scaling committee of the Association for the Advancement of Automotive Medicine (AAAM). It was developed in 1971 for use in assessing motor vehicle injuries and stratifying victims of motor vehicle crashes. The first AIS included only blunt injuries. However, it has been revised and updated to now provide a reasonably accurate picture. The latest AIS score is the 2005 revision (AAAM, 2005[5]).

The AIS classifies the injury severity based on the body region injured and the magnitude of the injury. The severity levels of injuries range from 1 (minor) to 6 (maximum, currently untreatable), as shown in Table 1.1. AIS scores of at least 3 indicate serious or life-threatening injuries.

Table 1.1: AIS score and injury severities

AIS Score	Injury
1	Minor
2	Moderate
3	Serious
4	Severe
5	Critical
6	Maximum (currently untreatable)

1.2.2. Head injury

In an automotive crash, head injuries occur because of either a direct impact against interior components or an indirect impact applied to the head and neck. Table 1.2 (Schmitt et al., 2009[130]) shows details of AIS classifications for head injuries.

This table indicates that serious–fatal head injuries (AIS 3+) include severe skull fractures and brain injuries. A contusion is a type of relatively minor hematoma of tissue in which capillaries and, occasionally, venules are damaged by trauma, allowing blood to seep into the surrounding interstitial tissues. A hematoma is an extravasation of blood outside the blood vessels, generally because of hemorrhage. A hematoma is a pocket or localized collection of blood, usually in liquid form, within the tissue. Diffuse axonal injury (DAI) is one of the most common and devastating types of traumatic brain injury (TBI). This implies that damage occurs over a more widespread area than in focal brain injury. DAI, which refers to extensive lesions in white matter tracts, is one of the major causes of unconsciousness and persistent vegetative state after head trauma. It occurs in about half of all cases of severe head trauma.

Table 1.2:   AIS classified head injury (Schmitt et al., 2009)

AIS code	Description
1	skin/scalp: abrasion, superficial laceration face: nose fracture
2	skin: major avulsion vault fracture: simple, undisplaced mandible fracture: open, displaced maxilla fracture: LeFort I and II
3	basilar fracture maxilla fracture: LeFort III total scalp loss single contusion cerebellum
4	vault fracture: complex, open with torn exposed or loss of brain tissue small epidural or subdural hematoma
5	major penetrating injury (>2 cm) brain stem compression large epidural or subdural hematoma diffuse axonal injury (DAI)
6	Massive destruction of both cranium and brain (crush injury)

1.2.3. Neck injury

Table 1.3 indicates neck injuries and their classification in terms of AIS grades (AAAM, 2005[5]). In general, injuries to the upper cervical spine are considered more serious and life threatening than those at a lower level.

Table 1.3:   Spinal injuries according to AIS score (AAAM, 2005)

AIS code	Description
1	skin, muscle: abrasion, contusion (hematoma), minor laceration
2	vertebral artery: minor laceration cervical/thoracic spine: dislocation without fracture thoracic/lumbar spine: disc herniation
3	vertebral artery: major laceration cervical/thoracic spine: multiple nerve root laceration
4	cervical/thoracic spine: spinal cord contusion incomplete
5	cervical/thoracic spine: spinal cord laceration without fracture
6	Decapitation cervical spine: spinal cord laceration at C3 or higher with fracture

According to the AIS classification for neck injuries (Table 1.3), fractures in upper cervical bones are always graded as a fatal injury (AIS 6). In addition, most experimental studies considered injury mechanisms according to the kinematics of cervical bones. However, AIS 3 or 4 injuries on the neck are related to spinal cord contusions or nerve root lacerations. To understand the tolerance to serious–fatal injuries of the neck, it is necessary to consider the impact responses of the spinal cord.

1.2.4. Chest injury

Table 1.4 shows the AIS rating for skeletal and soft tissue chest injuries (AAAM, 2005[5]). The severity of a skeletal injury is classified in terms of rib fractures. For example, 2–3 rib fractures or sternum fracture are graded as AIS 2 injury of the chest, and 4 or more rib fractures on one side or 2–3 rib fractures with hemothorax or pneumothorax are graded as AIS 3 injury. The rib cage protects internal organs from external impacts. However, the forces encountered in a severe automotive crash are generally large enough to fracture the ribs and sternum. Impact with the chest wall or the passage of compression waves could tear the main arteries within the thorax or injure the walls of the heart. The lungs can also be lacerated by the ends of fractured ribs. Therefore, lung and heart injuries are graded as AIS 3 or more severe injuries. The various injury types appear to be dependent on the rate of loading because of the viscoelastic nature of the tissues involved (Schmitt et al., 2009[130]). At low rates of loading, the injury is due to deformation of the rib cage or crushing. For automotive crashes, both the deformation and the rate of loading play an important role in injury causation.

Table 1.4:   AIS rating for skeletal and soft tissue chest injuries (AAAM, 2005)

AIS code	Skeletal injury	Soft tissue injury
1	one rib fracture	contusion of bronchus
2	2-3 rib fractures; sternum fracture	partial thickness bronchus tear
3	4 or more rib fractures on one side; 2-3 rib fractures with hemothorax or pneumothorax	lung contusion minor heart contusion
4	Flail chest 4 or more rib fractures on each of two sides 4 or more rib fractures with hemo- or pneumothorax	Bilateral lung laceration minor aortic laceration major heart contusion
5	Bilateral flail chest	Major aortic laceration lung laceration with tension pneumothorax
6		Aortic laceration with hemorrhage not confined to mediastinum

1.3. Human Body Surrogating Technologies

Studies using Post Mortem Human Subjects (PMHSs) or animal subjects have laid the foundations of current injury biomechanics.   However, several limitations are faced in elucidating injury criteria and tolerances from PMHS studies.   Some experimental studies investigated many test cases to consider a wide variety of biological differences, but others often suffered from a lack of enough test cases.   Furthermore, subjects cannot be collected prospectively, and the assumed test conditions were limited.   Therefore, human body surrogating technologies are necessary to simulate the impact responses of the human body and investigate injury mechanisms under various conditions.   Currently, hardware models of anthropomorphic test devices (ATDs) and computational models based on multibody or finite element (FE) methods are available for this purpose.

ATDs, commonly called "dummies," are often used as human surrogates.   The height and weight distribution, shape, and stiffness of these dummies are designed to realistically imitate human beings. Additionally, the global mechanical responses of these ATDs mimic human responses in an automotive crash. These ATDs are instrumented to measure various parameters, including sternal displacement relative to the spine, acceleration at the chest center of gravity (CG), and rate of chest deflection.   These and other parameters, or combinations thereof, are correlated with the presence of injury and used as predictors of thoracic injury risk for a given occupant, restraint condition, and set of impact characteristics.   However, crash dummies cannot be used to elucidate the injury mechanism or predict the appropriate injury risk of bony structures or internal organs.

The most popular multibody code used in the field of impact biomechanics is the Mathematical Dynamic Model (MADYMO) model developed by TNO Automotive (Delft, Netherlands).   Huang et al. (1994b)[54] developed a MADYMO multibody model of a whole body to study gross human motions in a side impact.   All joints and body segments were connected with linear/nonlinear springs and/or dampers. Happee et al. (2000)[44] developed a MADYMO-based small female human model using facet surfaces to represent the exterior body geometry and flexible elements to allow thoracic deflection based on a hybrid multibody FE modeling technique.   These multibody modeling approaches are very useful because their computational cost is very low and parametric adjustments can be easily made to study various design iterations.   Nevertheless, it was decided that the pure FE modeling approach should be used because of its flexibility in modeling multiple material compositions and complex model geometry as well as its capability to incorporate experimentally obtained material properties directly into the model without additional studies to fit the multibody code requirements.   Additionally, FE models have the advantage of being able to represent the impact responses of internal organs such as the brain and thoracic or abdominal organs.

Numerous FE models of the human body have been developed and validated against PMHS test data.   Most FE models include three-dimensional (3D) elastic-plastic skeletal bodies and viscoelastic or hyperelastic soft tissue parts.   For example, head models feature most essential components of the head including the scalp, skull, cerebrospinal fluid (CSF), dura mater, falx cerebri, and brain.   Injuries could be determined based on the strain or stress values observed in the FE models.   Bone fractures could be simulated by the plastic strain of elastic-plastic materials or the mesh elimination method, which are prepared

in explicit FE codes. Explicit codes such as LS-DYNA (LSTC, Livermore, CA) or Pam-Crash (ESI, Paris, France) have been widely used for developing and analyzing FE models in impact biomechanics. It is generally believed that mathematical modeling techniques have also been used to better understand injury mechanisms.

1.4. Investigation of Injury Mechanisms in Previous Studies

1.4.1. Brain injury (specifically, injury predictors)

Injury predictors obtained from the head FE models are very useful for gaining a detailed understanding of brain injury mechanisms under impact situations with linear and/or angular accelerations. However, it is difficult to apply these FE-based injury predictors to directly evaluate experimental data of head impact responses. FE-based injury predictors need several hours for a total FE analysis from pre-processing to post-processing. In addition, a head model interrelated with the predictors must be used for the analyses.

In the field of impact biomechanics, the injury severity for the human head has generally been predicted using the Head Injury Criterion (HIC). HIC is the only injury metric used for the head of crash dummies in vehicle safety standards. It is defined in terms of the linear acceleration and is used to predict skull fractures and brain contusions (Hertz, 1993[51]; Versace, 1971[152]). At the same time, pedestrians sustain head injuries associated with angular head acceleration as often as those associated with linear head acceleration in car-to-pedestrian accidents (Feist et al., 2009[31]). In particular, angular acceleration contributes to the generation of concussive injuries such as DAI as well as subdural hematomas (Thibault and Gennarelli, 1985[148]). As HIC is defined only by the resultant linear acceleration with respect to time, it is difficult to find a correlation between HIC and rotational head motion.

Historically, biomechanical studies have focused on characterizing brain injuries with rotational head motions using animal models (Ommaya et al., 1967[109]). Some other studies proposed brain injury criteria with angular accelerations (Ommaya and Hirsch, 1971[110]; Lowenhielm, 1974[85]; Ewing et al., 1975[29]; Margulies and Thibault, 1992[88]). However, these criteria are not currently used because they were developed with a limited number of specimens and head motion patterns and were not sufficiently validated for head injuries in real-world accidents. Additionally, the injury thresholds derived from animal experiments cannot be directly applied to living humans.

The high occurrence of concussions in contact sports, particularly helmeted football[1], has attracted the attention of scientists as a unique opportunity to collect biomechanical data to characterize mild traumatic brain injury (MTBI) (Broglio et al., 2010[12]; Guskiewicz et al., 2010 [41]; Rowson et al., 2009[126]; Schnebel et al., 2007[131]). Note that the word "football" denotes helmeted football in this thesis. In general, the heads of football players are covered by helmets with facemasks, and therefore, the risk of skull fractures due to football head impacts is quite lower than that of automotive crash cases. However, the impact forces on the

---

[1] helmeted football, i.e., American football

helmet may generate strong rotational head motion owing to the large moment arm resulting from the facemask's distance away from the CG of the head. Although the severity of brain injuries due to football impacts is milder than that of automotive pedestrian head injuries, data characterizing concussive head impacts in humans would be valuable in evaluating brain injury predictors with angular accelerations.

1.4.2. Spinal cord injury

The central nervous system (CNS) is the control center for the entire nervous system. According to the definition of the AIS, CNS injuries in the brain and spinal cord are generally categorized as severe injuries (AIS 3+). Most severe CNS injuries are related to automotive impacts. According to the National Automotive Sampling System (NASS) database for 2000–2004, the incidence of serious or severe brain injuries such as AIS 3+ injuries was 36.1%. This represented the most frequently injured body region for AIS 3+ injuries. On the other hand, neck injuries represented only 0.26% of all AIS 3+ injuries. Even though the incidence of spinal cord injury (SCI) was lower than that of brain injury, improving vehicle crashworthiness could reduce the incidence rate of SCI (Anderson and Viano, 1986[2]; Holly et al., 2002[52]; Carr et al., 2004[13]; Dryden et al., 2005[25]; Dvorak et al., 2005[26]).

A survey of the National Spinal Cord Injury Statistical Center (The National SCI Statistical Center, 2005[103]) revealed that motor vehicle crashes accounted for 47.5% of reported SCI cases since 2000. The potential sequelae of CNS injuries include memory loss, inability to concentrate, speech problems, motor and sensory deficits, and behavioral problems (Pope and Tarlov, 1991[122]; Dvorak et al., 2005[26]). Additionally, SCI causes significant initial and ongoing expenses for medical treatment and rehabilitation (Dryden et al., 2005[25]; Cobb et al., 2005[20]). For example, in the US, first-year health and living expenses after SCI have been estimated to range from $250,000 to $683,000 (Cobb et al., 2005[20]). Therefore, it is important to understand the mechanisms of SCI and TBIs in automotive crashes to reduce the number of patients and social costs due to CNS injuries.

During the last few decades, several studies have investigated the effects of vehicular restraint systems on severe injuries of the occupant's head and neck in frontal impacts (Clarke et al., 1971[18]; Patrick et al., 1972[114]; Walsh and Kelleher, 1978[157]; Cheng et al., 1982[16]; Deng, 1995[21]). Deng (1995)[21] conducted a series of parametric studies to investigate the effects of an airbag restraint and suggested inherent performance tradeoffs among various restraint conditions. His study reported that airbag restraints had the potential to reduce severe head injury at an impact velocity of 35 mph, but they increased the risk of injuries to the head and neck at an impact velocity of 30 mph compared to the use of a seatbelt alone. Hanks et al. (2003)[43] reported that drivers protected with an airbag alone suffered from 140% more SCI than those protected with both an airbag and a seatbelt. Additionally, Smith et al. (2005)[136] suggested that 84% of cervical SCI patients at higher delta-V[2] (delta-V > 47 kph) had airbag protection and, in a few cases, the airbag appeared to be responsible for the SCI. These studies indicated that even if current restraint systems were successful in preventing head injury, it did not guarantee that the neck would be protected as well.

---

[2] delta-V: difference of vehicular velocity between before and after the crash

Additionally, there is a noteworthy finding that some patients with brain injury also sustain cervical spinal injury or SCI (Pope and Tarlov, 1991[119]; Bilston, 1998[9]; Holly et al., 2002[52]).   Therefore, brain and spinal cord injuries must be considered together as injuries of the whole CNS.

A number of isolated human brain FE models have been proposed (Zhang et al., 2001[169]; Takhounts et al., 2003[142]; Kleiven and von Holst, 2001[73]; Willinger and Baumgartner, 2003[162]) and used to investigate injury predictors.   The Wayne State University Brain Injury Model (WSUBIM; number of elements: 314,000) was proposed with some injury criteria for brain injuries by Zhang et al. (2001)[169], and this model was applied to four cases of real-world vehicle crash impacts (Franklyn et al., 2005[32]).   Takhounts et al. (2003)[142] developed a Simulated Injury Monitor Finite Element Head Model (SIMon FEHM; number of elements: 7,800) and proposed three metrics as the brain injury predictors.   Willinger and Baumgartner (2003)[162] developed a ULP head model (number of elements: 74,000) and proposed that the von Mises stress is an injury predictor of brain injury.   However, all the proposed models described only the isolated human head.   They are useful for studying brain injuries but are not appropriate for investigating injuries to the entire CNS including the spinal cord.

Bilston (1998) [9] suggested that the mechanism of SCI can be assumed as an intrusion of the vertebrae into the spinal canal.   This supposed SCI mechanism can be observed in clinical studies or case analyses.   Cervical vertebral fractures or traumatic disc protrusions were observed in severe crash cases, which had a high possibility of SCI occurrence (Dvorak et al., 2005[26]; Yoganandan et al., 1989[166]; Smith et al., 2005[136]).   Even though no evidence of fractures or dislocation was noted, spondylosis or kyphosis causes a narrowing of the anteroposterior dimension of the cervical spinal canal and compresses the spinal cord (Hart et al., 2000[46]).   Although many detailed FE models of the human neck have been developed (Kleinberger, 1993[72]; Yang et al., 1998[165]; Deng et al., 1999[22]; Meyer et al., 2004[96]; Halldin et al., 2000[42]), the spinal cord and spinal canal have not been represented in these models.   At the same time, some FE models that included the cervical spinal cord (Bilston, 1998[9]; Hasegawa and Shiomi, 2003[47]) have been proposed.   However, these models did not reflect the plasticity of the vertebral bodies, which was necessary to predict vertebral fractures.   Additionally, these models did not include the detailed structure of the spinal cord.

1.4.3. Chest injury

Patrick et al. (1965)[113] tested several embalmed cadavers statically and dynamically in frontal chest impact.   The anteroposterior static stiffness was found to vary from 32.4 to 70.0 kN/m when the chest was loaded by a 102-mm-wide bar.   The dynamic stiffness prior to rib fracture for impacts with a 152-mm-diameter padded pendulum was ~175.1 kN/m for loads up to 4 kN.   The stiffness increased with the loading rate.   Dynamic frontal impact data were also obtained by Nahum et al. (1970)[98] and Kroell et al. (1971)[76] using a 152-mm impactor.   Lateral chest tests were conducted using blunt impactors by Stalnaker et al. (1973)[137], Cesari et al. (1981)[15], Viano (1989)[154], Talantikite et al. (1998)[141], and Chung et al. (1999)[17].   Based on these test results, the maximum chest compression ratio (C_{max}) was proposed as an injury criterion of the chest.   This is the compressed chest depth in terms of the percentage of the initial

chest depth. The current Federal Motor Vehicle Safety Standard (FMVSS) 208 on chest compression is based on a recommendation by Neathery (1975)[105] who analyzed the Kroell data and found that a compression of 76 mm would result in AIS 3 chest injuries.

If the severity of chest injury is determined in terms of chest deflection, the threshold of chest deflection would depend on the initial size of the chest. The initial chest geometry and structure differ depending on the subject's gender and body size. However, the number of PMHS subjects is always limited, and therefore, it is almost impossible to obtain PMHS subjects having the desired body size or shape. Therefore, numerical human body models are preferable for investigating the effects of body parameters on the impact responses.

It is generally believed that compared to a mid-sized male driver, a small-sized female driver is at greater risk of automotive-related injuries because of her short stature (and associated forward seating position) (Melvin et al., 1993[91]; Manary et al., 1998[87]), lower structural strength (Kimpara et al. 2003[68]), and lower injury tolerance values (Patrick and Andersson 1974[115]). Further investigations using a numerical model of the human chest are necessary to consider the chest injury mechanisms and effects of initial chest structures.

1.4.4. Gender differences

Based on injury surveillance and laboratory data, females have been shown to have a higher chance of sustaining severe injuries compared to males, especially in the chest and lower extremity regions (Patrick and Andersson, 1974[115]; Mackay and Hassan, 2000[86]; Lenard and Welsh, 2001[82]). By analyzing real-world automotive frontal crashes using the NASS in the US and the Cooperative Crash Injury Study (CCIS) in the UK, Mackay and Hassan (2000)[86] found that females and the elderly are the two most vulnerable groups in the entire population. At any given level of the AIS, the median tolerable delta-V for females was considerably lower than that for males. For example, Roberts and Compton (1993)[125] reported that the delta-V associated with a 50% probability of an AIS 3+ chest injury in the frontal impact of unrestrained occupants was 38 km/h for females and 44 km/h for males. Welsh and Lenard (2001)[160] also reported similar trends when investigating chest injuries with a maximum AIS (MAIS) of 2 or greater. Considering only AIS 3–6 injuries using the NASS database from 1997 to 2001, for male drivers, head injury and chest injury were the most and second most frequent injury, respectively. However, the order of injury frequency was reversed for female drivers.

Currently proposed injury tolerances and criteria for female occupants are not based on laboratory data obtained from female subjects. Rather, they are scaled from experimental data obtained largely from male cadavers (Eppinger et al., 1984[27]; Mertz, 1984[93]; Mertz et al., 1989[94]; Irwin et al., 2002[58]). However, these geometric and/or stress-related scaling methods have never been validated, and geometric scaling alone may not take into consideration these differences in the material properties between males and females (Kuppa and Eppinger, 1998[78]). Therefore, the investigation of chest injuries for females would be a good first step toward reducing serious injuries or fatalities to females in an automotive crash.

1.5.   Research Objectives and Structure of This Doctoral Thesis

Traffic accident analysis suggested increases in injured and disabled persons due to automotive crashes in Japan.   Therefore, impact biomechanics has been applied to reduce the injury probabilities to the head and chest.   Injury analysis using the AIS score suggested that the head and chest were the two most frequent body regions observed to suffer from serious or more severe injuries (AIS 3+ injuries). Considering AIS 3 or more injuries and severe residuals, SCI could be remarkable along with head or chest injuries.   The results of traffic accident analyses also showed an increasing number of female drivers on the road and suggested the vulnerability of female occupants in automotive crashes.   Therefore, the research objectives of this doctoral thesis are to investigate the injury mechanisms of serious–fatal injuries using human body surrogating technologies.

Human body surrogating technologies are necessary to obtain a better understanding of injury mechanisms.   For example, ATDs would be good tools to simulate the impact responses of the human body using real vehicular models and/or safety devices.   However, several limitations are faced in experimental studies using ATDs to determine injury mechanisms and assess injury severities.   ATDs are generally designed as durable tools to sustain numerous impact loadings.   Therefore, this thesis selected FE models of the human head neck complex and chest as human body surrogating tools.   The impact responses of the FE models were validated against experimental data using PMHS subjects obtained from literatures.   Then, the human body FE models were used for analyzing serious–fatal injurious impact scenarios in the following chapters.

In previous studies, numerous isolated brain FE models were proposed for investigating brain injuries.   However, the proposed injury mechanisms and metrics for brain injury were not unified owing to the characteristic features of each FE model.   In addition, the injury mechanisms of SCI, another part of the CNS, were not investigated as frequently as those of the brain.   Therefore, in Chapter 2, a head-neck complex FE model in which both the brain and the spinal cord are represented was used for a series of parametric studies to determine how the anteroposterior head-neck dynamics affect the biomechanical responses of the human head-neck complex in simulated frontal impacts.

It is believed that rotational head kinematics could be one dominant injury mechanism in TBI. However, it is not clear what parameters contribute to the stress or strain of brain tissues or damage that cause injuries.   In Chapter 3, football head impacts are analyzed to determine the brain injury predictors based on the FE model.   In addition, correlation analyses are used to reveal new brain injury predictors based on head kinematics, in addition to the HIC.

Chapter 4 focuses on chest injuries.   According to traffic accident analyses, gender differences are found in serious–fatal injuries.   However, it is not altogether clear whether a gender difference exists in the biomechanical parameters, or which parameter has the most influence on the chest response for females in automotive crashes.   Therefore, in Chapter 4, a retrospective review is conducted using published data to elucidate the chest impact responses and injury thresholds due to biological differences such as age, gender, and size of the human body.   Data from 83 cadaveric frontal and lateral blunt impacts to the chest were selected to characterize the chest's biomechanical properties, and the variables selected for analysis were

relevant cadaveric information, test conditions, chest impact response, and resulting chest injuries. An additional series of three-point bending tests using 87 human ribs was conducted with various loading rates, and the bending responses were obtained by considering the rate dependency and gender differences.

Biological varieties were simply considered by the scaling methods in these designs. In general, scaling methods assume that the human body can be represented by simple mechanical systems, such as the spring-mass-damper system reported by Lobdell et al. (1973)[84]. Therefore, the relationship between the impact responses and the weight (or height) of the human body could be derived through dimensional analysis, a method that has been used to predict the weight and height of the human body (Happee et al., 2000[44]; Irwin et al., 2002[58]; Kent et al., 2004[66]; Mertz et al., 2003[95]). However, the human body is too complex to be represented by a simple system. The composition of the material and structure inside the organs could affect the biomechanical responses and injuries of the human body. Therefore, an accurate description and detailed modeling of the human body are important key factors in gaining a better understanding of the injury mechanisms during impacts. Therefore, in Chapter 5, two series of parametric studies are conducted using an FE human body model of an American mid-sized male. The first study aimed to determine the influence of the rib bone's material and structural properties on the chest impact responses. To achieve this objective, the FE human body models were modified with different biomechanical parameters assigned to various components of the chest. Similarly, another parametric study was conducted by varying the body weight and height and rib area moment of inertia to understand the effect of size on the impact biomechanics based on FE analysis techniques. Then, the significant biomechanical parameters for female chest responses were summarized.

In Chapter 6, an American 5th percentile small female chest model was developed using knowledge previously obtained in Chapter 4 and Chapter 5. As experimental data for female subjects is generally limited, it is difficult to obtain many test cases from a single literature or consistent test setups. Therefore, female test data were collected from various experimental studies.

Finally, in Chapter 7, specific conclusions from each chapter are summarized, and the main conclusion of this thesis and recommendations for future works are presented.

Chapter 2   Investigation of Anteroposterior Head-Neck Responses

A series of parametric studies using a brain-spinal cord complex finite element (FE) model were conducted to investigate the effects of restraint conditions on central nervous system (CNS) injuries. The injury predictors for the brain were based on the Cumulative Strain Damage Measure (CSDM), whereas those for spinal cord injuries were based on the ultimate strains of the spinal cord and pia mater.

Some of the results taken from this section have been published in the 2006 Stapp Car Crash Journal (Kimpara et al., 2006A[A3]).

2.1. Introduction

This study aims to investigate how the anteroposterior external dynamic inputs to the head and torso during frontal impacts affect the biomechanical responses of the human head-neck complex. Toward this end, the research focus was limited to the upper torso kinematics. A head-neck complex FE model including the brain and cervical spinal cord was applied in this thesis. As the external inputs considered for the model are related to the anteroposterior translational motions and sagittal rotations of the head-neck complex, validation results using three series of head impacts and two series of neck tests are effective for the purposes of this chapter. Consequently, a series of parametric studies was conducted to investigate the relationship between the assumed anteroposterior boundary conditions and the biomechanical responses of the brain and spinal cord.

2.2. Head-Neck Complex FE Model

A commercially available mid-sized human male model THUMS-AM50 (THUMS: Total Human Model for Safety; Toyota Motor Corporation and Toyota Central R&D Labs., Inc., Aichi, Japan; Iwamoto et al., 2002[60]; AM50: American Male 50th percentile) was used as a base model in this thesis to predict the biomechanical impact responses. This model was developed using with LS-DYNA (LSTC, Livermore, CA), a commercially available explicit FE code. THUMS-AM50 version 3 was used for impact analyses of the head and neck. The brain model of THUMS had already been validated against cadaver test data on a series of translational head impacts (Nahum et al., 1977[99]) and two series of rotational impacts (Trosseille et al., 1992[150]; Hardy et al., 2001[45]), and it was found to show high bio-fidelity (Kimpara et al., 2006[70]). The neck model was validated against a series of neck flexion tests (Thunnissen et al., 1995[149]). The Normalized Integral Square Error (NISE: Donnelly et al., 1983[24]), a quantitative evaluation method used to compare the time history curves of the pressures and displacements predicted by the model with those

obtained from test data, evaluated the brain responses predicted by the THUMS brain FE model as excellent or good for 93% of the assessed variables.

Only the neck part was modified from the original because a detailed model of the spinal cord is required to represent the impact responses of the CNS. In addition, another validation with a cervical axial compression test was added for the neck model.

2.2.1. Structure

The CNS in the neck region was represented by a spinal cord model. This model consisted of hexagonal solid elements representing the white matter, gray matter, and CSF and shell elements representing the denticulate ligament, pia mater, and dura mater. The spinal cord model was created based on a 2D detailed spinal cord model (Ichihara et al., 2003[56]) and was modified to fit the geometry of THUMS-AM50. Then, the model was integrated into the spinal canal of the cervical spine. Figure 2.1 shows an overhead view of the model at the C4 level including the cervical vertebra, disc, and spinal cord. The size and geometry of the spinal cord were determined from literature data (Tanaka, 1984[147]; Suzuki and Shimamura, 1994[139]), which described the anteroposterior and lateral diameter of the spinal cord at the C3 to C7 vertebral level. The thickness of the CSF was assumed as 2 mm at the cervical region according to the schemes of anatomical references (Clemente, 1985[19]; Kahle et al., 1986[61]; Martini et al., 2000[89]). It is believed that the cervical dura mater is loosely connected to the cervical vertebrae via connective tissue. Therefore, in the model, a component of solid elements simulating fat layers was added between the spinal cord and the vertebral wall. The cervical nerves, represented by seatbelt elements, connected the spinal cord to the cervical spines. The neck model consisted of 12,586 elements (5,348 solid, 6,102 shell, 361 discrete[3], and 775 seatbelt elements).
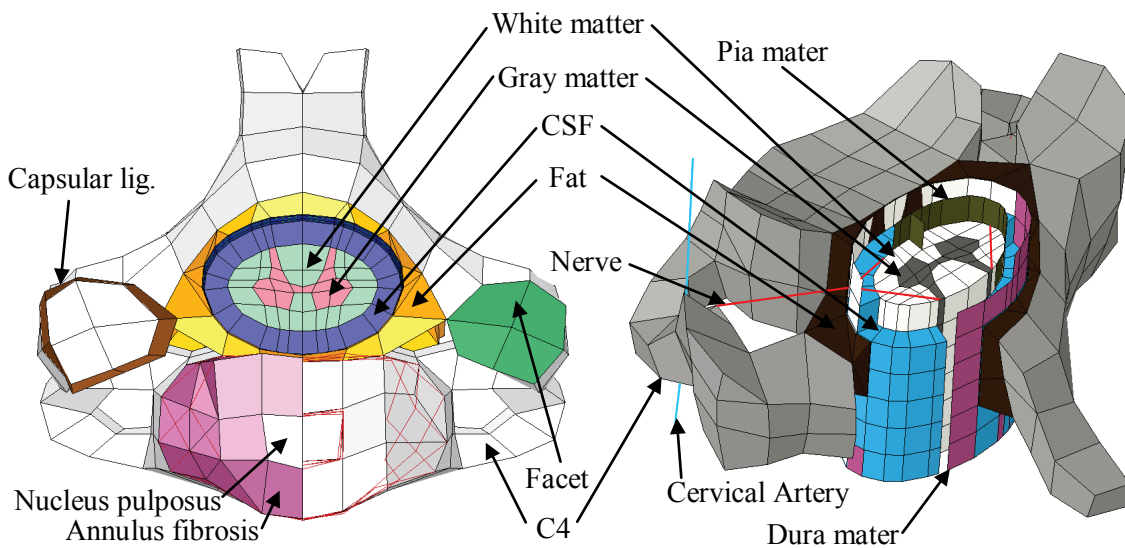
Figure 2.1: An overhead view of the cervical vertebra, disc, and spinal cord models at C4 level

---

[3] Discrete element: 1D discrete elements such as springs or dampers in LS-DYNA.

Figure 2.2 shows a lateral view of a 3D FE head-neck complex model. The head-neck models were continuously linked together to construct a single head-neck complex. The white and gray matters of the spinal cord were continuously linked to those of the brainstem to simulate a single brain-spinal cord complex.

Scalp
Skull
CSF
Muscles

Sagittal Sinus
White matter (Cerebrum)
Gray matter (Cerebrum)
White matter (Cerebellum)
Gray matter (Cerebellum)
White matter (Brainstem)
Gray matter (Brainstem)
White matter (Spinal cord)
Gray matter (Spinal cord)
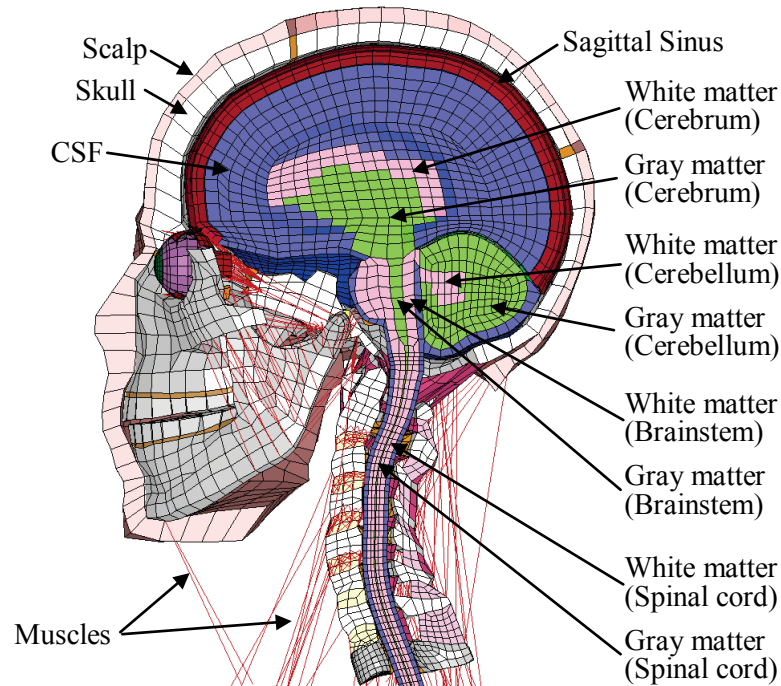
Figure 2.2: A lateral cross-sectional view of a 3D FE model of the head-neck complex

2.2.2. Material properties

(a) Spinal cord

Bilston and Thibault (1996)[8] conducted a tensile test on the human cervical spinal cord in vitro and determined the nonlinear material properties from their test specimens. Additionally, Bilston (1998)[9] conducted a parametric study of the material properties of the spinal cord using a 2D FE head-neck model. She found that the viscoelastic time-dependence did not significantly affect the stresses and strains of the spinal cord. The "wavy" nature of the fiber tracts would produce a nonlinear material behavior, and this might protect the neural fibers from injury at lower strains. Consequently, a hyperelastic material model type 181 was selected from the LS-DYNA material library for the spinal cord in this study.

Figure 2.3 shows stress-strain curves of the white and gray matters of the spinal cord obtained from bovine specimens (Ichihara et al., 2001)[55]. Ichihara et al. (2001) pointed out the difference in tensile properties between the white and the gray matter in the spinal cord. Ichihara et al. (2003)[56] also obtained six test specimens from the gray and white matter of bovine spinal cords. These specimens were tested under tension at various displacement rates ranging from 0.005 to 0.5 mm/s. Each tensile test was

completed within 5 min of sample preparation.   In this study, the obtained nonlinear curves were directly used in the material models for the gray and the white matter.
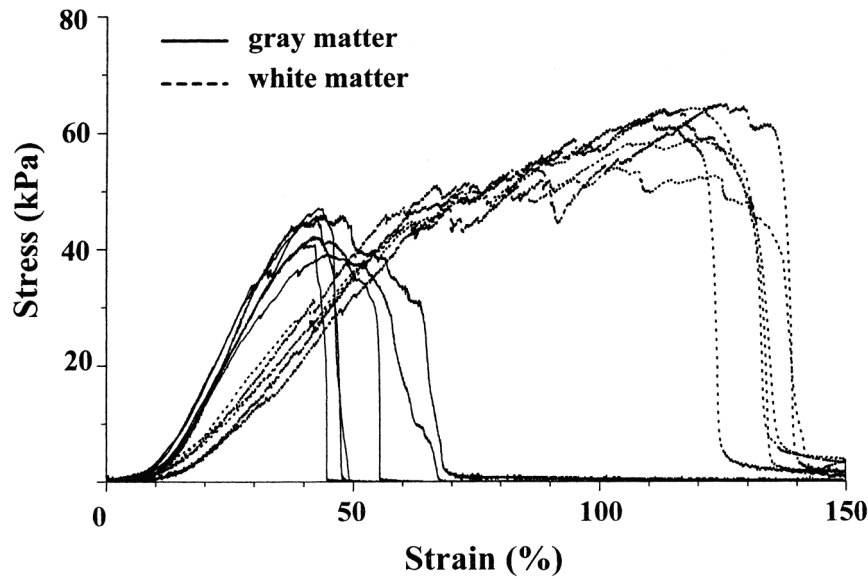
Figure 2.3:   Stress-strain curves of the white and gray matters of the spinal cord obtained from bovine specimens (Ichihara et al., 2001)

(b) Dura mater

The material properties of the cervical dura mater were determined from data reported by Yamada (1970)[164].   The cervical dura mater was represented using a nonlinear membrane material model (LS-DYNA material type 34).   Table 2.1 shows only the elastic components of the material properties used in the cervical dura mater in this study.

Table 2.1:   Material properties used in the cervical dura mater

		Density (kg/m³)	Young's modulus E (MPa)	Poisson ratio	Thickness (mm)	Reference
Dura mater	Anterior	1,100	44.1	0.30	0.33	Yamada (1970)
	Posterior	1,100	43.35	0.30	0.68	

(c) Pia mater

The material properties of the cervical pia mater were determined from the aforementioned experimental results conducted in this study.   They can be determined from the properties of the posterior median septum.   Young's modulus of 39.3 MPa, Poisson's ratio of 0.3, and thickness of 0.13 mm were determined for the pia mater; the corresponding values determined for the denticulate ligament were 63.9 MPa, 0.3, and 0.24 mm.

(d) Neck muscles

According to the results reported by Ono et al. (1997)[111], activation of the neck muscles is considered to occur within a range of 70–140 ms after impact.   As this study focuses on severe frontal impact scenarios with shorter phenomenological time duration, muscle activation would not be necessary. Therefore, only passive muscle responses were simulated.   The neck muscles were represented using tension-only bar elements based on the Hill-type muscle equation (LS-DYNA V970 material type S15) without activation to simulate an unaware condition prior to impact.   The passive muscle property was determined from the quasi-static tensile data of the sternocleidomastoid muscle (Yamada, 1970[164]).   The sternocleidomastoid, scalenus anterior, scalenus medius, scalenus posterior, longus capitis, longus colli, rectus capitis anterior, sternohyoid, multifidus, splenius capitis, semispinalis capitis, semispinalis cervicis, longissimus capitis, and longissimus cervicis muscles were considered in this study.

2.2.3. Validation for cervical axial compression

(a) Simulation setups

Pintar et al. (1995)[118] conducted a series of neck loading tests using 20 human cadaver head-neck complexes.   Figure 2.4 shows a diagram of the test setup.   The muscles and surrounding fat and soft tissues were removed from the spinal area to obtain the entire head to T2 ligamentous complex.   The test specimen was mounted into a fixative at T1-T2 inferiorly, and the cranium was left intact superiorly.   The cervical vertebral bodies were pre-aligned using a pulley-weight system and spring.   The occipital condyles (OC) were aligned over the center of the T1 vertebral body.   A flat plate with 20-mm-thick Ensolite padding was fixed to the piston device and impacted on the crown of the head at a speed of 2.5–8 m/s.   A corridor for the human neck dynamic force-deformation response was developed using the inferior load cell.   Table 2.2 shows a summary of the experimental data reported by Pintar et al. (1995)[118].   The term "Pre-align" in the table refers to the head position in the anterior-posterior direction.   However, other detailed impact conditions for each case were not reported in this literature.
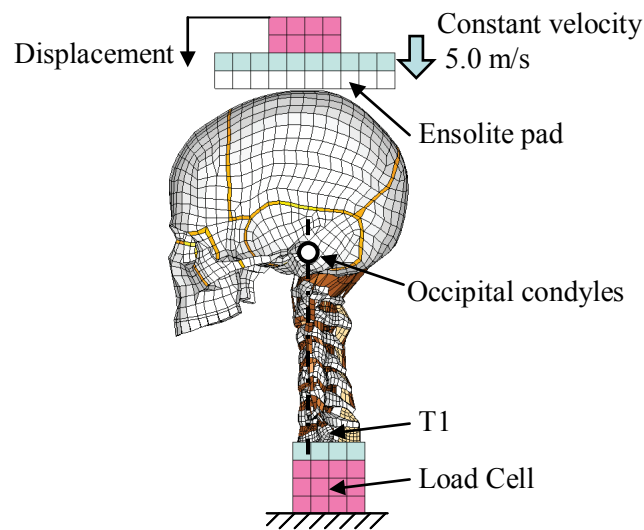
Figure 2.4:   Simulation setup of the head-neck model to simulate cervical axial compression

Table 2.2:   Summary of experimental results reported by Pintar et al., (1995) [118]

	Pre-Align (cm)	Failure load (N)	Neck disp. @failure (mm)	Injury
N01	-0.5	1183	16.4	Vertical fracture of C3
N02	0.0	3678	12.6	Compressive burst fracture of C5
N03	0.0	744	15.0	Wedge fracture of C4, compressive fractures of C2, C3
N04	0.0	5005	18.8	Wedge fracture of C6
N05	+0.5	6431	19.6	C3-C4 anterior longitudinal ligament tear with avulsion fracture of C3
N06	+0.5	3445	19.7	C2-C3 dislocation with ligamentous rupture
N07	+0.5	4580	17.7	Anterior vertebral body fracture of C4
N08	0.0	3906	22.3	Vertical fracture of C3 with lamina fracture
N09	0.0	5179	17.5	Anterior-superior chip fracture of C3
N10	0.0	3744	16.5	Compression fractures of C4, C7
N11	-0.5	4799	19.0	C3-C4 anterior longitudinal ligament tear; C4, C5 spinous process fractures
N13	+2.5	2884	13.9	Interspinous ligament tear at C6-C7
N14	0.0	3086	17.4	Compressive burst fracture of C5
N15	-0.5	1341	19.6	C6-C7 anterior longitudinal ligament tear with lamina fractures of C6, C7
N16	+3.0	2545	20.9	Entire posterior ligaments torn at C6-C7
N17	0.0	2732	14.5	Compression fracture of C5
N18	+0.5	2691	21.5	Mild compression of C7
N19	+2.0	2707	14.8	Entire posterior ligaments torn at C7-T1
N20	+1.0	2410	24.8	Compression burst fracture of C5 with posterior ligament rupture at C5-C6
N21	+0.5	3699	16.5	Compression burst fracture of C4 with posterior ligament rupture at C3-C4

In the simulations, a loading setup for axial compression (Figure 2.4) was represented with the neck model.   The alignment of the cervical vertebral bodies was changed to be straight in order to repeat the experimental setup.   T1 was fixed with a rigid base, and a loading device with Ensolite padding was dropped down at a constant velocity of 5 m/s.

(b) Results

Figure 2.5 shows the force-displacement curve obtained during axial loading on the head-neck complex. The black solid lines and gray dashed lines indicate the simulation result and experimental corridor, respectively. The force and displacement data were obtained from the inferior load cell and potentiometer on the piston device, respectively. The simulation results lied within the corridor.

The vertebral bone models of C1, C2, C3, and C4 showed yielding with plastic strain of more than 1.5% during compression loading, although mesh eliminations of the cervical vertebrae were not observed. The skeletal injuries predicted by the model qualitatively agreed with the autopsy reports of Pintar et al. (1995)[118]. Table 2.2 shows 15 cases of vertebral fractures and 9 cases of ligament tear or rupture in their compressive tests using 20 specimens.
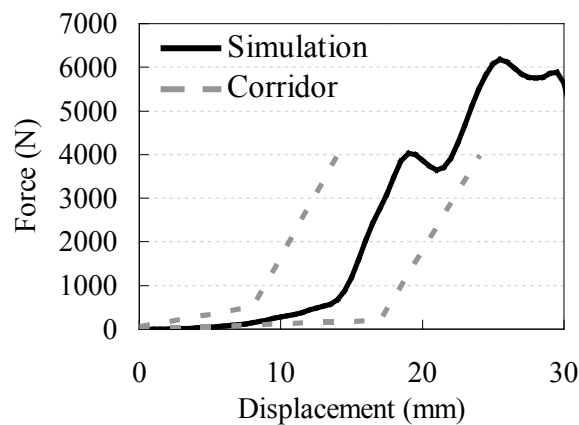
Figure 2.5: Force-displacement curves of the human head-neck during axial compression loading. Black thick line and dashed line respectively represent a simulation result predicted by the model and a test corridor obtained from Pintar et al. (1995)

Additionally, several ligament ruptures were represented in the model. The predicted ligament ruptures in the model were found in the posterior ligament at C5-C6, entire posterior ligaments at C4-C5, and alar ligament and capsular ligament at C0-C1. On the other hand, in the experimental data, Table 2.2 shows ligamentous rupture at C2-C3 for case "N06," interspinous ligament tear at C6-C7 for case "N13," entire posterior ligaments torn at C6-C7 for case "N16," and entire posterior ligament torn at C7-T1 for case "N19." Although some ligamentous damages were not clearly described in the literature, the ligamentous damages predicted by the simulation model agreed with the experimental data.

2.2.4. Cumulative Strain Damage Measure (CSDM)

The CSDM (Takhounts et al., 2003[142]) was used for evaluating the diffuse axonal injury (DAI) to the brain. The CSDM was defined as the volume percentage of the brain that exceeds a specified first principal strain (FPS) threshold. When the threshold of the FPS is set to 10%, the variable term is expressed as "CSDM 10%" in this study. For example, Figure 2.6 shows the difference between CSDM 10% and CSDM 20%, where the damaged volume in the former case is 49 vol%, which is greater than 1.2 vol% in the latter case.

(a) Strain threshold of 10%   **(b) Strain threshold of 20%**
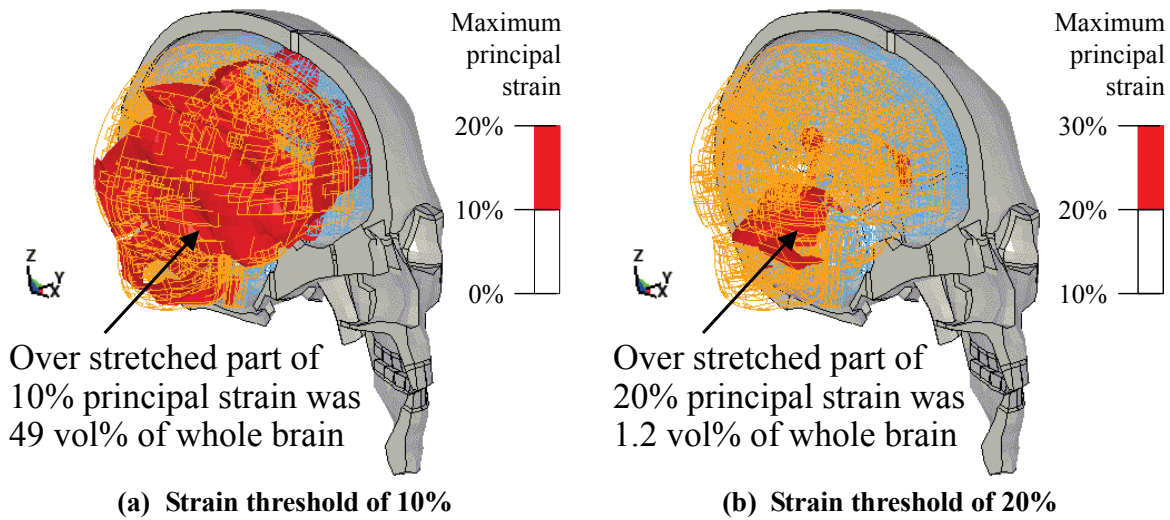
Figure 2.6:   A sample of strain distribution in the human brain FE model.   Elements that experienced over 10% (left) or 20% (right) of the principal strain were considered damaged.

2.3. Methods for Antero-posterior Head-Neck Impacts

2.3.1. Simulation setups

A series of parametric studies was performed to determine how the anteroposterior head-neck dynamics affect the biomechanical responses of the human head-neck complex in simulated frontal impacts. During a frontal automotive crash, the human body is restrained or receives direct impacts on the head, torso, and extremities. As vehicle occupants are stationary in the seats and restrained by seatbelts, it can be assumed that the anteroposterior dynamics to the head and torso could be the dominant inputs for the human head-neck responses and kinematics in frontal impacts.   The human neck might be injured owing to indirect force transmission.   The impact responses of the CNS region might be affected by the balance of external forces to the head and torso.   Consequently, a series of parametric studies was conducted using the validated head-neck complex model with different restraint conditions assigned to various restraint harnesses.   Figure 2.7 shows the mini-sled simulation setup.   All simulations were conducted using a commercially available FE solver, LS-DYNA 971 Rev. 4.2.1, Shared Memory Parallel (SMP) version (LSTC, Livermore, CA), using a single-core Intel Xeon 64-bit-based computer running Linux operating system.
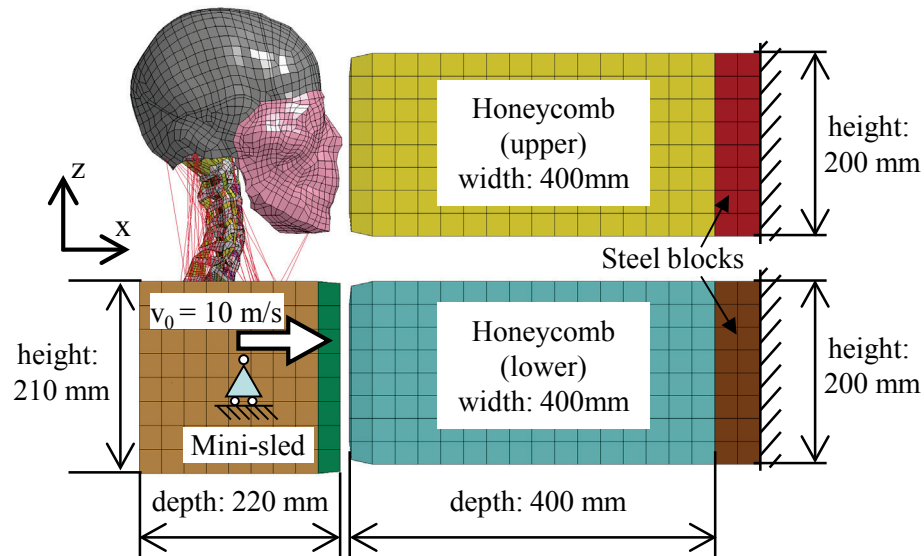
Figure 2.7:   Schematic diagram of mini-sled simulation setup

The boundary conditions prescribed for the parametric studies were set up by using a mini-sled configuration to represent an impact situation where the occupant was loaded in the anteroposterior direction only.   A lumped mini-sled simulated an upper torso.   The mini-sled model had a mass of 45.3 kg to represent the total mass of the chest, abdomen, and upper extremities (Robbins, 1983[124]) with a width of 440 mm, height of 210 mm, and depth of 220 mm.   For the simplicity of the boundary conditions, the translational (y and z directions) and rotational (around x-axis and z-axis) degrees of freedom of the mini-sled were constrained; however, a rotational degree of freedom around the y-axis was allowed.   The head-neck FE model was mounted on the mini-sled model.   To simulate a severe frontal impact situation, an initial velocity of 10 m/s was applied to both the head-neck complex and the mini-sled component along the direction from posterior to anterior.   Additionally, two honeycomb barriers were prepared to simulate various restraint conditions.   A flat honeycomb barrier had rounded edges with a width of 400 mm, height of 200 mm, and depth of 400 mm.   An upper honeycomb was placed at the head level, and a lower honeycomb was placed in front of the mini-sled model.   The strength and initial position of the two honeycombs were arbitrarily changed to produce various loading conditions.

2.3.2. Simulation matrix

Three different padded honeycombs with crush strengths of 100 psi (0.689 MPa)[4], 15 psi (0.103 MPa), and 1.5 psi (10.3 kPa) were prepared.   In particular, the crush strength of 1.5 psi was comparable to that of the deployed airbag (Yang et al., 1998[165]).   The side of the honeycomb opposite the impact site was attached to the steel block, which was rigidly fixed to the global coordinate system.   A pair of upper and lower honeycombs with various crush strengths was arranged to receive the momentum of the head and torso parts, respectively.

Nine simulation cases were prepared for the frontal mini-sled impact simulations (Table 2.3). These cases represent several variations in the occupant restraints, as explained in detail below.   Case 01 represented a case of only torso restraint.   Case 02 represented soft restraints of the head and torso with strength equivalent to that of the deployed airbag.   In Cases 03, 04, and 05, the strength of the honeycomb was 10 times higher for the torso, head, and head and torso, respectively.   Cases 06, 07, and 08 were coordinated to observe the effects of contact timing.   The upper honeycomb barrier was shifted forward by 50 and 100 mm in Cases 06 and 07, respectively, whereas the lower honeycomb barrier was shifted forward by 50 mm in Case 08.   Case 09 represents a hard impact where a 100 psi honeycomb was used for both the upper and the lower barriers.

Table 2.3:   Simulation matrix

	Head	Torso
Case 01	N/A	15 psi
Case 02	1.5 psi	1.5 psi
Case 03	1.5 psi	15 psi
Case 04	15 psi	1.5 psi
Case 05	15 psi	15 psi
Case 06	1.5 psi + offset 50 mm	15 psi
Case 07	1.5 psi + offset 100 mm	15 psi
Case 08	1.5 psi	15 psi + offset 50 mm
Case 09	100 psi	100 psi

---

[4] Crush strength: the greatest compressive stress that a brittle solid can sustain without fracture.

2.4. Results

Figure 2.8 shows the predicted overall kinematics of the model at 0 and 30 ms for simulating a mini-sled impact with closing velocity of 10 m/s.   The response modes of the head-neck complex are observed to vary according to the arrangement of the honeycomb barrier.   In Case 01, the torso part rebounded when the torso drove 138 mm forward.   Then, the head-neck part was swung forward without any restraint.   In Case 02, the head was stopped at 102 mm forward displacement, whereas the torso kept moving forward until a displacement of 268 mm.   In Case 03, the head traveled by ~99 mm and the translational motion stopped, whereas the torso stopped at 131.9 mm forward displacement with a little delay of 9 ms.   In Case 04, the head stopped early at a displacement of 68.7 mm, whereas the torso drove forward by more than 250 mm.   In Case 05, the head started to rebound at 68.1 mm displacement, whereas the torso moved forward until 131.6 mm displacement.   In Case 06, the head traveled forward by 143.7 mm from the initial position, whereas the torso stopped at 133.7 mm displacement from the initial position.   The timings of the head and torso stopping were almost comparable.   In Case 07, the head moved forward by 187.1 mm from the initial position, whereas the torso moved forward by 134.3 mm.   The body stopped earlier than did the head.   In Case 08, the head stopped at 102.6 mm displacement, whereas the torso stopped at 183.8 mm displacement from the initial position.   In Case 09, the head rebounded after 38.1 mm displacement, and the torso was at 45.3 mm displacement at almost the same time.

The results of the parametric study are summarized in Table 2.4.   The relative displacement in the X translational direction (ΔDisp-X) corresponds to the relative displacement between the head and the torso. CSDM 10% expresses the damaged volume percentage of the whole brain, which experiences FPS greater than the strain threshold of 10%.

Table 2.4:   A summary of parametric simulation results

	Head	Torso	ΔDisp-X (mm)	CSDM 10% (vol %)	White matter, Max FPS (%)	Gray matter, Max FPS (%)	Pia mater, Max FPS (%)	Number of ruptured ligaments
Case 01	None	15 psi	+207	0.50	29.7	24.7	14.2	11
Case 02	1.5 psi	1.5 psi	-213	52.3	37.3	31.4	51.6	14
Case 03	1.5 psi	15 psi	-51	27.0	34.7	31.8	23.1	4
Case 04	15 psi	1.5 psi	-246	88.7	37.7	35.1	66.4	16
Case 05	15 psi	15 psi	-93	71.8	35.6	33.9	33.9	11
Case 06	1.5 psi + 50 mm	15 psi	+26	21.0	21.6	19.1	10.6	0
Case 07	1.5 psi + 100 mm	15 psi	+60	17.8	22.4	20.6	8.2	1
Case 08	1.5 psi	15 psi + 50 mm	-106	33.4	36.2	34.0	36.9	9
Case 09	100 psi	100 psi	-41	71.9	33.7	29.2	25.9	2
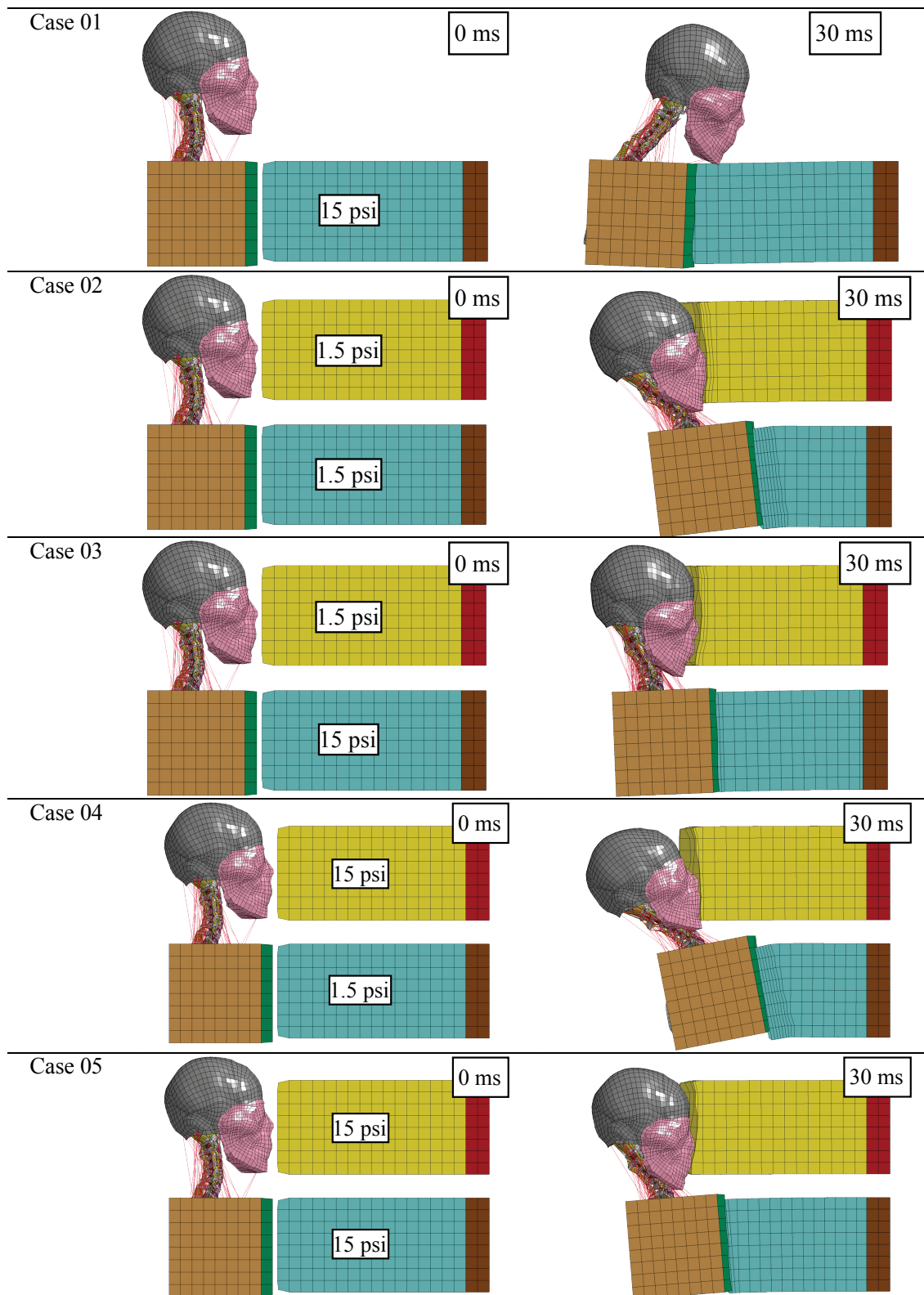
Figure 2.8:   Overall kinematics of the head-neck model with initial velocity of 10 m/s at 0 and 30 ms
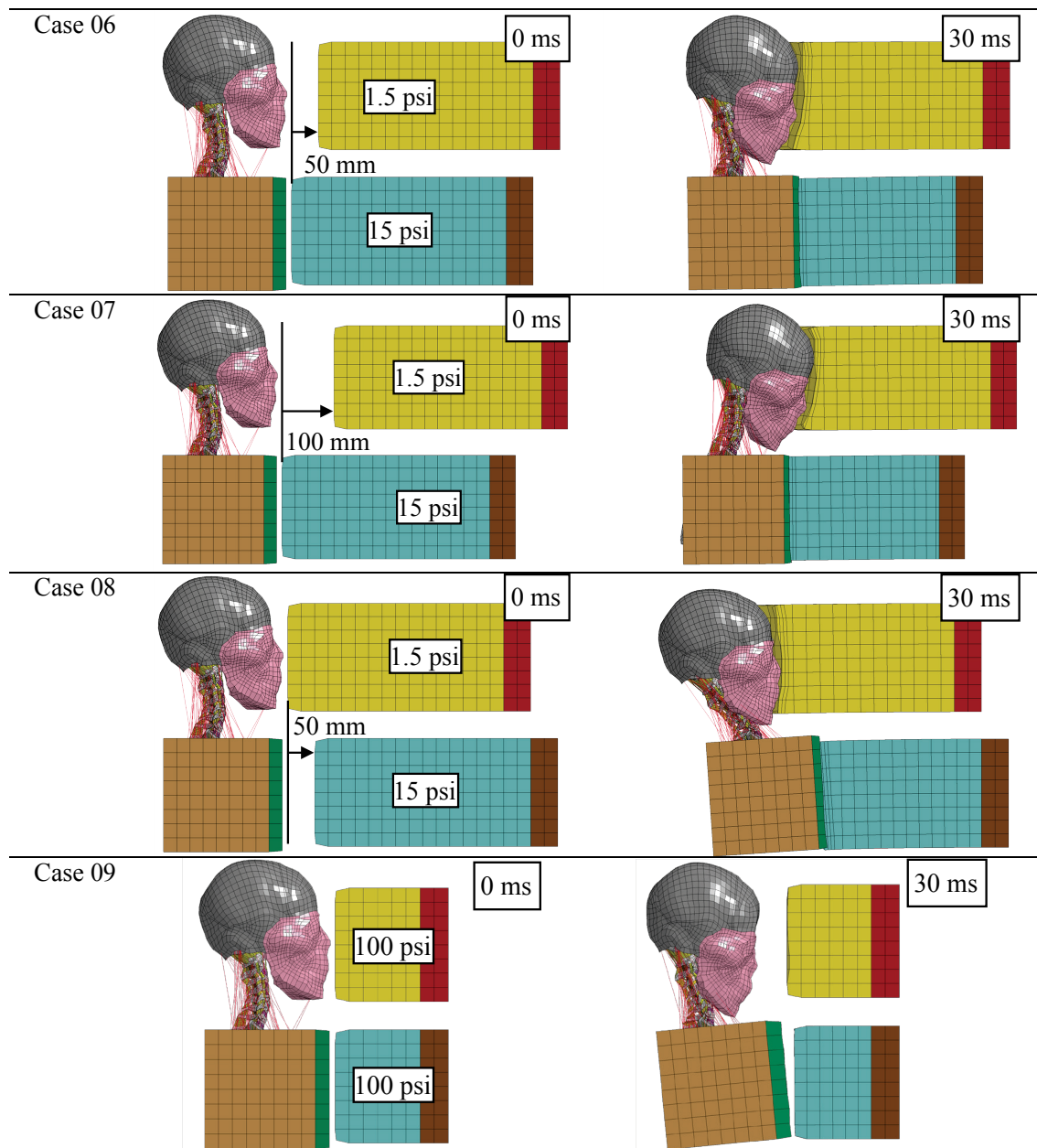
Figure 2.8(contd.): **Overall kinematics of the head-neck model with initial velocity of 10 m/s at 0 and 30 ms**

This study used CSDM with FPS thresholds of 10%, 20%, and 30% for analyzing the brain responses. Figure 2.9 shows the damaged volume percentage of the whole brain, which has experienced 10%, 20%, or 30% strain levels. In Case 04, 88.7% of the total brain volume experienced FPS of 10% or greater. The volume percentage in Case 04 was the highest in all simulation cases. The boundary condition for Case 04 was arranged with a stiffer head restraint and soft torso restraint. The secondary higher volume percentage cases were observed in Cases 05 and 09. These cases had a head restraint arranged with stiff honeycombs.
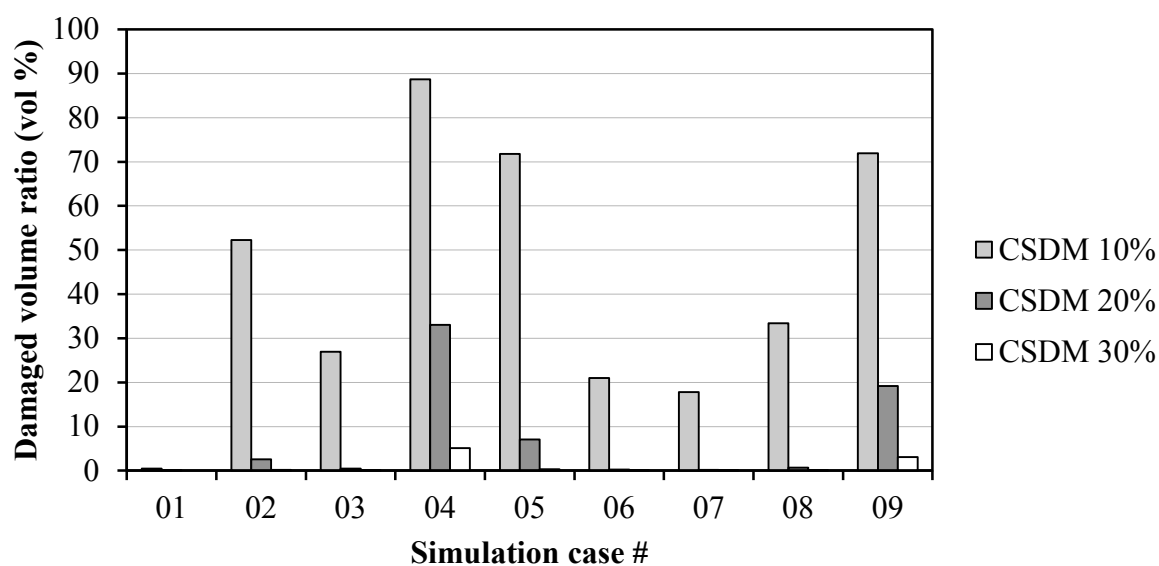
Figure 2.9: Volume percent of the whole brain, which has experienced 10%, 20%, or 30% strain levels
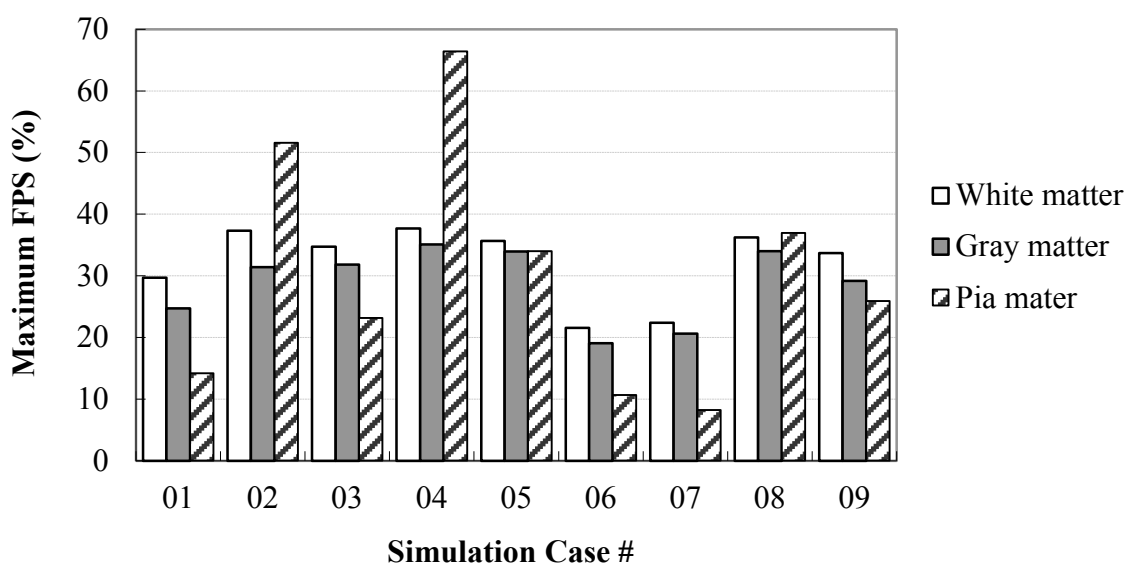
Figure 2.10: Maximum FPS of white and gray matter and pia mater of spinal cord.

Figure 2.10 shows the maximum peak values of the FPS obtained from white and gray matter and pia mater of spinal cord.   The white, gray, and striped bars represent the results of white matter, gray matter, and pia mater of the spinal cord, respectively.   The peak values of the FPS were compared among the simulation cases.   For the spinal cord, the peak FPS of white matter was greater than that of gray matter.   It was found that the difference in stiffness between white and gray matter affected the difference in peak FPS. Cases 06 and 07 showed FPS of less than 25% in the white matter, gray matter, and pia mater of the spinal cord.   Cases 02, 04, and 08 showed higher values of FPS (>35%) for the pia mater.

In this study, the material model for the spinal cord was assumed to be hyperelastic rubber to represent the nonlinear tensile behavior.   However, the damage or yielding of the spinal cord could not be represented in the model owing to the limitation of the material definition.   According to the stress-strain curves of the spinal cord (Figure 2.3; Ichihara et al., 2001[55]), the gray matter and white matter of the spinal cord yielded at a total strain of ~30%–40% and ~55%–60%, respectively.   Additionally, the tensile test results of the pia mater showed failure at a total strain of ~30% as well.   The predicted values of the FPS of the white matter in all cases were less than 50%.   However, the FPS of gray matter in Cases 02, 03, 04, 05, and 08 were in excess of 30%.   For the pia mater, Cases 01, 03, 06, 07, and 09 showed FPS less than 30%.

Table 2.5 lists the ligaments damaged during the impact loadings.   In this model, the mesh

Table 2.5:   Predicted damage to the ligaments during the impact loadings

	Cervical Ligaments	Thoracic Ligaments (only C7-T1)
Case 01	Alar ligament, Apical dental ligament, Anterior atlantoaxial ligament, Ligament cruciform atlantis, ISL(C1-C2), ISL(C4-C5), ALL(C6-C7), LN(C6-C7)	ALL(C7-T1), PLL(C7-T1), ALL(T1-T2)
Case 02	ISL(C1-C2), PLL(C2-C3), ISL(C2-C3), LN(C2-C3), ALL(C6-C7), ISL(C6-C7), LN(C6-C7)	ALL(C7-T1), SSL(C7-T1), ALL(T1-T2), PLL(T1-T2), CL(T1-T2), SSL(T1-T2), ALL(T2-T3)
Case 03	-	CL(C7-T1), SSL(C7-T1), ALL(T1-T2), SSL(T1-T2)
Case 04	ISL(C1-C2), PLL(C2-C3), LN(C2-C3), ISL(C2-C3), PLL(C3-C4), PLL(C4-C5), ISL(C4-C5), LN(C5-C6), ALL(C6-C7)	ALL(C7-T1), CL(C7-T1), ALL(T1-T2), PLL(T1-T2), CL(T1-T2), SSL(T1-T2), ISL(T1-T2)
Case 05	ISL(C1-C2), ALL(C2-C3)	ALL(C7-T1), CL(C7-T1), ITL(C7-T1), SSL(C7-T1), ALL(T1-T2), PLL(T1-T2), CL(T1-T2), SSL(T1-T2), ISL(T1-T2)
Case 06	-	-
Case 07	Anterior atlant axial ligament	-
Case 08	PLL(C2-C3)	ALL(C7-T1), CL(C7-T1), SSL(C7-T1), ALL(T1-T2), PLL(T1-T2), CL(T1-T2), SSL(T1-T2), ISL(T1-T2)
Case 09	ALL(C2-C3)	SSL(C7-T1)

*ALL: Anterior Longitudinal Ligaments, LN: Ligamentum nuchae, PLL: Posterior Longitudinal Ligament, ISL: Interspinous Ligament, TL: Transverse Ligament, CL: Capsular Ligament, SSL: Supraspinous Ligament

elimination method was used to represent the ligament ruptures.   Cases 01, 02, and 04 showed a high degree of ligament damage.   The predicted ligament damage was mainly concentrated in the upper and lower cervical areas.   In Cases 03 and 06, no cervical ligaments were damaged or ruptured.   Additionally, in Cases 06 and 07, the thoracic ligaments were not damaged as well.

2.5.   Discussion

A series of parametric studies was performed using the validated head-neck model to determine how the anteroposterior head-neck dynamics affected the biomechanical responses of the human head-neck complex in simulated frontal impacts.   Because the model consisted of body parts from the head to the upper torso, external forces were applied to the human body through the head and torso only.   The cases simulated in the parametric study included soft contacts to mimic an airbag restraint system, hard contacts to represent stiffer restraints or impacts against the interior structures, and offset restraints between the head and the torso.   The CNS injuries, including the brain and spinal cord injuries, might be controlled by balancing the external forces applied to the head and torso.

According to the anatomical reference (Clemente et al., 1985[19]), the spinal cord may not move easily.   The deformation of the spinal cord correlates with the relative displacements of the vertebrae.   The spinal cord consists of white and gray matter.   As the pia mater is wrapped around the spinal cord, it can be considered the external surface of the spinal cord.   The dura mater is wrapped around the pia mater with a layer of CSF between them.   Although the spinal cord, which is wrapped within the pia mater, floats in the CSF, denticulate ligaments connect the pia mater to the dura mater (Perese, 1960[117]).   The dura mater is attached with a fatty connective tissue in the spinal canal.   These anatomical boundary conditions of the denticulate ligaments and fatty connective tissue may not allow the relative motion of the spinal cord.   Additionally, nerve roots, which originate from the spinal cord, reach the vertebrae.   This structural connection also supports the constraint effect to the spinal cord.   Owing to these anatomical structures, the thoracic motion may not affect the length of the cervical spinal cord.   In this study, all parts of the pia mater, dura mater, nerve root, and denticulate ligaments were carefully represented in the FE model.   Even if the thoracic vertebral bodies showed significant motion, its effect on the injury mechanism of the spinal cord may be minor.   Consequently, it is believed that the assumed head-neck model with a mini-sled is sufficient to investigate the injury mechanism of the brain and cervical spinal cord.

The translational and rotational accelerations to the head have been recognized as significant external inputs to assess the risk of brain injury (Unterharnscheidt, 1971[151]; Gennarelli et al., 1971[38]; etc.). Additionally, the mechanism of spinal cord injury can be considered an intrusion of the vertebrae into the spinal canal (Bilston, 1998[9]).   Therefore, the external inputs to the head-neck in the anteroposterior directions could have a sensitive effect on the probability of brain and spinal cord injuries.   Thus, the parametric simulations performed in this study are considered a type of sensitivity analysis to understand the relationship between the boundary conditions and the responses of the brain and spinal cord.

Case 01, which had no restraint for the head, had the lowest score in the CSDM.   Additionally, the cases of soft contact to the head (Cases 02, 03, 06, 07, and 08) showed relatively lower severity in terms of the volume percentage of the damaged brain.   On the contrary, Case 04 had the highest score in the CSDM. This is probably because the head strongly impacted against a hard honeycomb barrier, and larger relative displacement occurred between the head and the torso.   Cases 05 and 09 had a relatively high score in the CSDM owing to the head restraint honeycomb with higher strength.   Therefore, when only head injury was considered, brain injury could be reduced by preventing the head from direct hard impacts or to restrain the head with soft airbags or cushions.   However, in this study, we estimated the brain injury by using only the CSDM because this study aimed to predict a severe brain injury as DAI.   Further consideration is needed to predict moderate and minor brain injuries by using other injury criteria and to consider how the injury severity to the head can be reduced.

For spinal cord injury criteria, the FPS was used to predict cervical spinal cord injuries of the gray matter.   The failure thresholds for the gray and white matter and pia mater were determined as FPS strains of 55%, 30%, and 30%, respectively, whereas the stress-strain properties were obtained from the uniaxial tensile tests using the animal specimens.   The results of the parametric studies indicate that the FPS of the white matter did not exceed a yield strain of 55% in all cases, whereas that of the gray matter exceeded a yield strain of 30% in Cases 02, 03, 04, 05, and 08.   As the gray matter is more fragile than the white matter (Ichihara et al. 2001[55]), the strain of the gray matter is more sensitive than that of the white matter.   The strain of the pia mater also exceeded the failure threshold strain of 30% in Cases 02, 04, 05, and 08. Young's modulus of the spinal cord was roughly estimated as only 1% of that of the pia mater.   If the pia mater were to rupture, the spinal cord would be flushed out.   Therefore, the gray matter and pia mater would be better injury predictors of the spinal cord.   In Cases 02, 03, 04, 05, and 08, the spinal cord was likely to be damaged.

The cases with greater FPS in the pia mater, such as Cases 02, 04, 05, and 08, showed backward head-neck extension.   In Cases 02 and 05, the stiffness of the honeycomb barriers was balanced between the head and the torso.   However, the deceleration length between the head and the torso was unbalanced because of the significant difference in the body mass between the head (4.39 kg) and the torso (45.3 kg). The inertial effect of the torso was greater than that of the head.   Therefore, the total displacement of the head was significantly shorter than that of the torso, and as a result, their relative displacement increased.   In Case 04, a stiffer honeycomb for the head reduced the deceleration length, and therefore, the relative displacement increased more significantly.   These results could suggest that the inertial effect of the human body plays an important role in the relative displacement between the head and the torso.   In Case 08, the displacement of the torso was relatively larger than that of the head because the head was restrained earlier. On the other hand, Case 01 predicted large forward head-neck extension; however, the FPS of the spinal cord was lower than the failure threshold strain.

With regard to predicting ligament rupture, Cases 01, 02, 04, and 05 showed a large amount of cervical ligament damage or rupture.   In these cases, the relative displacement between the head and the torso was extremely large and the head-neck complex showed hyperextension.   This neck kinematics can

lead to larger stretching in the cervical ligaments, in turn causing their rupture. Cheng et al. (1982)[16] conducted a series of cadaveric sled impact tests using a pre-deployed airbag. Two of six cases showed damage to the cervical ligaments. However, the simulation results shown in Table 2.5 seem to be somewhat overestimated. This is because a recent study preliminarily suggested that modeling the neck muscles with solid elements could reduce the stress from the vertebrae or ligaments in FE models (Hedenstierna et al., 2006[50]), whereas this study used discrete bar elements for cervical muscles and a breakable elastic-plastic material law for the cervical ligaments. Therefore, further study is required to qualify the number of ligament ruptures.

Considering the balance of the simulation results in terms of the brain injury, spinal cord injury, and cervical ligamentous injuries, Cases 06 and 07 showed a smaller amount of assumed CNS injury metrics, including brain and spinal cord injuries, under the simplified anteroposterior constraints. In these cases, the head-neck model was restrained by the arrangement of the soft restraint for the head with some forward offset and a hard restraint for the torso. However, as the current study emphasizes only the anteroposterior motion, the simulation setup could not represent the 3D kinematics for a real world occupant restrained asymmetrically with a three-point belt. A further study must be conducted to investigate real world injury prevention.

2.6. Conclusions

A 3D FE model of the head-neck complex was used to simulate the biomechanical responses of the entire CNS at the same time. The predicted results of the anteroposterior head-neck responses during severe frontal impacts showed that soft or no head contact could reduce the score of an injury predictor for DAI. With regard to the neck responses, the inertial effect of the human body plays an important role in the relative displacement between the head and the torso. Additionally, backward neck extension would increase the strain of the spinal cord. In either forward or backward extension, the large relative displacement between the head and the torso stretched the cervical ligaments. This study showed that a better configuration for the head-neck response is an arrangement of a soft restraint for the head with some forward offset and a hard restraint for the torso. However, the results obtained from the parametric study show only one of the potential mechanisms of CNS injuries in frontal impacts. To elucidate the CNS injury mechanism of occupants in real world frontal impact situations, a further study is required to simulate the interaction between the occupant and the vehicular internal structure by using the occupant FE model and vehicular internal structure FE model.

Chapter 3   Mild Traumatic Brain Injury Predictors

The brain finite element (FE) model was used for developing two criteria based on angular accelerations for traumatic brain injury (TBI), which we call Rotational Injury Criterion (RIC) and Power Rotational Head Injury Criterion (PRHIC) in this study.   Concussive and nonconcussive head acceleration data obtained from football head impacts were used to develop new injury criteria.

Some of the results taken from this chapter have been published in the 2011 International Journal of Automotive Engineering[A6], 2011 Transactions of Society of Automotive Engineers of Japan (Transactions of JSAE[A7]), and 2012 Annals of Biomedical Engineering[A8].

3.1. Introduction

In previous studies, numerous injury predictors (Gadd, 1966[36]; Ommaya et al., 1967[109]; Versace, 1971[152]; Margulies and Thibault, 1992[88]; Newman et al., 2000b[107]; Kleiven, 2007[74]; Takhounts et al., 2011[144]) based on translational or rotational head motions have been proposed.   These criteria will be beneficial to direct estimations via the measurement of 6 degree-of-freedom (DOF) head accelerations from crash dummy or human volunteer subjects.   As the computing times for these predictors are very short, they enable real-time analyses for evaluating the concussive severity in the field study.   However, the differences among these predictors have not yet been investigated.

This study aims to evaluate the characteristics of brain injury predictors based on head motions. In addition, it attempts to propose new injury criteria based on rotational head motion as mild traumatic brain injury (MTBI) predictors.   Toward this end, this chapter investigates the correlations among injury criteria based on head motions and FE-based injury predictors as calculated using a human head/brain FE model.

3.2. Methods

This study proposed two brain injury criteria with angular accelerations based on an investigation and understanding of retrospective researches on brain injury criteria.   The human brain FE model introduced in Chapter 2 was employed to obtain FE-based injury predictors describing the brain responses during head impacts.   Two datasets of head accelerations due to football impacts, including nonconcussive and concussive data, were used for investigating the validity of our two proposed injury criteria and the FE-based injury predictors.   Correlation analyses were conducted to determine the relationships between the proposed injury criteria and the FE-based injury predictors.   In addition, a logistic analysis was used to estimate the 50% probabilities of the proposed injury criteria for MTBI using concussive football impact

data.   Finally, the proposed injury criteria were evaluated with another set of pedestrian head impact data for severe TBI in diffuse axonal injury (DAI).

3.2.1. Head-motion-based brain injury criteria

From an investigation of retrospective researches on brain injury criteria, 9 variables for head-motion-based brain injury criteria were selected in this study.   First, four head motion variables—maximum linear acceleration (MLacc), maximum angular acceleration (MAacc), maximum linear velocity (MLvel), and maximum angular velocity (MAvel)—were employed as basic variables for injury criteria.   All acceleration and velocity variables were defined on a local coordinate system of the head. Second, an additional five injury criteria were defined in this study as described below.

Figure 3.1 shows a comparison of the tolerance curves (black solid curved lines) of both the effective linear acceleration and the angular acceleration with respect to time duration on log-log coordinates. The severity Index (*SI*) proposed by Gadd (1966)[36] was a precursor to the Head Injury Criterion (*HIC*).   *SI* was designed to show strong agreement with the Wayne State University Tolerance Curve (WSUTC: Figure 3.1(a), Patrick et al., 1963[112]); it is given by equation (3.1).

$$SI = \int A^n dt = TA^n \leq 1{,}000 , \quad\cdots\cdots\cdots\cdots\cdots\cdots\cdots\cdots\cdots\cdots\cdots\cdots\cdots\cdots\cdots\cdots \quad \textbf{(3.1)}$$

where A is the effective value of either the linear acceleration, force, or pressure, which is a response function producing the threshold of injury, T is time duration, and n is a weighting factor equal to 2.5.

Ommaya et al. (1967)[109] proposed a tolerance curve for the peak angular acceleration versus time duration using data on concussed and nonconcussed monkeys (Figure 3.1(b)).   It could be observed that the
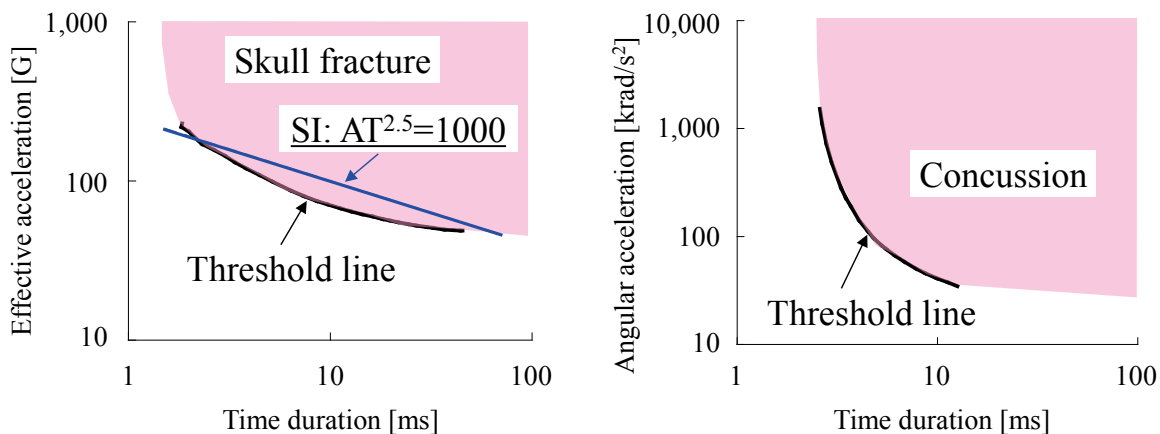
(a) Effective acceleration-time tolerance curve   (b) Angular acceleration-time tolerance curve

Figure 3.1: Comparison of linear and angular accelerations vs. time duration tolerance curves on log–log coordinates.   (a) Effective acceleration-time tolerance curve for forehead impact to a hard, flat surface with a line of *SI* threshold (Patrick et al., 1963[112]; Gadd, 1966[36]).   (b) Tolerance curve for angular acceleration amplitude and time duration using concussed and nonconcussed monkeys (Ommaya et al., 1967).

gradients of the curves are different between the effective acceleration and the angular acceleration. Although the peak angular acceleration from monkey subjects would differ from the effective variable of angular acceleration measured by human subjects, the tolerance curves for both the linear and the angular accelerations have acceleration inversely proportional to the time duration. Therefore, this study postulates that the injury tolerance curve for rotational head motion can be expressed as a function of the angular acceleration with respect to time duration in a manner similar to the WSUTC.

An important feature of *SI* is a downward linear line in the log-log coordinates for the effective acceleration versus time duration (Figure 3.1(a)). Versace (1971)[152] represented the effective acceleration "*A*" by the waveform average as given in equation (3.2). Then *SI* was modified as *HIC*, which is the current injury metric for head injury used in the Federal Motor Vehicle Safety Standards (FMVSS) 208; it is given by equation (3.3).

$$A = \frac{1}{(t_2 - t_1)} \int_{t_1}^{t_2} a(t)dt , \qquad \text{(3.2)}$$

$$HIC = \left[(t_2 - t_1) \left\{ \frac{1}{(t_2 - t_1)} \int_{t_1}^{t_2} a(t)dt \right\}^{2.5} \right]_{max} , \qquad \text{(3.3)}$$

where $a(t)$ is resultant linear acceleration, and t_1 and t_2 represent the initial and final integral times which *HIC* is calculated over (t_1 and t_2 are selected to maximize *HIC*). Determining *HIC* involves a computational solver that seeks the maximum value of *HIC* over a portion of the pulse. The maximum time duration was initially set as 36 ms; however, current standards use 15 ms. Therefore, the variable term for *HIC* is expressed as "HIC_{15}" in this study. HIC_{15} of 700 was estimated to have a 5% risk of Abbreviated Injury Scale (AIS) 4+ head injury (Prasad and Mertz, 1985[123]).

Kleiven (2007)[74] proposed a linear combination of HIC_{36} and the maximum resultant angular velocity as a brain injury predictor. Kleiven's linear combination (*KLC*) is given by equation (3.4).

$$KLC = 0.004718 \cdot \omega_r + 0.000224 \cdot HIC_{36} , \qquad \text{(3.4)}$$

where ω_r is the maximum resultant angular velocity.

When the assumption that a function similar to the WSUTC can express the injury tolerance curve for rotational head motions is permitted, the linear acceleration term of *SI* (equation (3.1)) can be substituted with the angular acceleration to approximate another injury tolerance curve for rotational head motion. In a similar fashion to *HIC*, a new injury criterion called the *RIC* was derived by substituting the resultant angular acceleration of $\alpha(t)$ for the resultant linear acceleration of $a(t)$ in equation (3.3). *RIC* is defined as follows:

$$RIC = \left[(t_2 - t_1) \left\{ \frac{1}{(t_2 - t_1)} \int_{t_1}^{t_2} \alpha(t)dt \right\}^{2.5} \right]_{max} \Bigg/ C_{RIC} , \qquad \text{(3.5)}$$

where C_{RIC} is a constant (=$1.0e^4$). This value designed the threshold of *RIC* as ~1000 to represent 50% probability of brain injury due to football impacts.

On the other hand, Newman et al. (2000b) [107] set the exponent "n" of equation (3.1) to simply 2 and not 2.5 and found that the expression has the physical meaning of the rate of change in kinetic energy or power.   Considering the magnitude of the rate of change in kinetic energy, the Head Injury Power (*HIP*) was proposed as a power expression of the human head to predict head injuries due to both linear and angular accelerations; it is given by the following equation:

$$HIP = \sum_{i=1}^{3} m \cdot a_i \cdot \int a_i dt + \sum_{i=1}^{3} I_{ii} \cdot \alpha_i \cdot \int \alpha_i dt , \quad \cdots\cdots\cdots\cdots\cdots\cdots\cdots\cdots\cdots\cdots \textbf{(3.6)}$$

where m is mass of the head (kg), a_i is the linear acceleration (m/s^2), I_{ii} is the moment of inertia (MOI) (kg·m^2), and α_i is the angular acceleration (rad/s^2) when the head is assumed to be a rigid body. Considering the inertial properties of a mid-sized male, the coefficient of mass is 4.5 kg, and those of the MOI for the x, y, and z directions are 0.016, 0.024, and 0.022 kg·m^2, respectively.   Newman et al. (2000b)[107] also determined the 50% probability of *HIP* for MTBI as 12.8 kW.

As this study focuses on rotational head motion, the rotational components of *HIP*, i.e., *HIP_rot*, was separated from the original *HIP* equation (3.6).   In a manner similar to equation (3.5), this study substituted *HIP_rot* (equation (3.7)) for the resultant linear acceleration of $a(t)$ in equation (3.3) and proposed the *PRHIC* as the following equation:

$$HIP\_rot = \sum_{i=1}^{3} I_{ii} \cdot \alpha_i \cdot \int \alpha_i dt , \quad \cdots\cdots\cdots\cdots\cdots\cdots\cdots\cdots\cdots\cdots \textbf{(3.7)}$$

$$PRHIC = \left[(t_2 - t_1) \left\{ \frac{1}{(t_2 - t_1)} \int_{t_1}^{t_2} HIP\_rot \, dt \right\}^{2.5} \right]_{\max} \Big/ C_{PRHIC} \quad \cdots\cdots\cdots \textbf{(3.8)}$$

where C_{PRHIC} is a constant (=1.0e^3).   This value designed the threshold of *PRHIC* as ~1000 to represent 50% probability of brain injury due to football impacts.

The time durations for angular acceleration obtained from football head impact data were greater than 15 ms of the maximum time duration for *HIC*.   Therefore, the maximum integral time duration for *RIC* and *PRHIC* was set to 36 ms, which was the original time duration of *HIC*.   Therefore, this study proposed two new injury criteria—RIC_{36} and $PRHIC_{36}$.

In summary, in addition to the four head motion variables—MLacc, MAacc, MLvel, and MAvel—five functions—HIC_{15}, *HIP*, *KLC*, RIC_{36}, and $PRHIC_{36}$—were used as injury criteria in this study.

3.2.2. FE-based brain injury predictors

An isolated human brain FE model was used to obtain FE-based brain injury predictors in this study.   Figure 3.2 shows a human brain FE model and the center of gravity (CG) of the head.   The brain FE model was segmented out from the head-neck FE model (see Chapter 2) with a few modifications.

FE-based brain injury predictors with various types of strains were effective to predict brain responses and injury outcomes (Kleiven, 2007[74]).   Therefore, this study also selected 10 FE-based brain injury predictors with various types of strains obtained from whole brain elements, which included the maximum principal strain (MPS), maximum shear strain (MSS), maximum strain rate (MSR), maximum
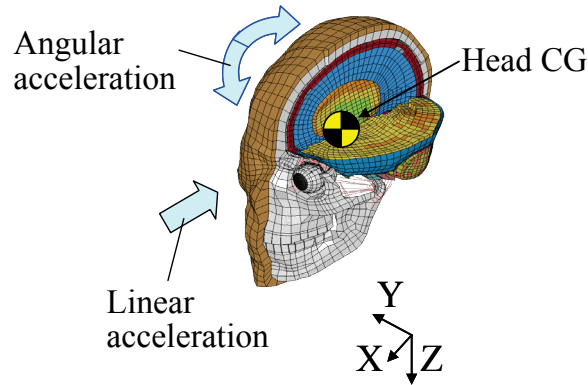
Figure 3.2: Human brain FE model and location of CG

product of strain and strain rate (MPSS), and Cumulative Strain Damage Measure (CSDMs; see Section 2.2.4). In particular, Viano and Lövsund (1999)[156] considered MPSS a "Hotspot" as they believed that it would be best predictor for TBI of the human brain. The CSDMs used in this study included CSDM 10%, 15%, 20%, 25%, 30%, and 35%, with six grades of strain thresholds to distinguish the severity of damage in DAI.

This study used the human brain FE model to predict brain injuries without any skull fractures. Therefore, the skull was modeled as a rigid body, and linear and angular accelerations measured in experimental studies were directly inputted as boundary conditions of the head through the skull. All simulations were conducted using a commercially available FE solver, LS-DYNA 971 Rev. 2, Shared Memory Parallel (SMP) version (LSTC, Livermore, CA), on a single-core Intel Xeon 64-bit-based computer running Linux operating system.

3.2.3. Head acceleration data

The head acceleration data utilized in this study represent 6DOF skull accelerations measured at the head CG. Two datasets with football head acceleration data were used: one contained nonconcussive head acceleration data (Rowson et al., 2009[126] and 2011[127]) collected directly from living human subjects (referred to as 6DOF device data) and the other contained concussive head acceleration data from National Football League (NFL) head impacts reconstructed using Hybrid III dummies (Newman et al., 2000a[106]). Both the 6DOF device data and the NFL data were used for correlation analyses between the proposed head injury criteria and the abovementioned FE-based brain injury predictors.

6DOF measurement devices were installed in the helmets of Virginia Tech football players throughout the 2007 and 2008 college football seasons. All instrumented players were either offensive or defensive linemen. Each player that participated in the study gave written informed consent with Institutional Review Board (IRB) approval from both Virginia Tech and the Edward Via College of Osteopathic Medicine. The linear and angular accelerations were recorded for every impact that the instrumented players experienced during games and practices. A total of 4,709 impacts were recorded during practices and games for the 19 instrumented players. No instrumented player sustained MTBI in this study. To investigate the relationships of linear and angular head accelerations at more severe levels, this

study selected 251 cases that had great linear acceleration, angular acceleration, linear velocity, or angular velocity from the 6DOF device dataset.

In total, 31 impact events that involved 58 players and included 25 concussions from NFL data were reconstructed using Hybrid III dummies based on game video (Pellman et al., 2003[116]).   As NFL data contain both concussive and nonconcussive head impacts, a logistic regression analysis was conducted for only NFL data to obtain the injury risk curves of the proposed injury criteria predicting MTBI.

In addition, a set of pedestrian head acceleration data obtained from Dokko et al. (2003)[23] was used to evaluate the proposed head injury criteria and the thresholds obtained from the injury risk curves. Two car-to-pedestrian accidents with severe head impacts were reconstructed using a multibody model and a pedestrian FE model to obtain 6DOF head acceleration data.   One case (case No. H032-86) includes DAI and subarachnoid hemorrhages, and another (case No. H070-85) includes DAI, subdural hematoma, and contusion.   We could not find any descriptions on the occurrences of skull fractures for both accident cases in the literature (Dokko et al., 2003[23]).

3.2.4. Statistical analyses and application of brain injury predictors

Correlation analyses were performed between 9 variables of head-motion-based brain injury criteria and 10 variables of FE-based brain injury predictors to investigate the relationship between the proposed injury criteria with angular accelerations and the FE-based brain injury predictors, especially CSDM.

In addition, logistic regression analyses were performed to determine the predictive capabilities of the head-motion-based brain injury criteria and FE-based brain injury predictors.   The Modified Maximum Likelihood Method (MMLM) proposed by Nakahira et al. (2000)[100], one of the methods used for logistic regression analyses, was adopted using MS Excel to determine the primary injury predictors.   The goodness of curve fit predicted by MMLM was evaluated using the Combined Evaluation Method (CEM).   Both methods are based on two assumptions of injury probabilities: (A) "the injury probability approaches zero when injury factors approach zero" and (B) "obtained injury risk curves possess the maximum goodness of fit."   The CEM method is used to evaluate these two assumptions.   The estimator for assumption B (EB) is defined as equal to the log likelihood.   Greater EB indicates better goodness of curve fit.   As this method has been used as an effective method in previous studies (Willinger and Baumgartner, 2003[162]), this study presumes the injury risk probability as logistic curves determined by the MMLM method.   As a result, the injury thresholds for 50% probability of proposed brain injury criteria for MTBI were obtained.

In addition, the 9 head-motion-based brain injury criteria were also calculated using 6DOF head accelerations reconstructed from two sets of car-to-pedestrian accident data with severe head impacts (Dokko et al., 2003[23]), and the validity of the proposed brain injury criteria was investigated.

3.3.   Results

3.3.1.   Correlation analyses between FE-based and head-motion-based brain injury criteria

First, the correlations between four head-motion-based injury criteria and five head motion variables were investigated using the NFL data and 6DOF device data.   The values of the correlation coefficients are summarized in Table 3.1, where results obtained from the NFL and 6DOF device databases are indicated in the upper and lower parts in each column, respectively.   Correlation coefficients greater than 0.89, which are equivalent to a coefficient of determination of 0.80, are indicated by a bold underline. Significant correlations ($R \geq 0.90$) of HIC_{15} and HIP with MLacc were observed in both the 6DOF device and the NFL databases.   Although HIP was a linear combination of the translational and rotational head kinetic power, HIC_{15} and HIP were somewhat correlated with the MAacc in the NFL dataset ($0.63 < R < 0.75$), whereas the correlations of these two criteria with MAacc in the 6DOF device dataset were not significant ($p > 0.05$). KLC, another linear combination of translational and rotational head kinematics, was significantly correlated with MAvel in the NFL dataset ($R = 0.91$), whereas the correlation coefficients with MLacc and MLvel were very minor in the 6DOF device dataset ($-0.13 < R < -0.11$, $p > 0.05$).   On the other hand, the injury criteria of RIC_{36} had strong correlations ($R > 0.80$) with MAacc in both datasets. $PRHIC_{36}$ somewhat correlated with MAacc and MAvel ($0.47 < R < 0.77$), whereas the correlation coefficients of $PRHIC_{36}$ with MLacc or MLvel were the smallest among all the injury criteria ($R < 0.09$).

Table 3.1:   Coefficients of correlation between head-motion-based brain injury criteria and head-motion-based NFL (upper) and 6DOF device data (lower)

Injury criteria	[†1] MLacc	[†2] MLvel	[†3] MAacc	[†4] MAvel
HIC_{15}	**<u>0.93**</u>	0.889**	0.60**	0.38*
	<u>0.93</u>	0.68**	-0.04	-0.27**
HIP	**<u>0.89**</u>	**<u>0.93**</u>	0.72**	0.58**
	<u>0.92</u>	0.72**	0.08	-0.15*
[†5] KLC	0.70**	0.82**	0.78**	**<u>0.91**</u>
	-0.13	-0.11	0.61**	0.71**
RIC_{36}	0.50**	0.66**	0.81**	0.86**
	-0.03	-0.09	**<u>0.90**</u>	0.63**
$PRHIC_{36}$	0.08	0.31	0.49**	0.77**
	-0.04	-0.02	0.59**	0.56**

*: $p<0.01$, **: $p<0.001$

[†1] *MLacc*: Maximum linear acceleration,   [†2] *MLvel*: Maximum linear velocity,

[†3] *MAacc*: Maximum angular acceleration,   [†4] *MAvel*: Maximum angular velocity,

[†5] *KLC*: A linear combination of *HIC* and maximum angular velocity proposed by Kleiven (2007)[74],

Second, the correlations between 10 FE-based predictors and 9 head-motion-based brain injury criteria are summarized in Table 3.2 using the NFL data and 6DOF device data. MLacc, MLvel, *HIC*, and *HIP* showed weak correlations with FE-based brain injury predictors. MAacc, MAvel, and *KLC* showed moderate correlation with the MPS, MSS, and MPSS in both datasets (R > 0.62). On the other hand, the two proposed injury criteria—RIC_{36} and $PRHIC_{36}$—showed strong correlations with FE-based injury predictors. RIC_{36} correlated significantly with MPS, MSS, MPSS, and CSDM 10%, whereas $PRHIC_{36}$ was only correlated with the CSDMs with strain thresholds greater than 20%. As the brain elements were represented by a nearly incompressible solid material, MPS and MSS were notably correlated with each other. In particular, significant correlations in both the NFL data and the 6DOF device data were found between RIC_{36} and CSDM 10% (R ≥ 0.92) and between $PRHIC_{36}$ and CSDM 30% (R ≥ 0.90). Figure 3.3 shows their plots and estimated regression lines. The estimated regression lines for the NFL data and 6DOF device data were qualitatively matched together in correlation between RIC_{36} and CSDM 10% in Figure 3.3 (a). However, the regression lines for the relationship between $PRHIC_{36}$ and CSDM 30% (Figure 3.3 (b)) were not matched between the NFL data and 6DOF device data owing to biased data plots. This is probably because few severe impact data points were included in the NFL and 6DOF device data.

Table 3.2: **Coefficients of correlation between FE-based and head-motion-based injury predictors based on NFL (upper) and 6DOF device data (lower)**

FE-based injury predictors	MLacc	MLvel	HIC_{15}	HIP	KLC	MAacc	MAvel	RIC_{36}	$PRHIC_{36}$
[†1] MPS	0.49**	0.67**	0.51**	0.72**	0.87**	0.76**	0.87**	**0.93****	0.76**
	-0.09	-0.03	-0.06	0.06	0.82**	0.69**	0.79**	0.68**	0.55**
[†2] MSS	0.47**	0.65**	0.48**	0.69**	0.86**	0.76**	0.87**	**0.92****	0.76**
	-0.09	-0.04	-0.06	0.06	0.82**	0.70**	0.79**	0.70**	0.57**
[†3] MSR	0.08	0.03	0.07	0.02	0.01	0.06	-0.03	0.05	-0.07
	-0.08	-0.10	-0.11	-0.09	0.59**	0.10	0.15	0.08	0.10
[†4] MPSS	0.55**	0.62**	0.50**	0.69**	0.80**	0.85**	0.78**	0.88**	0.76**
	0.07	0.01	0.09	0.23**	0.64**	0.83**	0.62**	**0.89****	0.70**
[†5] CSDM 10%	0.36*	0.52**	0.36*	0.58**	0.75**	0.69**	0.80**	**0.94****	0.68**
	-0.08	-0.11	-0.08	0.08	0.48**	0.75**	0.59**	**0.92****	0.84**
[†5] CSDM 15%	0.19	0.33	0.20	0.41*	0.66**	0.50**	0.77**	0.79**	0.85**
	-0.01	-0.03	-0.03	0.12	0.39**	0.57**	0.46**	0.79**	0.889**
[†5] CSDM 20%	0.13	0.24	0.14	0.32	0.59**	0.42*	0.72**	0.66**	0.83**
	0.03	0.01	0.00	0.15	0.35**	0.49**	0.42**	0.72**	**0.92****
[†5] CSDM 25%	0.13	0.23	0.12	0.30	0.60**	0.44**	0.73**	0.65**	0.85**
	0.07	0.07	0.05	0.19*	0.34**	0.49**	0.40**	0.72**	**0.91****
[†5] CSDM 30%	0.16	0.33	0.17	0.39*	0.66**	0.51**	0.78**	0.76**	**0.94****
	0.07	0.06	0.05	0.18*	0.29**	0.42**	0.35**	0.64**	**0.90****
[†5] CSDM 35%	0.09	0.26	0.09	0.33	0.59**	0.48**	0.75**	0.70**	**0.95****
	0.07	0.07	0.05	0.17*	0.26**	0.40**	0.33**	0.61**	0.85**

*: $p<0.01$, **: $p<0.001$

[†1] MPS: Maximum principal strain,　[†2] MSS: Maximum shear strain,　[†3] MSR: Maximum strain rate,

[†4] MPSS: Maximum product of strain and strain rate,　[†5] CSDM: Cumulative Strain Damage Measure.

Additional correlation analysis on RIC_{36} and $PRHIC_{36}$ with exponent values of 1.0, 2.0, and 3.0 was conducted to investigate the physical dimension of the original RIC_{36} and $PRHIC_{36}$. Table 3.3 shows the correlation coefficients between the injury criteria RIC_{36} and $PRHIC_{36}$ with changed exponent values and six variables that correlated well with these criteria, namely, MAacc, MAvel, MPS, MPSS, CSDM 10%, and CSDM 30%. RIC with exponent values of 1.0 and 2.0 would be related with the physical dimensions of angular velocity and rotational power of head motion, respectively. MAacc was strongly correlated with $RIC_{36}^{2.0}$ and $RIC_{36}^{2.5}$ (R > 0.90) in the 6DOF device dataset, whereas MAvel was correlated with $PRHIC_{36}^{1.0}$ in both the NFL and the 6DOF device datasets (R > 0.93). Although $RIC_{36}^{1.0}$ appeared to have an angular-velocity-related dimension, the correlation coefficients between $RIC_{36}^{1.0}$ and MAvel were not so great in both datasets (R < 0.89). However, RIC_{36} and $PRHIC_{36}$ with exponent values equal to or greater than 2.5

(a) RIC_{36} vs. CSDM 10%   (b) $PRHIC_{36}$ vs. CSDM 30%
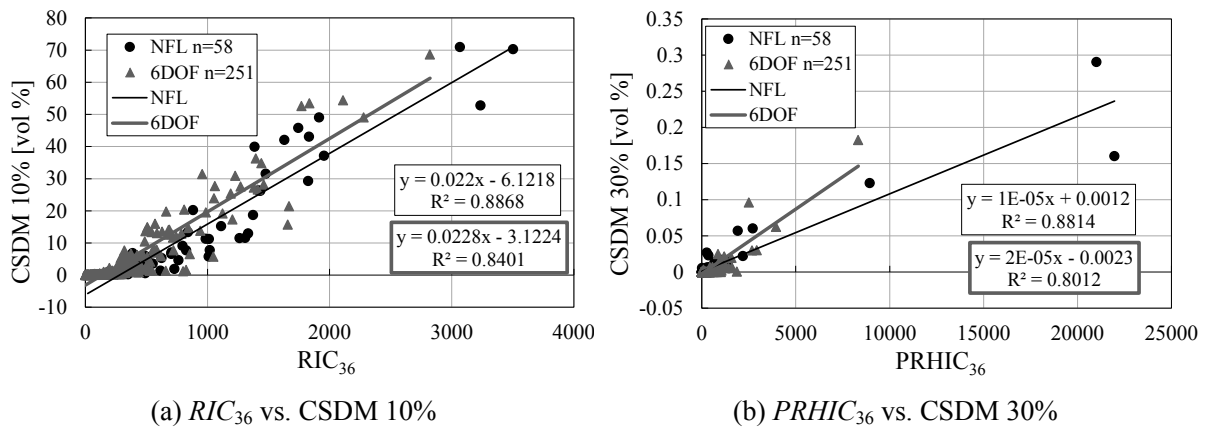
Figure 3.3: Correlations of CSDMs against RIC_{36} and $PRHIC_{36}$

Table 3.3:   Coefficients of correlation for RIC_{36} and $PRHIC_{36}$ with different exponents based on NFL (upper) and 6DOF device data (lower)

	MAacc	MAvel	MPS	MPSS	CSDM 10%	CSDM 30%
$RIC_{36}^{1.0}$	0.75**	0.81**	0.84**	0.71**	0.83**	0.53**
	0.77**	0.80**	0.76**	0.71**	0.66**	0.37**
$RIC_{36}^{2.0}$	0.76**	0.83**	**0.90****	0.80**	**0.91****	0.67**
	0.90**	0.70**	0.73**	0.87**	0.87**	0.55**
$RIC_{36}^{2.5}$	0.81**	0.86**	**0.93****	0.88**	**0.94****	0.76**
	0.90**	0.63**	0.68**	**0.89****	**0.92****	0.64**
$RIC_{36}^{3.0}$	0.83**	0.86**	**0.92****	**0.93****	0.92**	0.82**
	0.87**	0.58**	0.65**	0.885**	**0.92****	0.71**
$PRHIC_{36}^{1.0}$	0.61**	**0.93****	0.83**	0.79**	0.78**	**0.94****
	0.55**	**0.95****	0.74**	0.60**	0.62**	0.43**
$PRHIC_{36}^{2.0}$	0.54**	0.83**	0.80**	0.79**	0.74**	**0.96****
	0.65**	0.68**	0.64**	0.75**	0.87**	0.81**
$PRHIC_{36}^{2.5}$	0.49**	0.77**	0.76**	0.76**	0.68**	**0.94****
	0.59**	0.56**	0.55**	0.70**	0.84**	**0.90****
$PRHIC_{36}^{3.0}$	0.45**	0.73**	0.72**	0.73**	0.63**	**0.91****
	0.53**	0.47**	0.47**	0.63**	0.78**	**0.93****

*: $p<0.01$, **: $p<0.001$

† MPSS: Maximum product of strain and strain rate, †† CSDM: Cumulative Strain Damage Measure

showed more significant correlations with CSDM 10% and CSDM 30% in both datasets (R > 0.89), respectively.

3.3.2. Logistic regression analyses and injury risk probabilities

Table 3.4 shows a summary of the MMLM evaluation value of EB as determined by the CEM and ranks the FE-based brain injury predictors and head-motion-based brain injury criteria by EB scores. As most of football impact data used in this study was mild impact data, the obtained EB scores indicate the possibility for predicting MTBI. The best FE-based injury predictor for MTBI was MPSS, followed by MPS, MSS, CSDM 10%, and CSDM 30%. With regard to the head-motion-based injury criteria, the EB values of RIC_{36} and $PRHIC_{36}$ were equivalent to those of FE-based injury predictors. Figure 3.4 shows logistic regression injury risk curves for RIC_{36} and $PRHIC_{36}$. Based on concussive NFL head impact data, an RIC_{36} of 1030 and $PRHIC_{36}$ of 870 represent 50% probabilities of sustaining MTBI. In addition, the 50% probabilities of MTBI as predicted by the brain model were determined as CSDM 10% of 18.2 vol%, CSDM 20% of 0.26 vol%, and CSDM 30% of 0.008 vol%.

Table 3.4: **Results of logistic regression analyses of MMLM's evaluation value (EB) determined by CEM, and 50% probability of each factor for NFL data (N = 58)**

	Injury predictor	Unit	MMLM	
			CEM (EB)	50% probability
FE-based	MPSS	s^{-1}	-0.491	10.5
	MPS	%	-0.506	31.8
	MSS	%	-0.510	31.6
	CSDM 10%	Vol %	-1.289	18.2
	CSDM 30%	Vol %	-1.472	0.008
Head motion based	RIC_{36}	-	-0.772	1030
	$PRHIC_{36}$	-	-1.521	870

(a) RIC_{36} vs. CSDM 10%   (b) $PRHIC_{36}$ vs. CSDM 30%
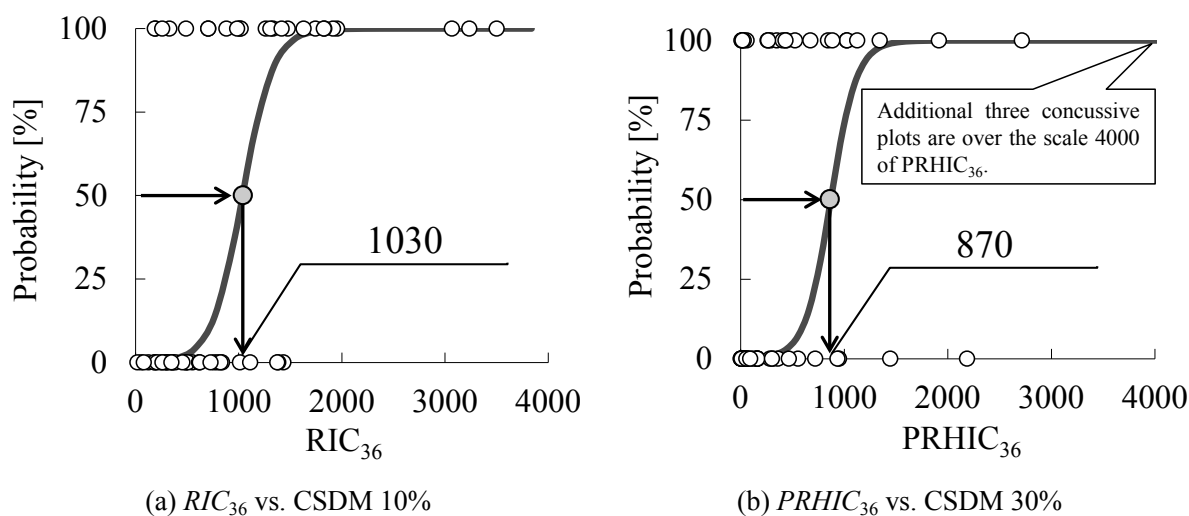
Figure 3.4: Injury risk probabilities for rotational head-motion-based injury criteria as determined by MMLM

3.3.3. Application to pedestrian head impacts with severe TBI

The injury probabilities for TBI have thus far been determined by the MAacc or angular velocity (Ommaya and Hirsch, 1971[110]; Lowenhielm, 1974[85]; Ewing et al., 1975[29]; Margulies and Thibault, 1992[88]). Figure 3.5 shows data plots of 6DOF sensors with the thresholds for DAI on a graph of angular acceleration versus angular velocity. Case No. H070-85 was already over the thresholds obtained from literature. On the other hand, Case No. H032-86 could be judged as injured based on the thresholds of Lowehielm (1974)[85] and Ewing et al. (1975)[29]; however, this same case was determined as noninjured based on the thresholds of Ommaya and Hirsch (1971)[110] and Margulies and Thibault (1992)[88].

Table 3.5 summarizes the results of 9 head-motion-based brain injury criteria for reconstructed pedestrian head impacts. The injury thresholds of HIC_{15}, HIP, RIC_{36}, and $PRHIC_{36}$ are also listed in this table. Case No. H032-86 did not exceed the injury threshold of HIC_{15}, whereas the HIP of 157 kW, RIC_{36} of 1200, and $PRHIC_{36}$ of 1490 were over the thresholds of 50% probabilities for MTBI. On the other hand, in Case No. H070-85, all injury criteria exceeded their thresholds for MTBI.
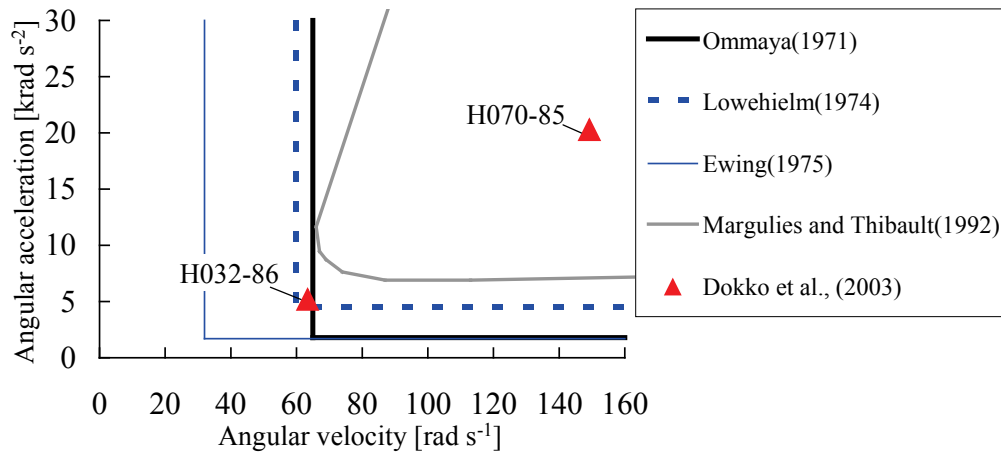
Figure 3.5: Angular acceleration vs. angular velocity of 6DOF sensor data with threshold lines obtained from literatures

Table 3.5: Variables of injury criteria using reconstructed pedestrian head impact data (N = 2) with injury thresholds

FE outputs	MLacc (m s^{-2})	MLvel (m s^{-1})	HIC_{15} (-)	HIP (kW)	MAacc (rad s^{-2})	MAvel (rad s^{-1})	RIC_{36} (-)	$PRHIC_{36}$ (-)
Thresholds	-	-	*700*	*12.8*	-	-	*1030*	*870*
H032-86	1839.3	30.9	396	157	5193.0	63.4	1200	1490
H070-85	3977.2	50.0	18806	581	20272.7	149.2	38300	344000

3.4. Discussion

3.4.1. Rotational head motion data

The characteristics of head motions between 6DOF device data and NFL data were different in the correlation between the linear and the angular accelerations.   The 6DOF data showed little correlation (R^2 = 0.25) between the linear and the angular accelerations (Rowson et al., 2009[126]), whereas the NFL data showed a more significant linear relationship between the linear and the angular accelerations (R^2 = 0.58) (Pellman et al., 2003[116]).   Rowson et al. (2009)[126] suggested a difference between the NFL data and the 6DOF device data.   They assumed that the correlation between the linear and the angular accelerations in NFL data would be due to the biased population structure toward concussive impacts.   In addition, the difference of neck stiffness between human subjects and Hybrid III dummy could be another likelihood to change the characteristics of head kinematics.   As 6DOF devices measure the head kinematics of the human subjects directly, 6DOF device data are more reasonable and reliable for determining a new injury criterion for the brain.

3.4.2. FE-based injury predictors

When the first principal strain (FPS) of each element in a brain FE model is considered an extension of an axonal filament, the classification of axonal injuries defined by Maxwell et al. (1997)[90] could be applied to the strain thresholds of CSDMs.   Axonal injuries can be categorized by two severities: primary axotomy and secondary axotomy.   Primary axotomy indicates severe damage of an axon filament associated with strain of more than 20%.   Secondary axotomy includes several stages, where the focal loss of axonal transport is associated with 5%–10% strain; axonal swelling, with 10%–15% strain; and axonal bulbs, with 15%–20% strain.   Some researchers showed that strains at the brain tissue level had a linear correlation with strains at the axonal level based on an experimental mechanical investigation using animal brain tissues (Tamura et al., 2007[146]).   Therefore, we hypothesized that CSDMs with lower strain thresholds such as 10%, 15%, and 20% could be related with mild TBI and those with higher strain thresholds such as 25%, 30%, and 35%, with severe TBI, in an effort to determine the most appropriate strain threshold for TBI.

The selection of brain FE models would affect the relations between the head accelerations inputted to the models and the brain responses predicted by the models.   The logistic regression analysis performed in this study estimated MPSS as the best FE-based injury predictor for MTBI.   This result agreed with those obtained by King et al. (2003)[71], who suggested MPSS in the midbrain region as the best predictor for concussion using their brain FE model with linear viscoelastic brain elements.   On the contrary, Willinger and Baumgartner (2003)[162] suggested the von Mises stress in the whole stress as the best predictor of concussion using a brain FE model with a linear viscoelastic material including cerebrospinal fluid (CSF) using the Arbitrary Lagrangian-Eulerian (ALE) method.   Kleiven (2007)[74] showed the relations between the local tissue brain responses of pressure, strain, product of strain and strain rate, as well as CSDM and the injuries using their brain FE models by considering a variant material definition of hyperelastic and linear viscoelastic.   Even though these studies analyzed the same data from the NFL reconstructions used in this

study, the different FE models suggested different FE-based injury predictors. This is probably because the differences in the selected material properties, mesh geometry, validation quality against experimental data, and utilized FE codes would affect not only the predicted brain response but also the resulting injury predictors and conclusions. Therefore, further investigations on how brain responses and damage mechanisms should be simulated by using FE models are necessary to determine which head kinematic variables increase the magnitude of strain or stress in the whole brain.

As four injury predictors—MPS, MSS, MSR, and MPSS—among the 10 injury predictors indicate the maximum values in whole brain elements, they could be significantly affected by the mesh size of the brain FE model. On the other hand, the CSDM with lower strain thresholds tends to present axonal damage spreading throughout the brain and brainstem. CSDM 10% for 50% probability of MTBI in football head impacts was 18.2 vol% damage of the whole brain. On the other hand, CSDM with higher strain thresholds tends to predict damaged elements with a much smaller area of the midbrain region. CSDM 30% for 50% probability of MTBI was only 0.008 vol% damage of the whole brain. According to our hypothesis described previously, CSDM 30% could be related with severe TBI. As the volume percentage of each brain element ranges from 0.0004 to 0.027 vol% with an average value of 0.0066 ± 0.0045 vol%, 0.008 vol% of the brain may correspond to a volume percentage of 1–2 solid elements in the brain model. Therefore, the MPS of 30% would also be considered one of the injury thresholds for severe brain injury. However, as the injury risk curves predicted in this study were based on concussive football head impacts, all predicted injury thresholds indicate 50% probabilities of MTBI. Therefore, the predicted threshold for CSDM 30% might not be appropriate for severe TBI. This is also the reason why the goodness of logistic curve fit for the MTBI predictor of CSDM 10% was better than that for the severe TBI predictor of CSDM 30%. Although further investigations and a comparison with 6DOF head acceleration data including severe head impacts and clinical observations are still needed to determine which FE-based injury predictors can precisely represent the injury mechanisms of concussion and DAI, CSDMs representing a volume percentage of damaged elements in whole brain elements could be better injury predictors for TBI.

3.4.3. Investigation of physical meanings of *RIC* and *PRHIC*

Gadd (1966)[36] stated that injury is some function of both the intensity of the loading and its time duration. However, it is difficult to express the physical meanings of the *SI* variable owing to the unnatural physical dimension. Therefore, Newman et al. (2000b)[107] substituted the exponent of 2.5 in equation (3.1) with 2.0 to obtain the physical meaning of the rate of change in kinetic power. A similar investigation conducted in the current study (Table 3.3) did not show significant correlations between MAvel and $RIC_{36}^{1.0}$, which might be related to the physical dimension of the angular velocity. This would be because the limited time duration of $RIC_{36}^{1.0}$ of up to 36 ms could not represent MAvel calculated from the whole accumulation of the integrated angular acceleration. On the other hand, $PRHIC_{36}^{1.0}$ was significantly correlated with MAvel. Although $PRHIC_{36}^{1.0}$ was related to the physical dimension of the kinetic energy, owing to the limited time duration for time integration of up to 36 ms, the magnitude of $PRHIC_{36}^{1.0}$ would be affected by kinetic power rather than energy. Therefore, $PRHIC_{36}^{1.0}$ might correlate with MAvel, which constitutes a

part of the rotational kinetic power.   However, either $RIC_{36}^{1.0}$ or $PRHIC_{36}^{1.0}$ did not correlate with any injury predictors predicted by the Total HUman Model for Safety (THUMS) brain model.   The current study indicates that RIC_{36} and $PRHIC_{36}$ with exponents greater than 2.0 had a significant correlation with FE-based injury predictors.   As $PRHIC_{36}$ with exponents greater than 2.0 corresponds to an uncommon physical dimension, further cautious verifications of the correlations and physical meanings of the original $RIC_{36}^{2.5}$ and $PRHIC_{36}^{2.5}$ are necessary.

3.4.4. Injury criteria for rotational head kinematics

In previous studies, Kleiven (2007)[74] and Newman (2000)[107] proposed KLC and HIP, which were linear combinations of translational and rotational head kinematic variables using the NFL dataset, respectively.   KLC and HIP represented different relationships, as shown in Table 3.1 and Table 3.2, owing to the difference in the weighting factors used for translational and rotational head kinematic variables.   However, the FE analysis showed that the translational kinematics may contribute insignificantly to the strains in the brain (Table 3.2).   This finding agreed with the FE analysis conducted by Kleiven (2007)[74].   When brain injury was determined by intracranial strains, injury criteria based on pure rotational head kinematics would be better than those including linear head kinematic variables for predicting TBI.

Based on the hypothesis of brain injury severity with axonal stretch as mentioned above, CSDMs with a greater strain threshold of 30% may predict severe TBI, whereas CSDM 10% may predict milder brain injuries such as concussion due to football head impacts.   Correlation analyses between FE-based brain injury predictors and head-motion-based injury criteria revealed that RIC_{36} was significantly correlated with CSDM 10% (R > 0.92), whereas $PRHIC_{36}$ was strongly correlated with CSDM 30% (R > 0.90).   Although MAvel showed strong correlations with the MPS (R > 0.79) or CSDM 10% (R > 0.59), the correlation coefficients of RIC were greater than those of MAvel when the THUMS brain FE model was used to predict the brain responses.   Therefore, this study recommends RIC_{36} and $PRHIC_{36}$ as different injury predictors for mild and severe TBI, respectively.

On the contrary, Takhounts et al. (2008)[143] reported that MAvel was correlated with CSDM 25% predicted by their SIMon brain FE model (Simulated Injury Monitor; Takhounts et al. (2003)[142]) in their linear regression analyses using the same 6DOF device data used in this study.   Then, they proposed another brain injury criterion based on head rotational kinematics called BRIC (Brain Injury Criterion: Takhounts et al., 2011[144]).   BRIC is calculated from the summation of the normalized MAacc and normalized MAvel. In terms of representation of different injury severities of TBI, Takhounts et al. (2011)[144] adopted a method of severity ratios that scales injury severities up or down from the injury severity of AIS 4+, whereas the current study prepared two different criteria—RIC_{36} and $PRHIC_{36}$.   Further investigation with additional head motion data including TBI cases are necessary to evaluate the predictive capabilities of head-motion-based injury criteria.

3.4.5. Applicability to car-to-pedestrian head impacts

Two case data of pedestrian head impacts obtained from Dokko et al. (2003)[23] were used to investigate the applicability of the proposed injury criteria to automotive head impacts with severe TBI.   The pedestrian FE model used was validated against three cases of Post Mortem Human Subject (PMHS) whole body pedestrian impact tests.   The body kinematics and trajectories of the whole body were duplicated, and contact points on the vehicular body showed good agreement with actual cases (Dokko et al., 2003[23]). Although the reconstruction of the pedestrian impact and estimation of the rotational head motion of the pedestrian are difficult owing to many uncertain physical conditions and lack of evidence, the simulation-based reconstruction of pedestrian head impacts is one of the best methods available currently. Therefore, the predicted 6DOF head motions are considered acceptable for further analysis to predict brain injuries.

Case No. H070-85 of pedestrian head impact (Table 3.5) had an extremely high *HIC* value, and therefore, severe head injury could be expected without any rotational injury criteria.   On the other hand, Case No. H032-86 had an *HIC* value lower than the threshold of 700.   If the head injury in this case was assessed using only *HIC*, brain injuries could be ignored.   Some injury threshold based on angular acceleration and velocity could not judge this case as injured (Figure 3.5).   However, RIC_{36} and $PRHIC_{36}$ exceeded the proposed injury thresholds for concussion in this case.   Although *HIP*, another injury criterion, exceeded the threshold for MTBI, the correlation analysis in this study did not show a high correlation coefficient between *HIP* and FE-based brain injury predictors.

Therefore, we propose to use HIC_{15}, RIC_{36}, and $PRHIC_{36}$ to investigate various head injuries. However, the proposed injury threshold with $PRHIC_{36}$ of 870 has a limitation in that the threshold was derived from mild and not severe TBI data.   Further studies are needed to better understand the head and brain injury mechanisms by investigating the relationships between skull fractures and brain injuries.   This may help produce more reliable head injury prediction tools for occupants and pedestrians in automotive accidents and players in football impacts.

3.5. Conclusions

This study analyzed nonconcussive and concussive football head impacts using a well-validated human brain FE model.   According to correlation analyses with brain strain variables, we found two new brain injury criteria based on the rotational head motion—*RIC* and *PRHIC*.   The following four specific conclusions can be drawn for the *RIC* and *PRHIC*.

1. RIC_{36} showed a significant correlation with CSDM 10% (R > 0.92), whereas $PRHIC_{36}$ was strongly correlated with CSDM 30% (R > 0.90).

2.   Based on a hypothesis of brain injury severity with axonal stretch, CSDMs with a greater strain threshold of 30% may predict severe TBI, whereas CSDM 10% may predict milder brain injuries such as concussion due to football head impacts.

3.   The current study determined thresholds for 50% probabilities of sustaining MTBI as RIC_{36} of 1030 and $PRHIC_{36}$ of 870 based on concussive NFL head impact data.   However, as $PRHIC_{36}$ could be considered the injury predictor for severe TBI, its injury threshold should be verified using further case data of severe TBI head impacts.

4.   All criteria—HIC_{15}, RIC_{36}, and $PRHIC_{36}$—are necessary for various head injury analyses as injury criteria based on translational and rotational head kinetics would predict different head injuries of skull fracture, brain contusion, and mild or severe TBI.

Chapter 4   Retrospective Review of Chest Impacts

Some of the results taken from this section have been published in the 2003 IRCOBI conference, Lisbon (Portugal) (Kimpara, et al., 2003[A1]) and presented at the 5th Combined Meeting of the Orthopaedic Research Societies of Canada, USA, Japan, and Europe, which was held in Banff, Canada, in October 2004 (Kimpara, et al., 2004[B1]).

4.1. Introduction

During impact, the rib cage provides crucial protection to vital internal organs.   Because of this function, many static tests have been conducted on human ribs to determine their mechanical properties such as force, deflection, Young's modulus, and fracture tolerance (Granik and Stein, 1973[40]; Got et al., 1975[39]; Cesari et al., 1981[15]; Begeman et al., 1990[7]).   This chapter aims to determine the chest impact responses and injury thresholds due to age and gender differences based on a retrospective review of published data.

Dynamic investigations have suggested that blunt impacts or pendulum-type tests are a better assessment of chest stiffness than sled tests.   This is because blunt impacts against a stationary subject do not need to account for the inertial effect.   Therefore, this study utilized male and female cadaveric subject data obtained from blunt chest impact tests (Nahum et al., 1970[98]; Kroell et al., 1971[76]; Stalnaker et al., 1973[137]; Kroell et al., 1974[77]; Cesari et al., 1981[15]; Viano, 1989[154]; Talantikite et al., 1998[141]; and Chung et al., 1999[17]) to evaluate the chest's biomechanical properties due to gender differences.

In addition, another series of rib bending tests was conducted with three different loading speeds. This test aimed to determine the rib's mechanical properties under high-speed loading conditions and rate dependencies in bending responses.

The results derived from this study can be useful in the development of new anthropomorphic test devices (ATDs) and mathematical models for small-sized females.

4.2. Methods
4.2.1. Retrospective study of blunt impact

Frontal pendulum impact data were taken from Post Mortem Human Subject (PMHS) tests conducted by Nahum et al. (1970)[98], Kroell et al. (1971)[76], Stalnaker et al. (1973)[137] and Kroell et al. (1974)[77] (Table 4.1).   All tests used pneumatic impactors with a diameter of 150 mm and were centered at approximately the mid-sternum level.   However, the mass of the impactor ranged from 1.6 to 23.6 kg and the impact velocities, from 4.0 to 14.5 m/s.   The backs of the subjects were unsupported in all tests, except for six subjects that were tested by Kroell et al. (1974)[77].   These were tested in the fixed-back

configuration.   Owing to the incomplete test results reported for subject Nos. 11FF and 63FM (Kroell et al. 1971[76] and 1974[77]), only 51 cases (40 males, 11 females) were available for frontal impact data analysis.

The datasets available for lateral pendulum impact analysis were much smaller.   A literature survey found data for only 26 males and 6 females (Cesari et al., 1981[15]; Viano, 1989[154]; Talantikite et al., 1998[141]; Chung et al., 1999[17]: Table 4.2).   In these studies, Viano (1989)[154] used a pneumatically driven pendulum impactor whereas the others used simple pneumatic impactors.   The impactors used in all tests were aligned at the level of the xiphoid process.   The mass of the impactor used by Cesari et al. (1981)[15] and Viano (1989)[154] was 23.4 kg compared to either 12 or 16 kg used by Talantikite et al. (1998)[141] and 50 kg used by Chung et al. (1999)[17].   Although six subjects were tested in the study reported by Chung et al. (1999)[17], two were tested with padding and were thus excluded from this study.   Chung et al. (1999)[17] measured the chest deflection from the lateral side of the 6th rib using a 40-channel chestband, whereas Viano (1989)[154] and Talantikite et al. (1998)[141] measured deflection based on film analysis.   Occasionally, chest deflection and force data were not tabulated in the original report and required digitization from the chest force-deflection curves or time histories to extract the needed information.   Moreover, Cesari et al. (1981)[15] did not report cadaveric response data such as the chest deflection and chest force.   Lastly, information on the subject height, chest force, viscous tolerance, chest stiffness, number of rib fractures, or chest injury was occasionally missing from these studies.   Hence, the data quality and quantity available for lateral impact analysis were worse than those used in frontal impact.

Data were analyzed for the following variables: test conditions, subject information, chest impact response, and resulting chest injury.   The variables of test conditions include the impactor mass, impact velocity, energy, and momentum.   Subject information includes the height, weight, gender, age, and chest depth and width of the test subjects.   The parameters of chest impact response include the maximum chest deflection (D_{max}), maximum chest compression ratio (C_{max}), maximum chest force (F_{max}), viscous criterion (VC_{max}), and initial chest apparent stiffness (K_a).   "Apparent stiffness" was defined as the slope of the initial force-deflection curve to indicate that it is not related to the traditional static stiffness and to distinguish it from "stiffness" used in this thesis to describe the material property.

Additionally, the number of rib fractures and Abbreviated Injury Scale (AIS) ratings were used for assessing the injury probabilities among the analyses using data of subject information and chest impact

Table 4.1:   Database of available PMHS test results for frontal blunt impact

Subject No.	Sex	Age	Height (m)	Weight (kg)	Chest Depth (mm)	Mass (kg)	Velocity (m/s)	F_{max} (kN)	D_{max} (mm)	C_{max}	VC_{max} (m/s)	K_a (kN/m)	Number Rib Fracture	AIS	Organ Injury
			PMHS Data			Impactor		Chest Responses					Chest Injuries		
Nahum et al. (1970)															
5FM	M	60	1.85	86	257	19.3	5.1	2.1	61.5	0.24	N/A	N/A	2	N/A	N/A
6FM	M	83	1.83	77	254	19.3	5.1	2.0	69.9	0.28	N/A	N/A	11	N/A	N/A
7FF	F	86	1.68	38	200	19.3	4.0	1.6	64.0	0.32	N/A	N/A	10	N/A	N/A
9FM	M	73	1.85	76	238	19.3	5.1	2.5	49.3	0.21	N/A	N/A	0	N/A	N/A
10FF	F	82	1.60	43	168	19.3	4.9	1.8	65.5	0.39	N/A	N/A	12	N/A	N/A
Kroell et al. (1971)															
12FF	F	67	1.63	63	186	22.9	7.2	4.3	78.7	0.42	11.58	135	22	4	1
13FM	M	81	1.68	76	246	22.9	7.4	4.6	109.2	0.44	17.09	147	21	4	1
14FF	F	76	1.56	58	216	22.9	7.3	4.5	94.0	0.44	14.55	324	7	3	1
15FM	M	80	1.65	53	200	23.6	6.9	4.7	78.7	0.39	12.20	170	13	4	1
18FM	M	87	1.77	66	219	23.6	6.7	4.2	91.4	0.42	12.33	521	14	4	1
19FM	M	19	1.70	66	203	23.6	6.7	4.3	76.2	0.38	10.63	338	0	1	0
20FM	M	29	1.80	57	203	23.6	6.7	3.9	71.1	0.35	9.51	1012	0	0	0
21FF	F	45	1.74	68	213	23.6	6.8	3.7	119.4	0.56	21.28	59	18	4	0
22FM	M	72	1.83	75	225	23.6	6.7	4.0	94.0	0.42	10.76	626	17	4	1
23FF	F	58	1.63	61	225	19.5	7.7	5.7	96.5	0.43	16.20	434	23	4	1
24FM	M	65	1.83	82	251	22.9	9.7	6.8	106.7	0.43	16.96	911	24	5	1
25FM	M	65	1.68	54	206	5.5	13.8	11.6	81.3	0.39	24.12	1487	18	4	1
26FM	M	75	1.73	64	248	1.9	11.2	5.3	45.7	0.18	7.24	1129	0	0	0
28FM	M	54	1.83	68	238	1.6	14.5	9.1	55.9	0.23	9.41	1050	0	0	0
Kroell et al. (1974)															
30FF	F	52	1.56	41	180	1.6	13.2	4.6	55.9	0.31	26.95	387	3	2	0
31FM	M	51	1.83	75	238	23.0	10.2	6.6	109.2	0.46	19.69	610	14	4	1
32FM	M	75	1.72	54	248	22.9	9.9	5.8	113.5	0.46	23.33	365	20	4	1
34FM	M	64	1.78	59	241	19.0	8.2	5.0	108.0	0.45	16.82	331	13	4	1
36FM	M	52	1.83	75	226	19.0	7.2	4.8	78.0	0.35	11.86	331	7	3	1
37FM	M	48	1.79	74	248	22.9	9.8	7.9	81.2	0.33	26.67	641	9	4	1
42FM	M	61	1.83	54	216	22.9	4.9	3.0	69.3	0.32	8.04	175	0	0	0
43FM	M	59	1.78	54	241	22.9	4.8	N/A	79.5	0.33	N/A	N/A	N/A	N/A	N/A
45FM	M	64	1.82	64	254	23.0	5.1	2.7	80.0	0.31	7.43	290	10	4	0
46FM	M	46	1.78	95	286	19.3	7.3	4.0	88.6	0.31	11.78	230	0	0	0
48FM	M	69	1.70	64	229	10.4	7.1	2.8	90.7	0.40	10.85	295	0	0	0
50FM	M	66	1.82	60	229	10.4	7.3	3.9	98.6	0.43	13.31	235	12	4	1
51FM	M	60	1.85	82	254	10.4	6.7	2.3	95.8	0.38	9.42	695	0	0	0
52FM	M	65	1.75	52	216	10.4	7.2	3.1	104.9	0.49	14.41	229	11	4	0
53FM	M	75	1.74	77	241	23.0	5.2	3.1	62.0	0.26	5.51	308	3	2	0
54FF	F	49	1.63	37	205	19.6	6.7	2.6	83.3	0.41	13.70	146	7	3	1
55FF	F	46	1.77	81	241	19.6	9.9	6.0	98.3	0.41	19.79	301	8	3	1
56FM	M	65	1.77	74	203	10.4	6.9	3.2	80.0	0.39	11.96	326	3	2	0
58FM	M	68	1.79	69	229	10.4	6.8	2.6	89.1	0.39	10.44	446	4	2	1
60FM	M	66	1.80	79	222	23.0	4.3	2.5	59.7	0.27	4.94	351	9	4	0
62FM	M	76	1.74	50	245	10.0	6.9	1.6	88.9	0.36	10.45	264	9	4	0
64FM	M	72	1.63	63	216	23.0	6.9	3.0	80.0	0.37	12.76	275	6	2	0
Stalnaker et al. (1973)															
C11	M	70	1.68	56	209	10.0	5.6	2.2	48.3	0.23	N/A	198	N/A	N/A	N/A
C15	M	65	1.58	35	179	10.0	5.7	2.9	51.8	0.29	N/A	569	N/A	N/A	N/A
C16	M	88	1.73	68	232	10.0	6.1	2.8	45.0	0.19	N/A	537	N/A	N/A	N/A
C17	M	49	1.80	70	226	10.0	6.7	3.1	48.0	0.21	N/A	844	N/A	N/A	N/A
C18	F	65	1.61	45	199	10.0	6.0	3.4	52.8	0.27	N/A	375	N/A	N/A	N/A
C19	M	52	1.78	92	206	10.0	5.6	2.5	50.0	0.24	N/A	N/A	N/A	N/A	N/A
C20	F	75	1.42	40	232	10.0	5.9	2.0	51.6	0.22	N/A	428	N/A	N/A	N/A
C21	M	62	1.83	51	189	10.0	6.8	2.7	45.7	0.24	N/A	489	N/A	N/A	N/A
C22	M	63	1.70	58	178	10.0	5.5	2.7	49.0	0.28	N/A	169	N/A	N/A	N/A
C23	M	58	1.78	70	206	10.0	6.0	2.7	49.0	0.24	N/A	734	N/A	N/A	N/A

Table 4.2:   Database of available PHMS test results for lateral blunt impact

Subject No.	Sex	Age	Height (m)	Weight (kg)	Chest Depth (mm)	Mass (kg)	Velocity (m/s)	F_{max} (kN)	D_{max} (mm)	C_{max}	VC_{max} (m/s)	K_a (kN/m)	Number Rib Fracture	AIS	Organ Injury
Viano (1989)															
863	M	49	1.76	107	375	23.4	9.4	6.9	98.3	0.26	1.53	135	14	4	1
RNY1	F	76	1.54	44	268	23.4	8.7	5.6	80.0	0.30	1.83	N/A	19	4	0
Cesari et al. (1981)															
K1	M	75	1.71	55	288	23.1	4.1	1.4	N/A	N/A	N/A	N/A	0	0	0
K2	M	75	1.71	55	288	23.1	6.2	1.8	N/A	N/A	N/A	N/A	8	3	1
M1	M	68	1.65	62	297	23.1	2.8	0.9	N/A	N/A	N/A	N/A	0	0	0
M2	M	68	1.65	62	297	23.1	4.8	1.9	N/A	N/A	N/A	N/A	7	2	0
N1	M	54	1.84	86	329	23.1	4.6	2.8	N/A	N/A	N/A	N/A	0	0	0
N2	M	54	1.84	86	329	23.1	5.7	3.6	N/A	N/A	N/A	N/A	0	0	0
N3	M	54	1.84	86	329	23.1	6.2	4.3	N/A	N/A	N/A	N/A	5	2	0
O1	M	70	1.60	79	319	23.1	4.5	2.1	N/A	N/A	N/A	N/A	0	0	0
O2	M	70	1.60	79	319	23.1	5.8	3.1	N/A	N/A	N/A	N/A	0	0	0
O3	M	70	1.60	79	319	23.1	7.5	4.1	N/A	N/A	N/A	N/A	19	4	0
P1	M	65	1.64	60	294	23.1	4.2	1.9	N/A	N/A	N/A	N/A	0	0	0
P6	M	65	1.64	60	294	23.1	5.6	2.6	N/A	N/A	N/A	N/A	4	2	0
R	M	80	1.80	92	336	23.1	6.8	2.9	N/A	N/A	N/A	N/A	9	4	0
S	M	79	1.64	64	300	23.1	5.8	2.2	N/A	N/A	N/A	N/A	14	4	0
T	F	79	1.44	40	268	23.1	5.2	1.9	N/A	N/A	N/A	N/A	10	4	0
Chung et al. (1999)															
CAD1	M	54	1.76	103	336	50.0	5.8	3.3	51.7	0.15	1.17	675	4	3	0
CAD4	M	71	1.72	76	335	50.0	6.3	3.8	61.0	0.18	1.07	1257	15	3	0
CAD5	F	79	1.67	71	330	50.0	5.6	2.4	55.5	0.17	1.33	98	11	3	0
CAD6	M	45	N/A	82	327	50.0	5.6	4.2	44.7	0.14	0.72	136	10	3	0
Talantikite et al. (1998)															
LCT01	M	65	1.76	55	290	12.0	6.0	2.2	62.5	0.22	1.33	109	3	2	N/A
LCT02	F	53	1.64	78	277	16.0	5.9	2.9	87.2	0.31	1.75	213	10	3	N/A
LCT03	F	80	1.57	30	245	16.0	6.1	1.9	63.6	0.26	0.93	132	18	4	N/A
LCT04	F	93	1.57	43	252	12.0	6.0	1.8	72.6	0.29	1.36	135	16	4	N/A
LCT05	M	84	1.60	42	285	11.9	8.2	2.9	102.0	0.36	2.59	161	9	3	N/A
LCT06	M	77	1.75	68	325	11.9	8.5	3.8	85.4	0.26	2.15	225	14	4	N/A
LCT07	M	72	1.81	82	340	16.0	7.2	3.9	96.8	0.28	1.70	115	11	4	N/A
LCT08	M	66	1.73	59	300	16.0	7.0	2.8	99.3	0.33	1.77	90	16	4	N/A
LCT09	M	65	1.65	66	300	16.0	5.7	2.6	73.9	0.25	1.26	83	6	3	N/A
LCT10	M	69	1.80	56	297	11.9	5.3	2.5	73.6	0.25	1.79	55	8	3	N/A
LCT11	M	71	1.69	71	290	12.0	8.5	3.8	80.5	0.28	2.00	N/A	6	3	N/A

response.   Cadaveric injury severity was based on the number and location of rib fractures, as specified by the Association for the Advancement of Automotive Medicine (AAAM), AIS version 1990 with 1998 updates (AAAM, 1998[4]).   According to Section 1.2.4, an AIS 3 injury represents four or more rib fractures on one side of the chest and three or less rib fractures on the other side.   An AIS 4 injury was defined by four or more rib fractures on each side of the chest.   Additionally, a binary system was used to distinguish any tests with or without seven or more rib fractures, AIS 3+ and 4+ injuries for logistic regression analysis.   Kent et al. (2001)[62] showed that seven or more rib fractures constitute a good indicator for flail chest injury (AIS 4+ chest injury; Table 1.4 in Chapter 1).

The linear regression method described by Zar (1984)[168] was used to investigate relationships among parameters succinctly.   In addition, the logistic regression method described by Menard (1995)[92] was used to determine injury probabilities.

4.2.2. Analyses for rib bending tests

This study used a series of rib bending test data based on three-point bending tests to characterize the biomechanical properties of human ribs.   The configuration of the test setup (Figure 4.1) used by Koh (2000)[75] was adopted for this study.   The data were 87 quasi-static and dynamic three-point rib bending test results using isolated 6th and 7th ribs dissected from 11 male and 13 female cadavers.   Anthropometric variables such as the height, weight, shoulder width, chest breadth, chest depth, and chest circumference for both data series were obtained from the subject database at the Wayne State University.

The test specimens used in this study ranged in age from 45 to 85 years and in weight from 34.9 to 87.1 kg.   For males, the average age was 65.1 ± 12.0 years; average mass, 70.2 ± 12.1 kg; and average height, 1.77 ± 0.06 m.   For females, the respective values were 69.7 ± 9.3 years, 61.4 ± 17.1 kg, and 1.51 ± 0.41 m.

The rib material properties are often determined through three-point bending tests.   Stein and Granik (1976)[138] found that the ultimate stress of human ribs increases with the strain rate.   However, the loading rate employed in their study was very low, ranging from 0.0085 to 0.2 mm/s, whereas loading rates causing blunt trauma are at least a thousand times higher.   Therefore, high-speed loading rates were also selected to determine the mechanical properties of the human rib at high loading rates.

A low-speed Instron materials testing machine (Model 1321 frame with a Model 8500 controller, Canton, MA) was used to load specimens at 0.169 mm/s (n = 23).   A band saw was used to cut the rib after the test to determine its cross-sectional properties.

Before testing, all muscles and soft tissues were gently removed from the specimens, which were then stored in plastic bags to retain moisture and kept in a cooler.   An antibacterial saline solution spray was used during the test to keep the specimen moist.   A low-speed Instron materials testing machine (Model 1321 frame with a Model 8500 controller, Canton, MA) was used to load specimens at either 0.169 mm/s (n = 23) or 16.9 mm/s (n = 23), whereas a high-speed Instron machine (Model 1331 frame with a Model 8500 controller) was used to achieve a loading rate of 1.69 m/s (n = 20) and 6.9 m/s (n = 21).   A three-point bending test fixture consisting of two aluminum posts separated by a distance of 76.2 mm and an aluminum loading head situated in the middle was used to load all specimens.   All supporting and loading edges have the same radius of 6.35 mm (Figure 4.1).   Figure 4.2 shows the high-speed testing fixture.   In the high-speed tests, the specimens were set in the vertical direction and impacted in the lateral direction because of the installation of the Instron Model 1331.   Therefore, specimens in the high-speed testing conditions were fixed with rubber bands.   After the bending tests, a band saw was used to cut the specimen so that the geometric properties of the ribs could be digitized and calculated (Figure 4.3).

STATISTICA (StatSoft, Inc., Tulsa, OK), a commercially available software, was used for all statistical analyses.
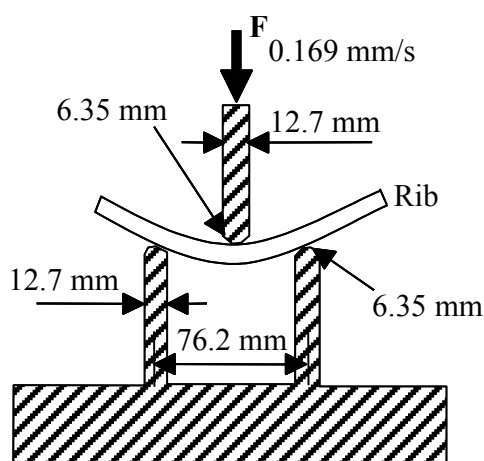
Figure 4.1:   Three-point bending test configuration of the ribs used by Koh (2000)
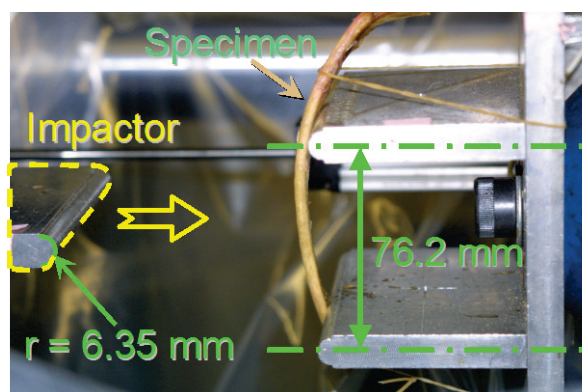
Figure 4.2:   Test setup for high-speed loading condition
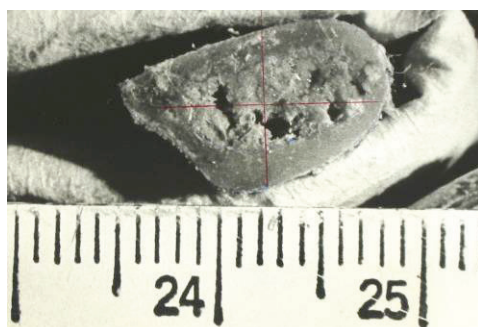
Figure 4.3:   A typical cross-sectional view of the rib used to calculate the cross-sectional area and moment of inertia

4.3.   Results from Blunt Impact Data for the Chest

4.3.1.   Relevant information on cadavers subjected to pendulum impacts

In the frontal impact group, the average age of the male and female subjects was 63.8 ± 13.9 and 63.7 ± 14.7 years, respectively.   There was no statistical difference between males and females in this regard.   However, in the lateral impact group, the average age of males (66.7 ± 9.8 years) was significantly lower ($p < 0.05$) than that of females (76.7 ± 13.0 years).   In the frontal impact group, the average height of male and female subjects was 1.77 ± 0.068 and 1.62 ± 0.092 m whereas in the lateral impact group, it was 1.71 ± 0.081 and 1.57 ± 0.081 m, respectively.   In the frontal impact group, the average weight of male and female cadavers was 66.9 ± 12.5 and 52.3 ± 14.7 kg whereas in the lateral impact group, it was 72.0 ± 15.9 and 51.0 ± 19.0 kg, respectively.   Statistically, in both groups, the male subjects used were taller and heavier than the female subjects.   Similarly, the males had relatively larger chest depth and width.   In the frontal impact group, the average chest depth of males and females was 227 ± 23 and 206 ± 22 mm whereas in the lateral impact group, it was 313 ± 22 and 273 ± 30 mm, respectively.

4.3.2.   Chest responses versus cadaveric anthropometrics

A linear regression analysis showed no significant correlation between the chest impact response data (D_{max}, C_{max}, F_{max}, and K_a) and cadaveric age, height, and weight ($p > 0.05$, $r^2 < 0.2$) for both frontal and lateral impacts.   Figure 4.4 shows a comparison of K_a between males and females owing to blunt impact in the frontal and lateral directions.   In frontal impact, the average K_a for males and females was 476 ± 324 and 267 ± 150 kN/m, respectively.   Based on a Student's t-test, the male chest was significantly stiffer than the female chest ($p < 0.05$).   In lateral impact, the average K_a for males (186 ± 158 kN/m) was higher than that for females (144 ± 49 kN/m) but was not statistically different.   It should be noted that only four female subjects were available for lateral impact analysis because no K_a data were provided for two of the six females tested.
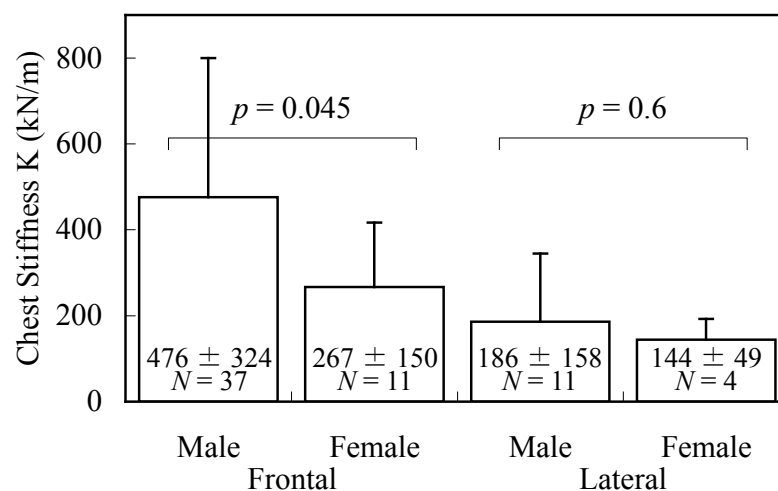
Figure 4.4:   Average value and standard deviation of initial chest apparent stiffness due to blunt impact, Left: male versus female response in frontal impact, Right: male versus female response in lateral impact

4.3.3. Chest response versus input test conditions

Figure 4.5 shows D_{max} as a function of the impact energy in frontal and lateral impacts. The analysis is limited to the impact energy range of 200–1200 J, and extrapolation of the regression lines beyond this range is not recommended. In frontal impact, the D_{max} increased with the impact energy. For both males ($p < 0.01$, $r^2 = 0.43$) and females ($p < 0.01$, $r^2 = 0.65$), D_{max} was somewhat linearly correlated with the impact energy. In frontal impact, the slope for females was 0.067 mm/J. It was steeper than that for males (0.049 mm/J), indicating that larger chest deflections were observed in females when subjected to the same impact energy, especially for high-energy impacts. In lateral impact, D_{max} did not correlate linearly with the impact energy ($p > 0.05$, $r^2 = 0.06$ for males and $p > 0.05$, $r^2 = 0.04$ for females). Thus, linear regression lines were not provided in Figure 4.5 (b).

(a) Frontal impact   (b) Lateral impact
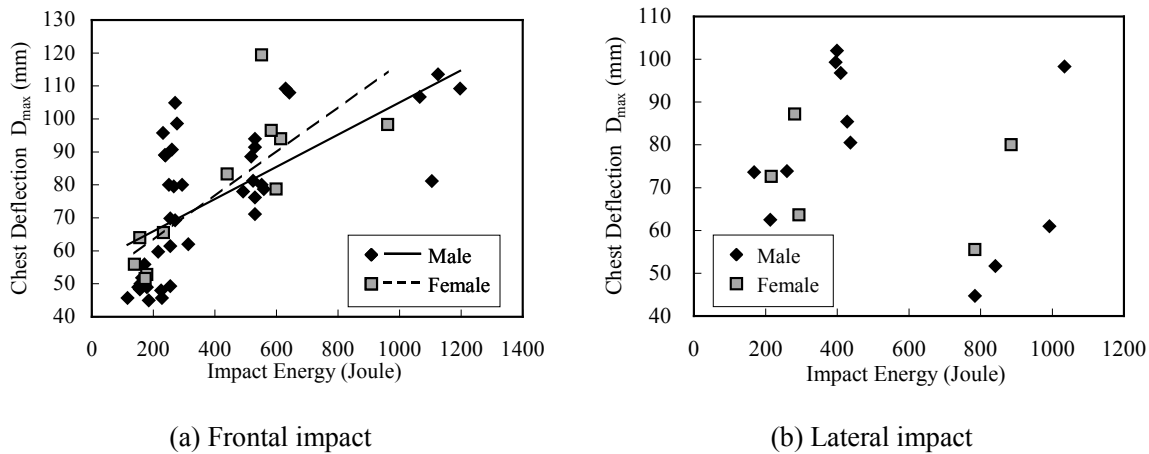
Figure 4.5: Maximum chest deflection (D_{max}) as a function of impact energy in frontal and lateral blunt impact

Figure 4.6 shows the linear correlation of C_{max} and F_{max} with impact energy in frontal impact. Both C_{max} ($p < 0.01$, $r^2 = 0.36$ for male and $p < 0.05$, $r^2 = 0.44$ for females) and F_{max} ($p < 0.01$, $r^2 = 0.32$ for males and $p < 0.05$, $r^2 = 0.54$ for females) increased significantly with the impact energy. For C_{max} versus impact energy, both the slope and the intercept for females were slightly higher, indicating that the chest compression ratio is higher in females; this is probably due to the fact that the female chest depth is smaller than that of males. In lateral impact, only F_{max} in males correlated linearly with the impact energy ($p < 0.01$, $r^2 = 0.58$). Other chest response parameters were not linearly correlated with impact energy.

(a) C_{max} vs. Impact energy

(b) F_{max} vs. Impact energy
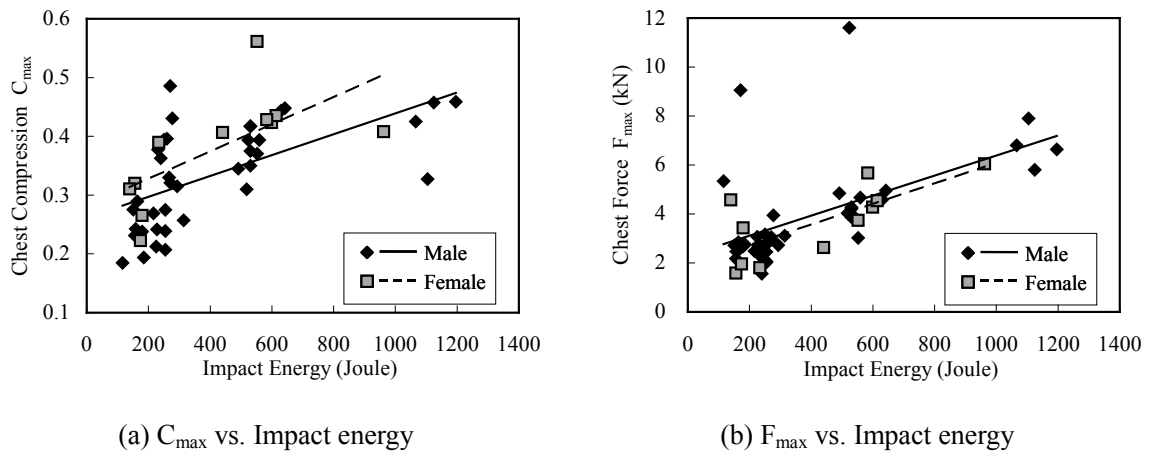
Figure 4.6: **Maximum chest compression ratio (C_{max}) and maximum chest force (F_{max}) as a function of impact energy in frontal blunt impact**

The impact energies used in various experimental studies of frontal impact can, upon inspection, be divided into three groups: low (~200 J), middle (~600 J), and high (~1,000 J). There were only four males and one female in the high impact energy group, and it was thus not possible to perform a Student's t-test on the data. Chest response data for the other two groups are shown in Table 4.3. The *p* values indicate a significant gender difference for C_{max} ($p < 0.05$) in the middle impact energy group. A comparison of the other parameters showed no statistical differences. In lateral impact, impact energies can be divided into two groups: low (~300 J) and high (~900 J). No significant gender difference was observed in chest responses.

Table 4.3: **Average and standard deviation of chest response for males and females for frontal impact**

Low impact energy	Male		Female		*p*	Female/Male
	N	Average ± S.D.	*N*	Average ± S.D.		
D_{max} (mm)	25	66.7 ± 19.5	5	58.0 ± 6.4	> 0.05	86.9%
C_{max} (%)	25	29.6 ± 8.1	5	30.2 ± 6.3	> 0.05	102.0%
F_{max} (kN)	24	3.05 ± 1.47	5	2.67 ± 1.29	> 0.05	87.6%

Middle impact energy	Male		Female		*p*	Female/Male
	N	Average ± S.D.	*N*	Average ± S.D.		
D_{max} (mm)	11	87.0 ± 12.7	5	94.4 ± 15.8	> 0.05	108.5%
C_{max} (%)	11	38.8 ± 4.3	5	45.1 ± 6.3	**< 0.05**	116.3%
F_{max} (kN)	11	4.91 ± 2.28	5	4.17 ± 1.11	> 0.05	84.8%

4.3.4. Chest injuries versus impact responses

Table 4.4 shows the results of logistic regressions for AIS 3+ and AIS 4+ injuries as well as chest injuries with seven or more rib fractures against the injury predictors D_{max}, C_{max}, F_{max}, and VC_{max}.   If we randomly choose a minimum χ^2 value of 5 to select the parameters for both male and female injury prediction, we could predict AIS 3+ injuries using D_{max} and C_{max} and injuries with seven or more rib fractures using D_{max} for frontal impact.   There were insufficient data to determine which response parameters could be used to predict these injuries for lateral impact.

While the χ^2 values were still high for VC_{max} as an injury predictor, negative logistic curves were found in the plots of VC_{max} versus seven or more rib fractures or AIS 3+ injuries for females.   This indicates a higher probability of sustaining seven or more rib fractures or AIS 3+ injuries with lower VC_{max}.   Because this conclusion is intuitively wrong, VC_{max} is not considered a good injury predictor.

Table 4.4:   Cross-reference of chest injuries by chest responses

Chest responses	Chest Injuries	Gender	Frontal impact			Lateral impact		
			N	χ^2	p	N	χ^2	p
D_{max}	Rib fractures 7+	M	30	8.3	**< 0.01**	12	1.9	> 0.05
		F	9	5.9	**< 0.05**		N/A	
	AIS 3+	M	28	7.9	**< 0.01**	12	0.7	> 0.05
		F	7	5.7	**< 0.05**		N/A	
	AIS 4+	M	28	9.0	**< 0.01**	12	6.8	**< 0.01**
		F	7	1.4	> 0.05	5	0.0	> 0.05
C_{max}	Rib fractures 7+	M	30	7.0	**< 0.01**	12	0.8	> 0.05
		F	9	4.7	**< 0.05**		N/A	
	AIS 3+	M	28	7.2	**< 0.01**	12	0.3	> 0.05
		F	7	5.7	**< 0.05**		N/A	
	AIS 4+	M	28	8.1	**< 0.01**	12	2.5	> 0.05
		F	7	3.7	> 0.05	5	0.7	> 0.05
F_{max}	Rib fractures 7+	M	30	1.8	> 0.05	26	2.4	> 0.05
		F	9	0.3	> 0.05		N/A	
	AIS 3+	M	28	1.9	> 0.05	26	5.5	**< 0.05**
		F	7	0.0	> 0.05		N/A	
	AIS 4+	M	28	1.7	> 0.05	26	4.3	**< 0.05**
		F	7	0.0	> 0.05	6	0.0	> 0.05
VC_{max}	Rib fractures 7+	M	28	9.1	**< 0.01**	12	0.6	> 0.05
		F	7	5.7	**< 0.05**		N/A	
	AIS 3+	M	28	9.1	**< 0.01**	12	0.3	> 0.05
		F	7	5.7	**< 0.05**		N/A	
	AIS 4+	M	28	9.2	**< 0.01**	12	1.0	> 0.05
		F	7	0.4	> 0.05	5	0.3	> 0.05

Figure 4.7 shows logistic plots of the probability of sustaining an injury with seven or more rib fractures in frontal impact as a function of D_{max} and C_{max}, respectively.   For a 50% probability of sustaining an injury with seven or more rib fractures, the values for D_{max} and C_{max} were 79 mm and 34% for males and 61 mm and 32% for females, respectively.   Figure 4.8 shows the logistic plots of the probability of sustaining AIS 3+ injuries in frontal impact as a function of D_{max} and C_{max}.   For a 50% probability of sustaining an AIS 3+ injury, the values for D_{max} and C_{max} were 81 mm and 35% for males and 68 mm and 36% for females, respectively.
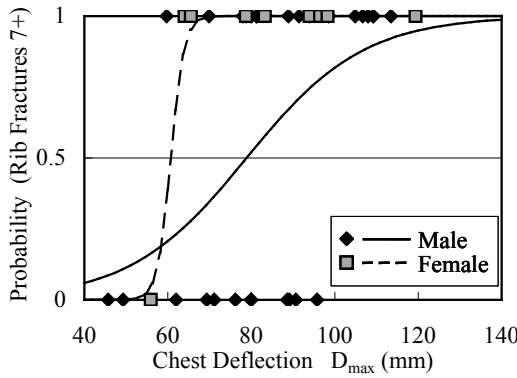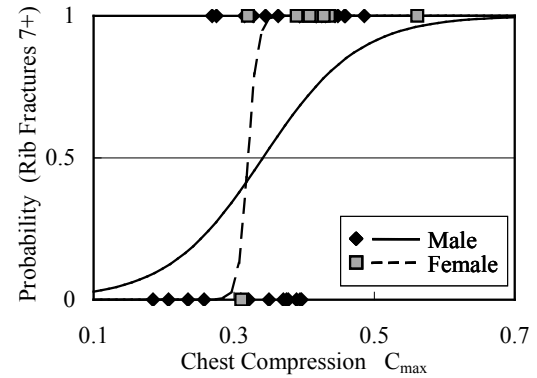
(a) Rib fractures 7+ injury vs. D_{max} (b) Rib fractures 7+ injury vs. C_{max}

Figure 4.7:   Logistic plots of probability of 7+ rib fractures due to D_{max} and C_{max} in frontal impact
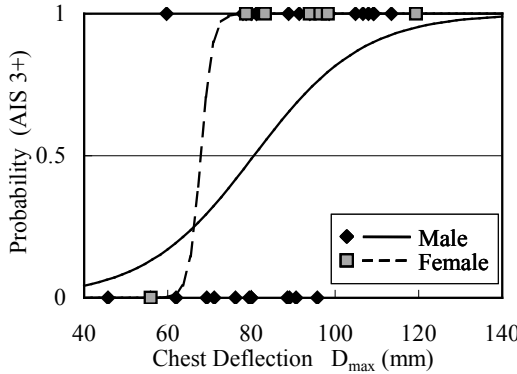
(a) AIS 3+ injury vs. D_{max} (b) AIS 3+ injury vs. C_{max}
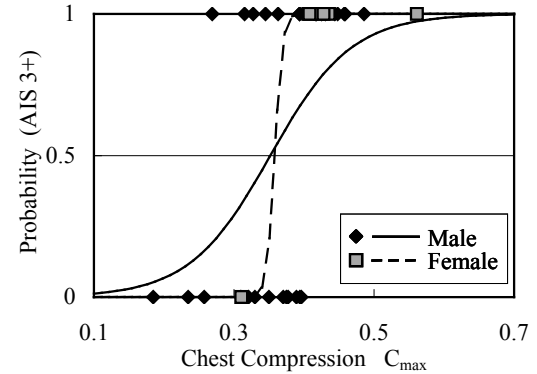
Figure 4.8:   Logistic plots of AIS 3+ chest injury probability due to D_{max} and C_{max} in frontal impact

4.4.   Results from Rib Bending Test Data

4.4.1.   Relevant information on test subjects

Linear regressions were conducted among anthropometric data of the test subjects and rib's cross-sectional area and area moment of inertia.   Table 4.5 lists the correlation coefficient (R) and significance level (p) in parenthesis, with bold face values indicating statistical significance.

Generally, female data shows statistical significance in many cross reference pairs, whereas male data shows only six pairs.   In particular, when the pair of variables, which indicates coefficients of correlation greater than 0.72, are arbitrarily chosen in both male and female data, strong correlations were observed among the weight of the human body, chest breadth, and chest circumference.   However, the chest depth, which is utilized for calculating the chest compression ratio, did not depend on any parameter of anthropometric data, such as height or weight.

The cross-sectional area and area moment of inertia of the rib cage showed somewhat significant levels in combinations of height versus cross-sectional area and shoulder width versus area moment of inertia.   However, the correlation coefficients of these pairs did not match between male and female data. For example, the correlation coefficients between height and cross-sectional area of the rib cage were negative in males and positive in females.   Therefore, this study could not find correlations of anthropometric data and cross-sectional geometric properties of the rib cage.

Table 4.5: Coefficients of correlation among the subject data and cross-sectional data of the rib cage.

Male (N=11)	Height	Weight	Shoulder width	Chest breadth	Chest depth	Chest circumference
Height						
Weight	0.29					
Shoulder width	0.07	0.02				
Chest breadth	0.24	**0.80****	0.26			
Chest depth	0.16	0.32	0.35	0.28		
Chest circumference	0.20	**0.85****	0.24	**0.72***	**0.74****	
Cross-sectional area of rib cage	**-0.43****	0.05	0.30	0.08	-0.10	0.04
Area moment of inertia	-0.27	0.22	**0.35***	0.23	-0.15	0.11
Female (N=13)						
Height						
Weight	0.36					
Shoulder width	0.07	-0.06				
Chest breadth	0.40	**0.75****	-0.32			
Chest depth	0.34	**0.61***	0.28	**0.61***		
Chest circumference	0.41	**0.94****	-0.18	**0.83****	**0.67***	
Cross-sectional area of rib cage	**0.56****	**0.51****	-0.03	**0.53****	**0.42****	**0.50****
Area moment of inertia	**0.44****	**0.62****	**-0.37***	**0.68****	**0.31***	**0.55****

*: $p<0.05$,   **; $p<0.01$

Boldface indicates those cases with $p < 0.05$.

4.4.2. Strain rate dependency

Figure 4.9 shows the ultimate stress as a function of loading rate (in log10 scale) for males (diamonds) and females (triangles).   Data from Stein and Granik (1976)[138] were also included in this figure (squares) for comparison.   Although an upward trend can be observed in the ultimate stress as a function of loading rate, it is not significantly different when the loading rate increased from 0.169 to 6,900 mm/s based on a Student's t-test.   Similarly, the average ultimate load increased with the loading rate; however, there was no significant difference between any loading rate pair.   For male specimens, the average maximum displacement (3.1 ± 0.7 mm) at a loading rate of 6,900 mm/s was significantly higher when compared to the cases with a loading rate of 0.169 mm/s (2.1 ± 0.6 mm) and 16.9 mm/s (2.2 ± 0.3 mm).   However, there was no difference in the maximum displacement in female ribs when comparing different loading rate pairs.   In terms of Young's modulus, only the 16.9 and 1,690 mm/s loading rate groups show statistical difference for males.   No other loading rate pairs exhibited statistical differences.
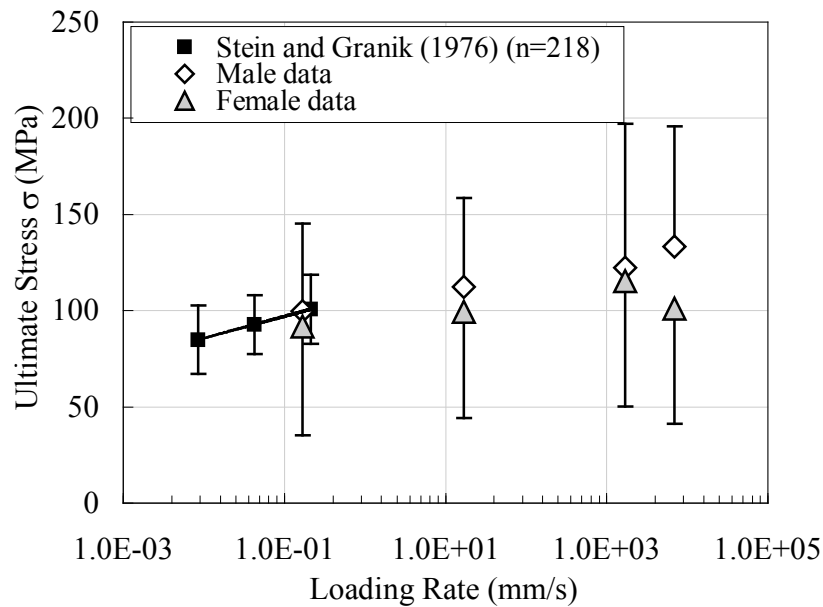
Figure 4.9:   Relationship between the ultimate stress and the loading rate

4.4.3. Gender difference

Table 4.6 shows the average and standard deviation of the anthropometric data of test subjects. Only height and shoulder width showed statistical gender differences.   In addition, the cross-sectional geometric properties of the rib cage showed significant gender differences.   Figure 4.10 shows a comparison of the geometric properties for male and female ribs.   Based on Student's t-tests, the cross-sectional area and moment of inertia for males (29.6 ± 7.9 mm^2 and 209.6 ± 94.2 mm^4) were significantly higher ($p < 0.05$) than those for females (23.2 ± 5.4 mm^2 and 104.1 ± 54.4 mm^4).   However, it is interesting to note that the size variables of the chest were not different between males and females, and even height or shoulder width showed gender differences.

Table 4.6:   Average and standard deviation of subject data

	Male (n=11)	*Female (n=13)*	*p*
Age [year]	65.1 ± 12.0	69.7 ± 9.3	> 0.05
Height [mm]	**1.77 ± 0.06**	**1.51 ± 0.41**	**< 0.05**
Weight [kg]	70.2 ± 12.1	61.4 ± 17.1	> 0.05
Shoulder width [mm]	**352.7 ± 50.6**	**298.0 ± 20.2**	**< 0.01**
Chest breadth [mm]	311.6 ± 20.4	309.5 ± 49.7	> 0.05
Chest depth [mm]	213.5 ± 33.5	199.9 ± 45.2	> 0.05
Chest circumference [mm]	941.9 ± 86.6	927.7 ± 115.4	> 0.05
	Male (n=39)	*Female (n=48)*	*p*
Cross-sectional area [mm^2]	**29.6 ± 7.9**	**23.2 ± 5.4**	**< 0.01**
Area moment of inertia [mm^4]	**209.6 ± 94.2**	**104.1 ± 54.4**	**< 0.01**
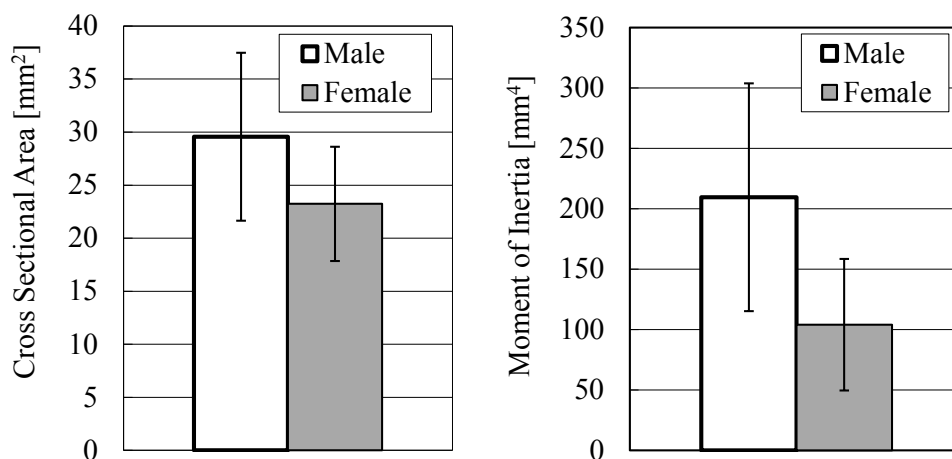
Figure 4.10: Cross-sectional area and moment of inertia are both significantly higher in male ribs

Table 4.7 shows the average and standard deviation of the rib bending test results. At a loading rate of 0.169 and 6,900 mm/s, the ultimate loads for males were significantly higher than those for females, but the same was not true for the other two loading rates. On the other hand, although the average ultimate stress and Young's modulus for male ribs were higher than those for females, no significant gender differences could be found ($p > 0.05$) from the average ultimate stress and Young's modulus in all loading rates.

Table 4.7:   Average and standard deviation of rib biomechanical properties

0.169 mm/s-loading rate	Male (n=10)	Female (n=13)	p
Ultimate load [N]	**310.1 ± 133.3**	**167.4 ± 131.9**	**< 0.05**
Max displacement [mm]	2.1 ± 0.6	2.3 ± 0.6	> 0.05
Ultimate stress σ [MPa]	99.9 ± 45.4	91.9 ± 56.7	> 0.05
Young's modulus [GPa]	9.94 ± 4.8	9.86 ± 4.3	> 0.05
16.9 mm/s-loading rate	Male (n=10)	Female (n=13)	p
Ultimate load [N]	355.0 ± 192.2	201.4 ± 196.5	> 0.05
Max displacement [mm]	2.2 ± 0.3	3.0 ± 1.3	> 0.05
Ultimate stress σ [MPa]	112.4 ± 46.1	99.5 ± 55.3	> 0.05
Young's modulus [GPa]	10.1± 2.3	9.0 ± 3.7	> 0.05
1,690 mm/s-loading rate	Male (n=9)	Female (n=13)	p
Ultimate load [N]	344.6 ± 223.8	205.8 ± 121.5	> 0.05
Max displacement [mm]	2.5 ± 0.8	2.9 ± 1.1	> 0.05
Ultimate stress σ [MPa]	122.2 ± 74.8	115.3 ± 65.0	> 0.05
Young's modulus [GPa]	6.2 ± 3.0	7.0 ± 3.2	> 0.05
6,900 mm/s-loading rate	Male (n=10)	Female (n=13)	p
Ultimate load [N]	**373.0 ± 188.3**	**198.8 ± 163.0**	**< 0.05**
Max displacement [mm]	3.1 ± 0.7	2.7 ± 0.9	> 0.05
Ultimate stress σ [MPa]	133.2 ± 62.5	101.1 ± 60.0	> 0.05
Young's modulus [GPa]	7.1 ± 3.8	7.9 ± 4.4	> 0.05

4.5. Discussion

This retrospective study analyzed data from 83 cadaveric pendulum-type impacts: 40 males and 11 females in frontal impact and 26 males and 6 females in lateral impact.   Because female subjects represented only 20% of the tested cadavers, we believe that more female subject tests are needed for gender differences to be evaluated fully.   One drawback of using published pendulum test results obtained from different sources for data analysis is that different test protocols were used.   To minimize the effect of this deficiency, linear regression against impact energy was used prior to the comparison of the biomechanical responses between genders.   Nevertheless, the findings derived from this study can be used to better understand the similarities and differences in the biomechanical properties between males and females.

In this retrospective study, the age distribution of the donors is shown in Figure 4.11.   This figure shows that most test subjects were 40–80 years old; this range may not be completely representative of the driving population.   Thus, although our findings indicated that there were no statistical correlations between the impact responses of the chest and the rib bending strength against age, these findings may be related to the fact that mainly elderly subjects were tested.   We believe that recent advancements in medical technology are responsible for this increase in life expectancy.   Many studies have shown the age-dependent material properties of the human bone.   However, these studies have focused on long bones such as the femur, humerus, tibia, and radius (Yamada, 1970[164]; Hayes, 1991[49]; Zioupos and Currey, 1998[170]).   The only age-dependent study on human ribs that we found was by Stein and Granik (1976)[138].   While this study reported that the breaking load, bending strength, and cross-sectional area decreased as the age of the test subjects increased, all 218 specimens were obtained from 79 male cadavers.   Consequently, the results cannot be used to test the hypothesis that the strength of the female rib was lower than that of the male rib.

The female chest was significantly more compliant than the male chest in frontal impact.   While this difference was not statistically significant, the male K_a was also higher in lateral impact.   Additionally, chest injuries in terms of the number of rib fractures tended to be less severe in males than in females when impacts of the same energy were considered.   However, even though the average impact responses in terms
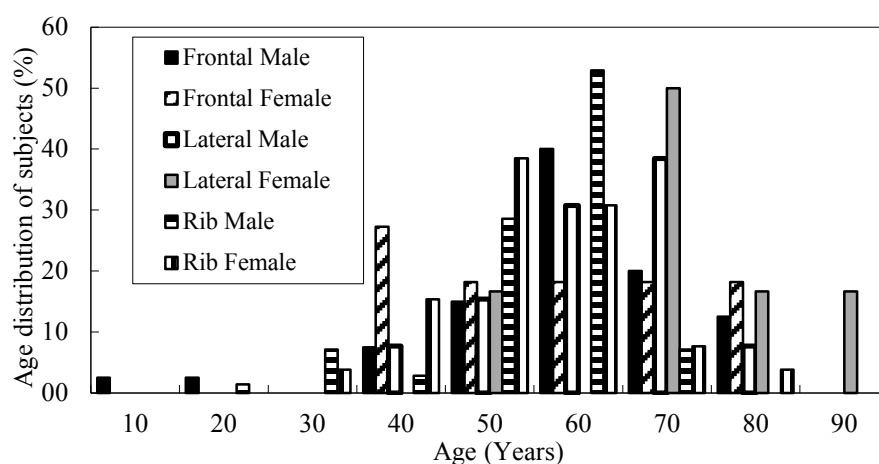
Figure 4.11: Age distribution of the test subjects used in this retrospective study

of C_{max} and D_{max} were higher and those in terms of F_{max} were lower in female subjects, the gender differences were not statistically significant.   The only exception was C_{max} in the 600 J impact energy group due to frontal impact.   In this impact energy group, C_{max} in male subjects averaged 38.8% compared to 45.1% among female subjects ($p < 0.05$).

The above findings could probably be better explained by results from three-point bending tests of isolated ribs taken from 70 male and 26 female age-equivalent cadavers in a previous study (Kimpara et al., 2003[68]).   In these tests, which used the same test protocol, we found that the average stiffness for males was 43% higher than that for females.   Additionally, the cross-sectional area of female ribs was ~19% smaller than that of male ribs ($p < 0.01$).   However, Young's modulus calculated from three-point bending tests and bone mineral density as measured from the ash content showed no difference between males and females.   We believe that the low bending stiffness observed in the female chests was due to the lower area moment of inertia of the ribs, which have a smaller cross-sectional area.

The equal stress-equal velocity scaling procedure proposed by Eppinger et al. (1984)[27] was used to scale all data to a 46.2 kg person, a representation of the fifth percentile female subject.   The basic scaling factor, lambda (λ), is defined in equation (4.1):

$$\lambda = \sqrt[3]{M_{af05}/M_{subject}}, \quad\cdots\cdots\cdots\cdots\cdots\cdots\cdots\cdots\cdots\cdots\cdots\cdots\cdots\cdots\cdots\cdots\cdots \quad \textbf{(4.1)}$$

where M_{af05} and $M_{subject}$ represent the mass of a fifth percentile American Female (AF05) and of the test subject, respectively.   To determine the 5th percentile female chest deflection, we use the product of λ and D_{max}.   To determine the 5th percentile female chest force, we use the product of λ^2 and F_{max}.

4.5.1. Frontal impact scaling

Figure 4.12 shows the normalized maximum chest deflection ($\lambda \cdot D_{max}$) and force ($\lambda^2 \cdot F_{max}$) versus the impact energy in frontal impact, scaled to the 5th percentile female from all male (diamond) and all female (square) subjects tested.   A linear regression was used to correlate the resulting 5th female representation scaled from the male (solid line) and female (dashed line) subjects.   Additionally, the raw data of D_{max} and
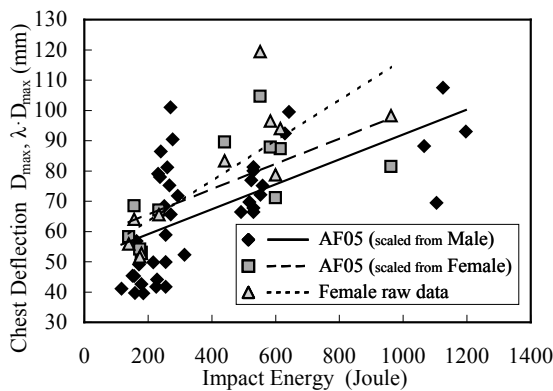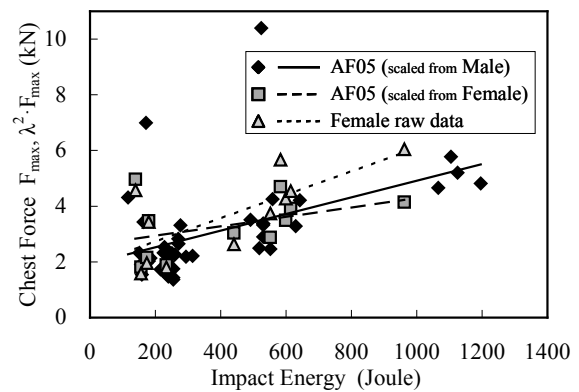
(a) D_{max} and $\lambda \cdot D_{max}$ vs. Impact energy   (b) F_{max} and $\lambda^2 \cdot F_{max}$ vs. Impact energy

Figure 4.12: Plots of normalized chest responses against impact energy in frontal impact

F_{max} obtained from all female subjects (triangle) and corresponding linear regressions (dotted line) are shown in the same figure for reference.

If the equal stress-equal velocity scale law correctly predicts the 5th percentile female responses, then the three regression lines should be close to each other.   Otherwise, it would indicate that in addition to the weight differences, other disparities may separate males from females.   Based on the linear regression of $\lambda \cdot D_{max}$ versus the impact energy, the slopes were very similar when comparing the scaled results using all male and female data.   However, there was an offset of 6 mm in $\lambda \cdot D_{max}$ between these two regression lines. The slope obtained from the linear regression of the female raw data was steeper than that obtained from the two scaled lines.

When considering D_{max} versus impact energy, as shown in Figure 4.5 (a), the results from the linear regression of D_{max} for the low and middle impact energy groups for males and females were approximately the same.   However, the slightly higher slope in females resulted in a larger difference when the impact energy increased.

For $\lambda^2 \cdot F_{max}$, it was observed that the slope of the linear regression between $\lambda^2 \cdot F_{max}$ and the impact energy was the greatest for the raw female data, followed by that obtained from all male scaled data and all female scaled results. $\lambda^2 \cdot F_{max}$ scaled from all female data was greater than that scaled from all male data for the low impact energy group; however, $\lambda^2 \cdot F_{max}$ scaled from all female data was less than that scaled from all male data for the high impact energy group.   In contrast, the slope and intercept of F_{max} versus impact energy for both genders, as shown in Figure 4.6 (b), were very similar.

4.5.2. Injury predictors

Using scaled and raw female data, the probability of sustaining an injury with seven or more rib fractures and AIS 3+ injuries in frontal impact is shown in Figure 4.13 (a) and (b), respectively. $\Lambda \cdot D_{max}$ shows chest deflection for a 5th percentile female scaled from all male (solid line) and female (dashed line) subjects tested.   These curves are compared with the logistic regression curve for raw female data, plotted as a dotted line in the same figure.   For a 50% probability of sustaining an injury with seven or more rib
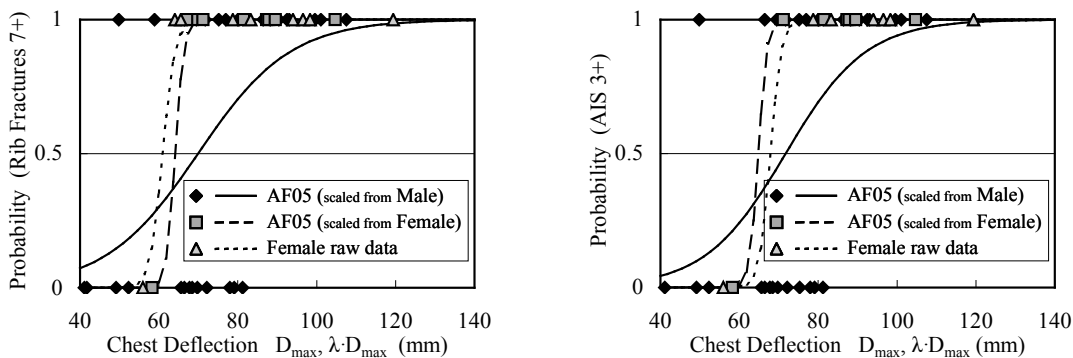
(a) Rib fractures 7+ injury vs. D_{max} and $\lambda \bullet D_{max}$ (b) AIS 3+ injury vs. D_{max} and $\lambda \bullet D_{max}$

Figure 4.13: Logistic plots of injury probability due to normalized chest deflection in frontal impact

fractures, the values for $\lambda \cdot D_{max}$ were 69.9 and 64.1 mm when scaled from all male and female results, respectively. The corresponding value for raw female data was 61 mm, as shown in Figure 4.7 (a). Similarly, for a 50% probability of sustaining an AIS 3+ injury, the respective values were 71.7 and 64.8 mm and the corresponding value for raw female data was 68 mm (Figure 4.7). The difference in $\lambda \cdot D_{max}$ scaled from all male data and from raw female data was ~13% for seven or more rib fractures and 5% for AIS 3+ injuries. Although this discrepancy is small, it should be noted that the logistic curves are widely divergent between the scaled male data and the raw female data.

The aforementioned findings were obtained by lumping all available impacts for logistic regression regardless of the impact energy. These data seem to suggest that D_{max} can be used to separate male responses from female ones. For a 50% probability of sustaining seven or more rib fractures, D_{max} was 79 and 61 mm for males and females, respectively. Similarly, for a 50% probability of sustaining AIS 3+ injuries, D_{max} was 81 and 68 mm for males and females, respectively. On the other hand, when three impact energy groups were considered separately, we found that D_{max} was not statistically different between males and females.

The slope obtained from the linear regression of C_{max} versus impact energy for females ($p < 0.05$, $r^2 = 0.44$) was ~31% steeper than that for males ($p < 0.01$, $r^2 = 0.36$). This indicates that a higher chest compression ratio was observed in females compared to males when subjected to the same impact energy (Figure 4.6 (a)). C_{max} for females was 2% ($p > 0.05$) and 16.3% ($p < 0.05$) greater than that for males in the low and middle impact energy groups, respectively (Table 4.3). The high impact energy group was not compared owing to the small number of specimens available. While there was a significant difference in C_{max} between males and females ($p < 0.05$) for the middle impact energy group, we found almost no difference in C_{max} for the prediction of a 50% probability of sustaining seven or more rib fractures or AIS 3+ injuries (Figure 4.8). For a 50% probability of sustaining seven or more rib fractures, C_{max} was 34% and 32% for males and females, respectively. Similarly, for a 50% probability of sustaining AIS 3+ injuries, C_{max} was 35% and 36% for males and females, respectively.

4.5.3. Lateral impact

In lateral impact, the linear relationships between the response variables (D_{max}, C_{max}, F_{max}, $\lambda \cdot D_{max}$, and $\lambda^2 \cdot F_{max}$) and the impact energy were not statistically significant probably due to the small number of cases available. More cadaveric pendulum impact data are needed for gaining a better understanding of lateral impacts to the chest.

Viano (1989)[154] proposed the use of VC_{max} and C_{max} as measures of chest injury tolerance for lateral impact. For a 25% probability of sustaining an AIS 4+ injury, the proposed injury thresholds for VC_{max} and C_{max} were 1.47 m/s and 38.4%, respectively. Figure 4.14 shows the logistic plots of the probability of sustaining AIS 4+ injuries in lateral impact as a function of VC_{max} and C_{max} obtained from this study. The tolerance in terms of VC_{max} and C_{max} for a 25% probability of sustaining an AIS 4+ injury was 1.32 m/s and 23.5% for males, both of which are lower than the values reported by Viano (1989)[154]. However, the logistic curve obtained for females for AIS 4+ injuries in terms of VC_{max} showed a negative

correlation (Figure 4.14 (a)).   This result is intuitively incorrect, and more research is needed regarding the use of VC_{max} as an injury predictor for female lateral impact.

<div align="center">(a) AIS 4+ injury vs. VC_{max} (b) AIS 4+ injury vs. C_{max}</div>
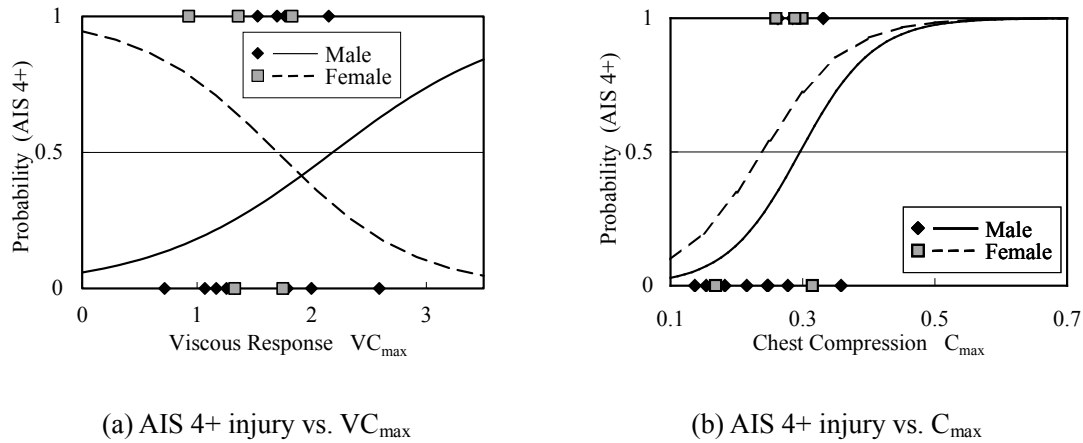
Figure 4.14: Logistic plots of AIS 4+ injury probability due to chest responses in lateral impact

In this study, only 17 female cadavers (11 for frontal and 6 for lateral impacts) were available to analyze the chest's biomechanical properties.   Lenard and Welsh (2001)[82] estimated that the probability of sustaining AIS 2 chest injuries for female occupants was much higher than that for male occupants in frontal impact.   However, we could not duplicate this analysis because only one female case (Cadaver No. 30FF, Kroell et al. 1974[77]) sustained an AIS 2 injury with three rib fractures, whereas the rest of the female cadavers sustained AIS 3+ injuries with seven or more rib fractures.   Therefore, more female low injury severity data are needed for an in-depth analysis of the differences in injury response and injury threshold between males and females.

4.5.4. Rib's biomechanical properties

One drawback in this study is the fact that only specimens from elderly cadavers were used.   For males and females, the average age was 65 and 70, respectively.   With a change of ~40,000 times in the loading rate from 0.169 to 6,900 mm/s, the ultimate stress increased only 33% and 10% in males and females, respectively.   It can accordingly be concluded that the human rib is not highly rate sensitive.

Significant gender differences were observed in the geometric properties of ribs in terms of their cross-sectional area and moment of inertia.   On the other hand, there is no gender difference in material properties such as the maximum displacement, ultimate stress, and Young's modulus.   The ultimate load shows a significant difference when comparing males and females for loading rates of 0.169 and 6,900 mm/s. As the rib's bending moment is a function of the products of their material stiffness and area moment of inertia, it is believed that gender differences in the rib's geometry cause the gender difference in the ultimate load.

4.6. Conclusions

Several conclusions can be drawn from this study based on a retrospective analysis of 83 frontal and lateral blunt cadaveric impacts and 87 isolated rib bending tests.   The variables analyzed include test condition, cadaveric anthropometric data, chest impact response, and resulting chest injury.

1. Female K_a (267 ± 150 kN/m) was considerably lower than that of males (476 ± 324 kN/m) for frontal impact, probably due to the smaller cross-sectional area of female ribs.

2. The D_{max}, C_{max}, and F_{max} somehow correlated linearly with the impact energy for both males and females for frontal impact.   This linear relationship will be useful in the development of a 5th percentile female numerical model and ATDs.

3. The slopes of the D_{max} and compression ratio versus impact energy for females are 37% and 31% steeper than those for males, respectively.   In general, the maximum deflection and compression ratio for females are considerably higher than those for males when subjected to the same impact energy.

4. Based on a linear regression analysis, data obtained from the isolated rib bending tests that were currently available in this study did not statistically correlate the age, height, weight, and chest depth and width of the cadavers tested for both males and females.   Age effects were not observed because the age group of the test subjects had a bias toward an older population.

5. There was no significant gender difference in Young's modulus and bone mineral density based on isolated rib bending tests.   However, the cross-sectional area and area moment of inertia were ~22% and 50.3% lower than those of male ribs, respectively.

6. The data analyses for the anthropometric properties of the rib bending test subjects shows that the chest depth and rib's geometry did not associate with the height or weight of the human body. Therefore, it is impossible to estimate the rib's cross-sectional properties from anthropometric data of height or weight owing to the inhomogeneous and complex nature of the human body.

7. The use of the equal stress-equal velocity scaling law to predict the 5th percentile female responses are not appropriate because this normalization method does not consider gender differences.

Chapter 5   Biomechanical Factors Affecting Thoracic Injuries

This chapter explains the numerical human body model used in this thesis for investigating the chest injury mechanisms.   Two series of parametric studies were conducted using this model.   The results obtained in this chapter have been presented in the Journal of Biomedical Engineering, Transaction of ASME (Kimpara, et al., 2006B[A4]), and Journal of Traffic Injury Prevention (Kimpara, et al., 2010[A5]).

5.1. Introduction

The retrospective analysis of frontal chest pendulum impact in Chapter 4 using data obtained from Nahum et al. (1970)[98], Kroell et al. (1971[76] and 1974[77]) and Stalnaker et al. (1973)[137] revealed that the maximum deflection and compression ratio for females are considerably higher than those for males when subjected to the same impact energy.   In addition, the three-point bending test results in Chapter 4 showed gender differences in the rib's cross-sectional area and area moment of inertia instead of material properties, while there were no loading rate dependencies in the rib's bending responses.   However, it is not altogether clear which biomechanical parameter has the most influence on the chest response or how sensitive the results are to the assumed values of the parameters.

It may be difficult to validate the responses of a specific percentile subject mainly because of the difficulty of obtaining an adequate number of specimens in any specific size group.   On the other hand, finite element (FE) models have been shown to be an excellent tool when determining the effect of geometric and material properties.   Consequently, this study aims to determine how the weight and height of the subjects, rib cage area moment of inertia, assumed stiffness, and mass density of the rib cage, internal organs, and superficial muscles affect the human chest impact responses in frontal and lateral pendulum impacts.   In this study, two series of parametric studies were conducted using a commercially available FE human chest model with different biomechanical parameters assigned to various chest components.   The findings of this study can provide information needed for improving the scaling methods applicable for the study of chest impact biomechanics.   In addition, some findings could lead to the suggestion of effective biomechanical properties for modeling a new 5th female FE chest model.

The validated chest model was used for conducting two series of parametric studies in the following sections.   The first parametric study was aimed at investigating the effects of the assumed stiffness and mass density of the rib cage, internal organs, and superficial muscles of the chest.   The second series was conducted to determine which of the body weight, height, and rib cage area moment of inertia influenced the impact responses of the chest.   The findings obtained from these studies would provide information needed for improving the scaling methods applicable for the study of chest impact biomechanics.

A linear regression analysis was conducted to evaluate the effect of variances in anthropometrics and to find the optimal injury predictor. STATISTICA (StatSoft, Inc., Tulsa, OK), a commercially available software, was used for statistical analyses.

Sections 5.3 and 5.4 present the simulation matrices and results of each parametric study.

5.2. Chest FE Model

A commercially available mid-sized human male model THUMS-AM50 (THUMS: Total Human Model for Safety, Iwamoto et al., 2002[60]; AM50: American Male 50th percentile) was used as a base model to predict the chest impact responses. THUMS-AM50 version 1.52 was used for chest impact analyses without any modifications. Most skeletal parts were represented using shell elements and solid elements corresponding to the cortical and cancellous bones, respectively. Furthermore, the length and width of the typical elements were sufficiently large so that the initial minimum time step was greater than 1 μs, except for the detailed brain and spinal cord models, to reduce the computational time.

Accurate material properties of the human body models are essential for predicting injuries. The experimentally measured material properties of biological tissues generally indicate complex nonlinear and viscoelastic behavior with a wide range of variation in terms of stiffness and strength. Unfortunately, the material models available in LS-DYNA are limited for the representation of these complex biomechanical materials. Therefore, the representative material properties were carefully assumed for each tissue model and selected from the LS-DYNA material library to represent the primary biomechanical behavior.

5.2.1. Geometry and structure

The rib cage consists of the spine, sternum, costal cartilage, and 12 pairs of ribs composed of cortical and cancellous bones. The ribs were modeled with solid elements with covering shell elements. The solid and shell elements correspond to the cancellous and cortical bones, respectively. The nonlinear articulations of the rib cage, which included the sternocostal joints and interchondral articulations, were treated as if they were directly connected, as also reported by Wang (1995)[158] and Lee and Yang (2001)[80]. However, the costovertebral joints, which are the costotransverse joints between the ribs and the vertebral body of the spine, were modeled as bone-to-bone contacts, and the joint stiffness was controlled by major ligaments. All ligaments were modeled using a tension-only elastic membrane or bar elements.

The geometrical parameters of the ribs reported in Chapter 4 were mostly obtained from the straight portion of the 6th and 7th ribs. The cross-sectional area and area moment of inertia measured from male cadaveric subjects were 29.6 ± 7.9 mm^2 and 209.6 ± 94.2 mm^4, respectively. On the other hand, in the model, the average cross-sectional area and associated area moment of inertia used for the FE model were 26.3 ± 1.8 mm^2 and 131.4 ± 32.0 mm^4, respectively. Although the geometrical parameters from the rib model were relatively smaller than those from the test data, these rib model parameter values were within the standard deviations of the test data.

5.2.2. Material properties

The material properties used for the bones and soft tissues in the baseline model were based on published experimental data (Abe et al., 1996[1]; Yamada, 1970[164]). Elastic-plastic material characteristics (LS-DYNA MAT Type 81 with element Type 16 [LSTC, Livermore, CA]) were used so that rib fractures could be simulated using the mesh elimination method, which deletes elements stretched over the strain thresholds. However, the mesh elimination method used in LS-DYNA is very sensitive to the size of the mesh as well as to the material properties selected (Moinerean et al., 1999[97]; Wang et al., 1997[159]). The effects of mesh size were investigated using either a four-layer fine mesh or one-layer coarse mesh model of the same outline geometry. Then, we concluded that the simulation results based on a failure strain of 3% matched well with the experimental data for the mesh density selected for this model.

For cancellous bone, different elastic-plastic material characteristics with failure strain of 10.3% (LS-DYNA MAT Type 24 with element Type 1) was selected based on Hayes and Gerhart (1985)[48], who reported that the failure strains of the cancellous bone ranged from 3% to 23% before it was fully crushed with a significant decrease in stiffness. Table 5.1 summarizes the material properties selected for the cortical bone of the ribs and sternum.

The internal organs in the chest cavity were modeled using a linearly viscoelastic cellular rubber material with confined air pressure (LS-DYNA MAT Type 87), and internal organs in the abdominal cavity were modeled using a crushable foam material law (LS-DYNA MAT Type 63). The superficial muscles were modeled using a linearly viscoelastic material, and the skin was represented by linearly elastic shell/membrane elements.

Table 5.1:   Material properties of the cortical bones used in this study

	Mass density (kg/m³)	Young's modulus (GPa)	Yield stress (MPa)	Shell thickness (mm)
Rib's cortical bone	2,000	10.2	65.3	0.7
Sternum's cortical bone	2,000	11.5	123.0	1.0

5.2.3. Validation for chest impact responses

The chest model was validated against the cadaveric pendulum impact test data reported by Kroell et al. (1971[76] and 1974[77]) for frontal impacts and Bouquet et al. (1994)[10] for lateral impacts. All simulation series were performed using a commercially available FE solver, LS-DYNA 970 or 971 (LSTC, Livermore, CA), on a 64-bit-based computer running Linux operating system. Post-processing of the simulation results was conducted using the LS-PREPOST post-processor (LSTC, Livermore, CA).

(a)   Simulation setups

Kroell et al. (1974)[77] reported that the fixed-back test configuration precluded whole body motion and provides no information regarding the effect of body weight and height. However, the present study

aimed to investigate the effects of the body weight or height of human subjects on the chest responses. Therefore, this study selected only the free-back test configuration of frontal chest impact because the mass of the body would affect the impact responses and reaction forces on the chest.

The model was positioned in an erect sitting position on a rigid flat surface with the back unsupported. For frontal impact, the center of the pendulum was positioned at the mid-sternum level (Figure 5.1). The pendulum had a mass of 23.4 kg and diameter of 150 mm, and it had a rounded edge. Two different impact velocities, 6.9 and 5.9 m/s, were used for frontal and lateral impact simulations, respectively. The results predicted by the model were sampled at 10 kHz, and contact force data were filtered using a Society of Automotive Engineers (SAE) digital low-pass filter at a channel frequency class (CFC) of 180 Hz.
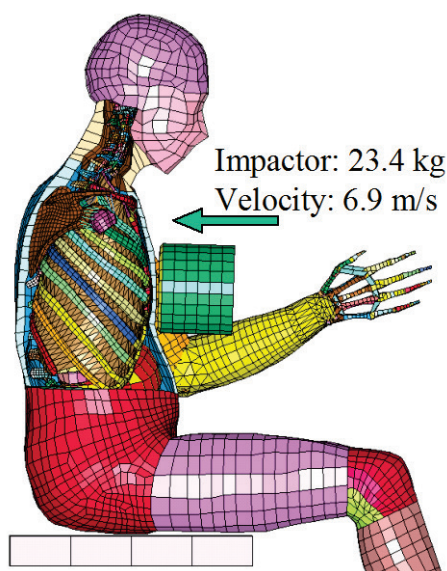
Figure 5.1: Simulation setup of the THUMS model for frontal pendulum chest impact

(b) Results

Figure 5.2 shows the force-deflection responses of the chest predicted by the model for frontal and lateral pendulum impacts, respectively.   The thick black line indicates the simulation results predicted by the model, and the dotted lines represent the upper and lower bounds of the corridors obtained from cadaveric pendulum tests.

(a) Frontal impact   (b) Lateral impact
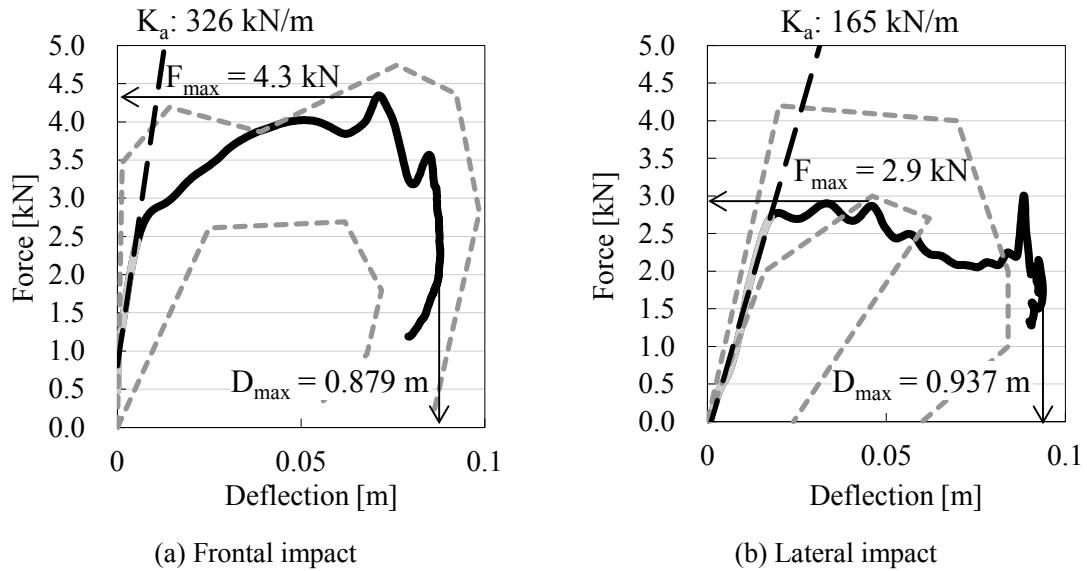
Figure 5.2:   Chest force-deflection responses predicted by the model.   The short dashed gray lines show the upper and lower bounds of the corridors obtained from cadaveric pendulum tests.   The long-dashed line represents the initial apparent stiffness (K_a) based on linear regression.

The initial chest apparent stiffness (K_a), maximum chest force (F_{max}), maximum chest deflection (D_{max}) in anteroposterior direction, and maximum chest compression ratio (C_{max}) obtained from D_{max} divided by the initial chest depth in the anteroposterior direction were calculated from the force-deflection curve predicted by the model.   The "apparent stiffness" of K_a was defined as the slope of the initial force-deflection curve (black dashed lines in Figure 5.2).   In addition, the eliminated shell element groups in the rib models were counted as the numbers of rib fractures (Rib Fxs) or fractured ribs (Fxed Ribs). However, the viscous criterion (VC) could not be recreated from the papers selected for this study because the viscous criterion reported by Viano et al. (1989)[155] was not available until 1989.

In frontal impact, the model predicted 15 rib fractures on 9 ribs, D_{max} of 87.9 mm, F_{max} of 4.3 kN, and K_a of 326 kN/m.   The initial force-deflection curve agreed with the test corridors.   However, the predicted number of rib fractures for the baseline model was reasonable compared to 10.1 ± 8.3 fractures obtained from Test Numbers 13FM, 15FM, 18FM, 19FM, 20FM, 22FM, and 64FM (Kroell et al., 1971[76] and 1974[77]).   The circles in Figure 5.3 indicate the locations of the rib fractures predicted by the model.
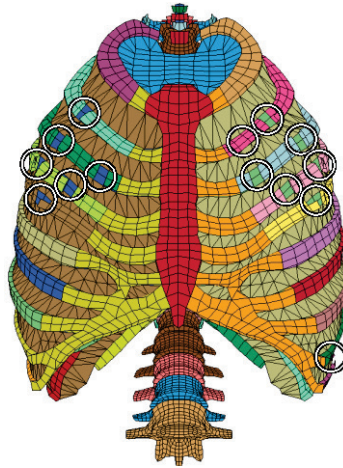
Figure 5.3:   Rib fracture locations predicted by the model at t = 45 ms in frontal chest impact

In lateral impact, the model predicted 22 rib fractures on 8 ribs, D_{max} of 93.7 mm, F_{max} of 2.9 kN, and K_a of 165 kN/m.   Bouquet et al. (1994) [10] gave multiple collisions to a single Post Mortem Human Subjects (PMHS).   Therefore, it is impossible to compare the number of rib fractures due to lateral chest impacts with the autopsy reports of the test.

While the force-deflection response predicted by the model was near the upper bound of the corridors for frontal impact (Kroell et al., 1971[76] and 1974[77]) and near the lower bound of the corridors for lateral impact (Bouquet et al., 1994[10]), most impact responses fell within the corridors.   Therefore, it is believed that this chest model could have acceptable accuracy for investigating chest injury mechanisms in further parametric studies.

5.3.   Effects of Assumed Stiffness and Mass Density of the Human Chest

The first parametric study was aimed at investigating the effects of the stiffness and mass density of the biological material properties on the impact responses of the whole chest in frontal and lateral directed loadings.   This study aimed to illustrate the relationships between the whole impact responses and the bony strength, which is influenced by aging effects and gender differences in rib thickness.

5.3.1.   Simulation matrix

The variables for the baseline model selected for this parametric study include Young's modulus (E: 10.2 GPa), yield stress (σ_y: 65.3 MPa), tangent modulus (E_t: 2.3 GPa), and mass density (ρ: 2,000 kg/m^3) of the ribs and sternum; shear modulus (G: 2.0 kPa) and E (1.7 MPa) of the internal organs; and bulk modulus (K: 2.3 MPa) and short- and long-term shear moduli (G_0 and G_∞: 3.5 and 1.2 MPa, respectively) of the superficial muscles.   The magnitude of these variables either increased or decreased by 50% from the baseline parameter to determine the overall effect due to the changes in each property.   Based on an analysis of data obtained from the rib bending tests, Young's modulus of male ribs ranged from 4.3 to 21 GPa with an average value of 7.21 ± 5.94 GPa (Chapter 4).   Thus, it is believed that a change of ±50% from the baseline

value was acceptable in terms of Young's modulus.   Although a large change of ±50% in the mass density seemed unrealistic, such a change could highlight its effect on the chest impact responses more clearly than a small change.

Figure 5.4 and Figure 5.5 show the stress-strain characteristics selected for the rib cage and internal organs.   In these figures, the solid black lines indicate the baseline model properties, and the solid gray lines and black dashed lines represent increased and decreased material properties, respectively.

A total of 106 simulations were conducted for both frontal and lateral pendulum impact.   To determine the effect of stiffness change, 27 simulations were conducted, representing three components (rib cage, internal organs, and superficial muscles) each of which had three levels (+50%, baseline, and −50%). Similarly, the effect of changing mass was simulated using 26 simulations for the same three components with three levels each except for the baseline case.   As all 53 cases have been conducted for both frontal and lateral directed impacts, a total of 106 cases were simulated.
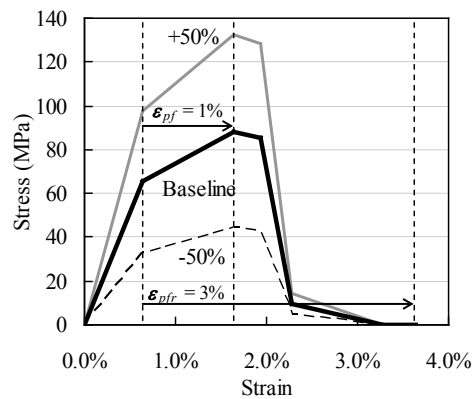
(a) Rib cortical bone
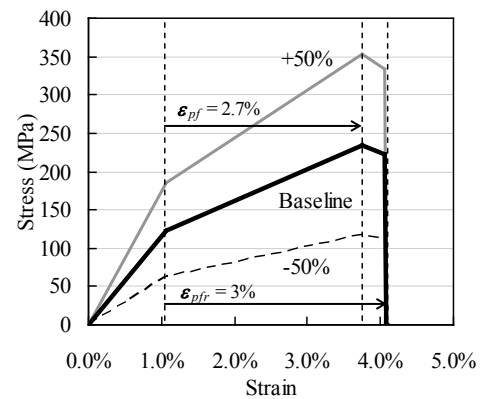
(b) Sternum cortical bone
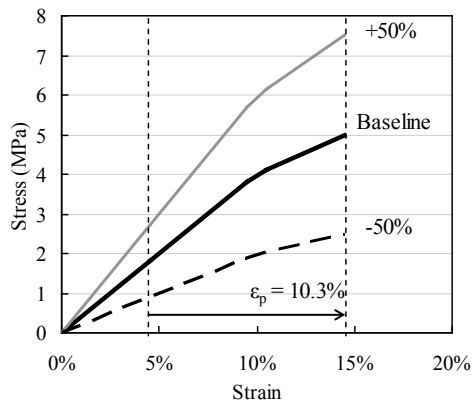
(c) Cancellous bone

Figure 5.4:   Description of elastic-plastic material properties of the ribs and sternum
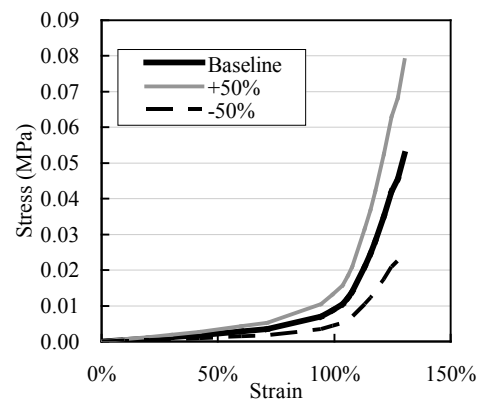
(a) Thoracic viscera
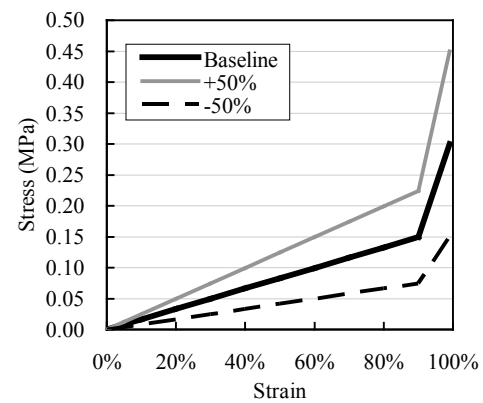
(b) Upper abdomen
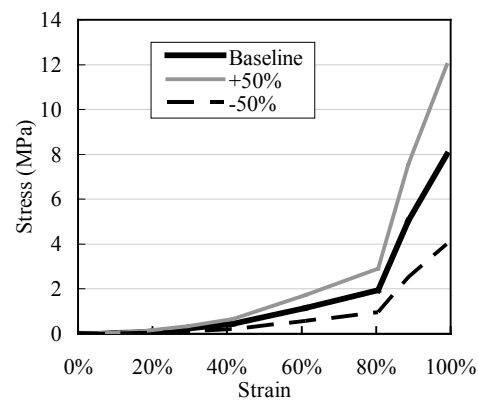
(c) Lower abdomen

Figure 5.5:   Stress-strain characteristics defining the material properties of the thorax and the abdomen

5.3.2. Results

(a) Effects of assumed material stiffness on chest response

Linear regressions have been conducted among the response variables of frontal and lateral chest impacts (K_a, F_{max}, D_{max}, and number of Fxed Ribs and Rib Fxs) and the stiffness of the rib cage, internal organs, and superficial muscles, as listed in Table 5.2 and Table 5.3. These tables list the correlation coefficient (R). A significance level (p) less than 0.05 was considered significant.

In frontal impact, F_{max} (R = 0.63) and number of fractured ribs (R = −0.83) and rib fractures (R = −0.91) were significantly correlated with the change in stiffness of the rib cage. Similarly, F_{max} (R = 0.67) and D_{max} (R = −0.82) were highly correlated with the stiffness of internal organs. K_a correlated only with the stiffness of the superficial muscles (R = 0.76).

In lateral impact, K_a correlated significantly with the stiffness of superficial muscles (R = 0.98). F_{max} also significantly correlated with the stiffness of superficial muscles (R = 0.79) and correlated well with the stiffness of the rib cage (R = 0.55). D_{max} correlated significantly with the stiffness of the rib cage (R = −0.88). Additionally, the number of fractured ribs (R = −0.78) and rib fractures (R = −0.89) showed a high correlation with the stiffness of the rib cage.

Table 5.2: **Linear regression of the frontal chest impact responses with the stiffness of the rib cage, internal organs, and superficial muscles (Bold face indicates significant correlations).**

Frontal N = 27	K_a	F_{max}	D_{max}	[*1] Fxed Ribs	[*2] Rib Fxs
Rib cage	**R = 0.39***	**R = 0.63****	R = -0.37	**R = -0.83****	**R = -0.91****
Internal organs	R = -0.09	**R = 0.67****	**R = -0.82****	R = -0.014	R = 0.009
Superficial muscles	**R = 0.76****	R = 0.019	R = -0.25	R = 0.000	R = 0.038

*: $p<0.05$,   **; $p<0.01$,   Boldface indicates those cases with $p < 0.05$.

[*1] Fxed Ribs: number of fractured ribs, [*2] Rib Fxs: number of rib fractures.

Table 5.3: **Linear regression of the lateral chest impact responses with the stiffness of the rib cage, internal organs and superficial muscles (Bold face indicates significant correlations).**

Lateral N = 27	K_a	F_{max}	D_{max}	[*1] Fxed Ribs	[*2] Rib Fxs
Rib cage	R = 0.14	**R = 0.55****	**R = -0.88****	**R = -0.78****	**R = -0.89****
Internal organs	R = -0.003	R = 0.10	R = -0.21	R = -0.03	R = -0.14
Superficial muscles	**R = 0.98****	**R = 0.79****	R = -0.38	R = 0.19	R = 0.11

*: $p<0.05$,   **; $p<0.01$,   Boldface indicates those cases with $p < 0.05$.

[*1] Fxed Ribs: number of fractured ribs, [*2] Rib Fxs: number of rib fractures.

(b) Effects of assumed mass density on chest response

As for the stiffness change, linear regressions were conducted among the response variables and the mass density of the rib cage, internal organs, and superficial muscles due to frontal and lateral impact, and the results are listed in Table 5.4 and Table 5.5.   Additionally, the total mass of the whole chest was added for a comparison of the mass density change.

In frontal impact, K_a was significantly correlated with the change in mass density (and weight of whole chest) of the rib cage and internal organs. F_{max} and D_{max} were significantly correlated with the mass density of the internal organs ($R = 0.93$ and $R = -0.72$, respectively).   Additionally, the number of fractured ribs was correlated with the mass density of the superficial muscles ($R = 0.73$).

In terms of lateral impact, K_a ($R = 0.998$), F_{max} ($R = 0.80$), and D_{max} ($R = 0.89$) were significantly correlated with the mass density of the superficial muscles and weight of the whole chest. F_{max} was also moderately correlated with the mass density of the internal organs ($R = 0.45$).   Additionally, the number of rib fractures was somewhat correlated with the mass density of the internal organs ($R = 0.56$) and the whole chest weight ($R = 0.49$).

Table 5.4:   Linear regression of the frontal chest impact responses with the mass density of the rib cage, internal organs, and superficial muscles (Bold face indicates significant correlations).

Frontal N = 27	K_a	F_{max}	D_{max}	[*1] Fxed Ribs	[*2] Rib Fxs
Rib cage	**R = 0.60****	R = -0.01	R = -0.13	R = -0.15	R = -0.07
Internal organs	**R = 0.53****	**R = 0.93****	**R = -0.72****	R = -0.24	R = 0.21
Superficial muscles	**R = 0.59****	R = 0.18	R = 0.33	**R = 0.39***	**R = 0.73****
Whole chest weight	**R = 0.82****	**R = 0.84****	R = -0.38	R = 0.04	**R = 0.60****

*: $p<0.05$,   **; $p<0.01$,   Boldface indicates those cases with $p < 0.05$.

[*1] Fxed Ribs: number of fractured ribs, [*2] Rib Fxs: number of rib fractures.

Table 5.5:   Linear regression of the lateral chest impact responses with the mass density of the rib cage, internal organs, and superficial muscles (Bold face indicates significant correlations).

Lateral N = 27	K_a	F_{max}	D_{max}	[*1] Fxed Ribs	[*2] Rib Fxs
Rib cage	R = 0.046	R = -0.01	R = 0.08	R = -0.18	R = 0.06
Internal organs	R = 0.004	**R = 0.45***	R = -0.13	R = 0.36	**R = 0.56****
Superficial muscles	**R = 0.998****	**R = 0.80****	**R = 0.89****	R = -0.06	R = 0.077
Whole chest weight	**R = 0.62****	**R = 0.85****	**R = 0.45***	R = 0.24	**R = 0.49***

*: $p<0.05$,   **; $p<0.01$,   Boldface indicates those cases with $p < 0.05$.

[*1] Fxed Ribs: number of fractured ribs, [*2] Rib Fxs: number of rib fractures.

5.4. Effects of Body Weight, Height, and Rib Cage Area Moment of Inertia

The second series of parametric studies aimed to elucidate the roles of body weight, height, and rib cage area moment of inertia on the impact responses of the whole chest in frontal directed loadings. This parametric study might indicate the effects of body size and scaling methods on the whole impact response and injury.

5.4.1. Simulation matrix

The selected body parameters in this study were body weight (W), height (H), and area moment of inertia of the rib cage (I_{Rc}) and of the ribs alone (I_{rib}). The three body sizes selected were those of a large male (AM95), mid-sized male (AM50), and small-sized female (AF05). Their respective body weights and heights were 102.6, 76.6, and 46.4 kg and 1.86, 1.75, and 1.51 m. To obtain the scale factor based on the equal-stress equal-velocity procedure proposed by Eppinger et al. (1984)[27], the body weight ratio λ_m was calculated first. Based on the weight ratio, the scaling factors for AM95 and AF05 were 134% and 60.6%, respectively. The length dimensions such as height, chest depth, and thickness of the cortical bones, ligaments, skin, and other tissues were scaled using the cubic root of λ_m ($\lambda_m^{1/3}$). Based on these two λ_m values, the corresponding cubic roots for AM95 and AF05 were 110.3% and 84.6% for $\lambda_m^{1/3}{}_{AM95}$ and $\lambda_m^{1/3}{}_{AF05}$, respectively. For simplicity, the length scaling factors used for $\lambda_m^{1/3}{}_{AM95}$ and $\lambda_m^{1/3}{}_{AF05}$ were 110% and 85%, respectively.

A total of 11 simulation models, including the baseline Model 0, were prepared for frontal pendulum impact simulations (Table 5.6). These models represented several variations in human anthropometry, as explained in detail below. In Model 1, all length dimensions such as the rib thickness, ligament length, and vertebral body height were increased by 10% to represent a large male whereas in Model 2, all length dimensions were reduced by 15% to represent a small female. Note that the mass density for Models 1 and 2 did not need to be changed to reflect the proper weight. Figure 5.6 shows the features of the baseline model (Model 0), large male model (Model 1), and small female model (Model 2).

Models 3 and 4 represented a person with all length dimensions being the same as those for AM50 but with weight of either AM95 or AF05. To achieve these goals, the mass density was multiplied by either 134% or 60.6% of the baseline model. Model 5 represents a tall and skinny person, with the height and cross-sectional properties of AM95 and weight of AM50. To achieve this goal, all length dimensions of the baseline model were multiplied by 110% and the mass density was multiplied by 75.1% (inverse of $\lambda_m{}_{AM95}$) so that the total mass remained the same as that for AM50. In Model 6, a heavy person with short stature, with the height and cross-sectional properties of AF05 and weight of AM50, was simulated using the same principle described for Model 5.

Models 7–10 were created to simulate persons with abnormal proportions in cross-sectional area compared to that of the baseline model. Model 7 represented the size of AM50, but the area moment of inertia for the rib cage (ribs and sternum) was increased to the same size as that used for AM95. In contrast, Model 8 represented the size of AM50, but the area moment of inertia for the rib cage (ribs and sternum) was the same as that for AF05. To achieve these goals of increasing or decreasing the moment of inertia without

changing the dimensions of the rib cage, an increase of 44.3% and a decrease of 47.2% were implemented in the cortical bone thickness of the ribs and sternum.   The cross-sectional geometry of the rib was assumed to have a rectangular shape.   Therefore, the thickness of the cortical bone for Models 7 and 8 was adjusted to match the area moment of inertia of AM95 (Model 1) and AF05 (Model 2), respectively.   For Model 7, the cortical bone thickness for the rib and sternum was increased from 0.70 to 1.01 mm and 1.00 to 1.44 mm, respectively.   Similarly, for Model 8, the cortical thickness for the rib and sternum was changed from 0.70 to 0.37 mm and 1.00 to 0.53 mm, respectively.   Models 9 and 10 assumed that the area moment of inertia for the rib was the same as that used in Models 7 and 8, respectively.   However, the area moment of inertia of the sternum was the same as that of AM50.

Table 5.6:   Simulation matrix for second series of parametric studies

Model No.	Mass density (%)	Human body		Area moment of inertia (Cortical bone thickness)	
		Weight	Height	Sternum	Ribs
0	100	AM50 (76.6)	AM50 (1.75)	AM50 (1.0)	AM50 (0.70)
1	100	AM95 (102.6)	AM95 (1.86)	AM95 (1.1)	AM95 (0.77)
2	100	AF05 (46.4)	AF05 (1.51)	AF05 (0.85)	AF05 (0.60)
3	134	AM95 (102.6)	AM50 (1.75)	AM50 (1.0)	AM50 (0.70)
4	60.6	AF05 (46.4)	AM50 (1.75)	AM50 (1.0)	AM50 (0.70)
5	75.1	AM50 (76.6)	AM95 (1.86)	AM95 (1.1)	AM95 (0.77)
6	163	AM50 (76.6)	AF05 (1.51)	AF05 (0.85)	AF05 (0.60)
7	100	AM50 (76.6)	AM50 (1.75)	AM95 (1.4)	AM95 (1.0)
8	100	AM50 (76.6)	AM50 (1.75)	AF05 (0.53)	AF05 (0.37)
9	100	AM50 (76.6)	AM50 (1.75)	AM50 (1.0)	AM95 (1.0)
10	100	AM50 (76.6)	AM50 (1.75)	AM50 (1.0)	AF05 (0.37)
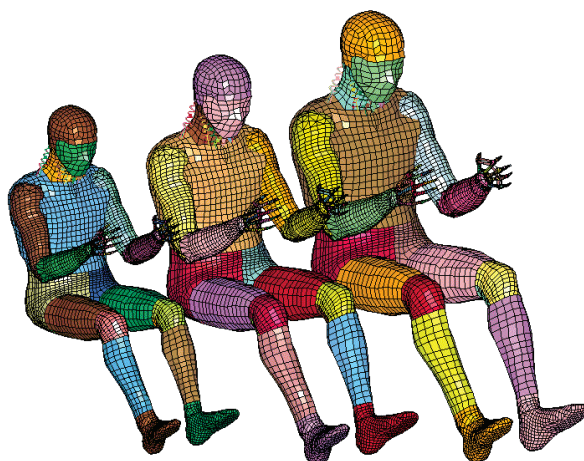
Figure 5.6:   FE Human models (from left): small female model (Model 2), baseline male model (Model 0), and large male model (Model 1)

5.4.2. Results

(a) Chest frontal impact responses of scaled human body

Figure 5.7 shows the force-deflection response curves for all simulations.　Table 5.7 lists all response variables for all simulations.　In this table, numbers shown in parentheses indicate the percentage change based on values predicted for the baseline model, and the shaded cells represent those cases with a decrease in the impact response for the sake of distinguishing those with increased and decreased model-predicted responses.

(a) Models 0, 1, and 2

(b) Models 0, 3, 4, 5, and 6

(c) Models 0, 7, 8, 9, and 10
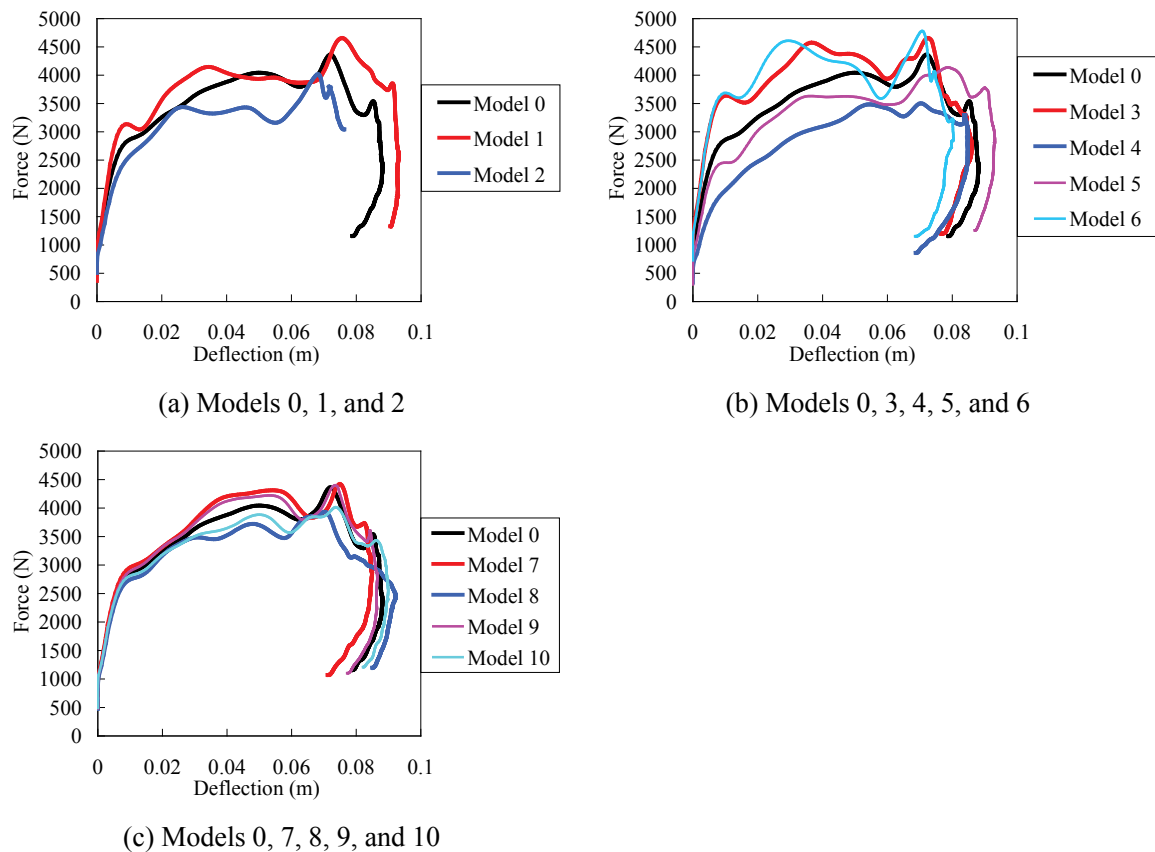
Figure 5.7: Comparison of force-deflection responses predicted by each simulation case compared to that predicted by the baseline model

Table 5.7:   Summary of the stiffness, peak force, maximum chest deflection, maximum compression ratio, numbers of fractured ribs and rib fractures of for each simulation case

Model No.	K_a [kN/m]	F_{max} [kN]	D_{max} [mm]	C_{max} [ ]	*[1] Fxed Ribs	*[2] Rib Fxs
0	326	4.3	88.1	37.3	9	14
1	338 (+3.7%)	4.7 (+6.7%)	93.1 (+5.7%)	35.8 (−4.0%)	8 (−1)	11 (−3)
2	268 (−17.7%)	4.0 (-8.0%)	76.3 (−13.4%)	38.0 (+1.9%)	11 (+2)	15 (+1)
3	362 (+11.0%)	4.7 (+6.7%)	86.1 (−2.3%)	36.4 (−2.3%)	9 (0)	16 (+2)
4	186 (−43.0%)	3.5 (-19.7%)	84.8 (−3.7%)	35.9 (−3.7%)	8 (−1)	11 (−3)
5	275 (-15.6%)	4.1 (-5.1%)	93.1 (+5.7%)	35.8 (−3.9%)	8 (−1)	11 (−3)
6	396 (+21.5%)	4.8 (+9.6%)	80.3 (−8.8%)	40.0 (+7.3%)	19 (+10)	25 (+11)
7	280 (-14.3%)	4.4 (+1.3%)	84.9 (−3.7%)	35.9 (−3.7%)	9 (0)	12 (−2)
8	261 (-20.0%)	3.9 (-9.9%)	92.2 (+4.6%)	39.0 (+4.6%)	16 (+7)	23 (+9)
9	273 (-16.3%)	4.4 (+0.9%)	86.6 (−1.7%)	36.6 (−1.7%)	10 (+1)	13 (−1)
10	266 (-18.5%)	4.0 (-8.0%)	89.9 (+2.0%)	38.0 (+2.0%)	15 (+6)	21 (+7)

*[1] Fxed Ribs: number of fractured ribs,   *[2] Rib Fxs: number of rib fractures

(b)   Linear regression analysis for parametric study of scaled human body

Linear regressions were conducted among the response variables (K_a, F_{max}, D_{max}, and C_{max}), injury variables (Rib Fxs and Fxd Ribs), and predictor variables (W, H, I_{Rc}, and I_{rib}).   Table 5.8 lists the correlation coefficient (R), with bold face values indicating statistical significance (significance level (*p*) value of less than 0.05).

Between the predictor and the response variables, K_a (R = 0.68) was somewhat correlated with W, D_{max} (R = 0.90) was highly correlated with H, and C_{max} (R = −0.72) was somewhat negatively correlated with H.   Additionally, C_{max} was negatively correlated with I_{Rc} (R = −0.86) and with I_{rib} (R = −0.85).   For the impact response variables, no significant correlations were observed.   The injury variables, Rib Fxs and Fxd Ribs, correlated well with the predictor variables I_{Rc} and I_{rib} (R < −0.72) and significantly with the response variable C_{max} (R > 0.93).

Table 5.8: Coefficients of correlation among the body data, impact responses, and injury data.

N=11	W	H	I_{Rc}	I_{rib}
			Predictors	
K_a	**0.68***	-0.19	-0.08	-0.05
F_{max}	0.28	-0.01	-0.25	-0.20
D_{max}	0.56	**0.90****	0.54	0.40
C_{max}	-0.17	**-0.72***	**-0.86****	**-0.85****
Rib Fxs	0.05	-0.55	**-0.74****	**-0.82****
Fxed Fibs	-0.06	-0.59	**-0.72***	**-0.77****

N=11	K_a	F_{max}	D_{max}	C_{max}
			Responses	
K_a				
F_{max}	0.08			
D_{max}	-0.09	0.12		
C_{max}	0.32	0.16	-0.34	
Rib Fxs	0.35	0.26	-0.16	**0.93****
Fxed Fibs	0.29	0.13	-0.21	**0.94****

*: $p<0.05$, **; $p<0.01$

Boldface indicates those cases with $p < 0.05$.

5.5. Discussion

5.5.1. Effects of biomechanical factors on initial apparent stiffness (K_a) and maximum contact force (F_{max}) of the chest

Linear regression analyses were widely adopted to investigate the relationships among the parameters succinctly. Although their functional relationships in real situations were not expressed by linear functions, linear regression analyses could suggest the existence of correlations.

The first series of parametric studies focused on how the assumed stiffness and mass density of the rib cage, chest internal organs, and superficial muscles affected the overall response of the human chest. Based on a linear regression of the first series of parametric studies, the stiffness of the superficial muscles influenced K_a in both frontal and lateral impacts. As muscle activation was not assumed in this study, the effects of muscle tone on the superficial stiffness were not determined. Additionally, a stiffer rib cage would statistically result in higher F_{max} in both frontal and lateral impacts. It was also found that either stiffer material property or greater mass density of internal organs increased F_{max} in frontal impacts, whereas this tendency was not observed in lateral chest impacts.

Eleven simulation models from the second series of parametric studies were used to determine the effect of the body weight (W), height (H), and I_{Rc} and I_{rib} on the model-predicted K_a and maximum contact

force (F_{max}).   Linear regression indicated that the body weight, an inertial parameter, can only explain some of the observed changes in K_a (R = 0.68; see Table 5.8).

K_a was influenced by the mass density (and, consequently, the total weight of the torso) of the superficial muscles.   These results indicated that K_a was mainly influenced by mass and inertial effects.   A parametric study using a lumped model (Lobdell et al. 1973[84]) was reported by Kent et al. (2003b)[65], which would be helpful in gaining a better understanding of these results.   In their study, the dominant contributors of force response at the instantaneous and very early period of impact were the inertia of the frontal chest wall and viscous component of the chest.   On the contrary, the elastic forces of the chest reach only 10% of the whole force magnitude.   The initial apparent stiffness K_a in this study represents the instantaneous force responses, and therefore, the correlation of K_a with the mass density of the superficial muscles and body weight W agrees with the inertial effect after immediate impact.

The changes in the height and I_{Rc} and I_{rib} did not correlate with K_a and F_{max}.   One possible reason is the fact that different tissues were exposed to the pendulum when different model sizes were simulated. Figure 5.8 shows the contact area imposed by the pendulum on the chest wall for the three body sizes (AM95, AM50, and AF05).   The sternum, costal cartilage, and ribs in Figure 5.8 are represented in dark, white, and gray color, respectively.   The figure shows that the entire sternum was in contact with the pendulum for AF05, whereas only a portion of the sternum was impacted in AM95.
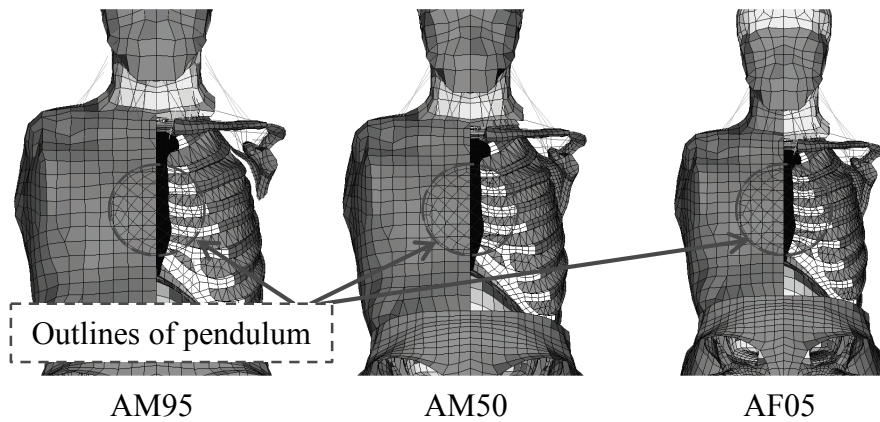
Figure 5.8:   Contact area of the pendulum on the chest for different body sizes (left: large male AM95, center: mid-size male AM50, right: small female AF05)

5.5.2. Effects of biomechanical factors on D_{max} and C_{max}

Based on a linear regression of the first series of parametric studies, a stiffer rib cage would result in less D_{max} in lateral impacts but not statistically significantly in frontal impacts.   It was also found that stiffer internal organs decreased D_{max} in frontal chest impacts.

Table 5.8 shows that D_{max} is significantly correlated with height (R = 0.90), whereas C_{max} is less significantly correlated with height (R = −0.72). C_{max} is highly correlated with I_{Rc} (R = −0.86) and I_{rib} (R = −0.85).   Figure 5.9 shows the negative correlation of C_{max} against I_{Rc}.
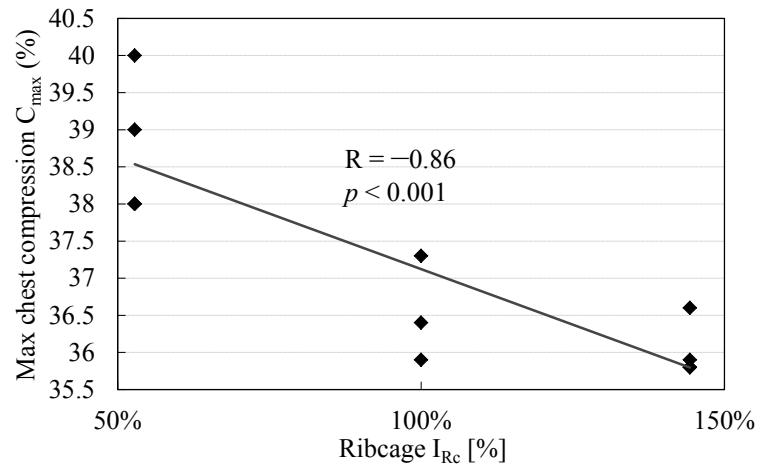
Figure 5.9:   Linear correlation of maximum chest compression ratio to area moment of inertia of the rib cage.

5.5.3. Effects of biomechanical factors on rib fractures

The location and number of rib fractures were predicted using the element elimination method available in LS-DYNA.   The stiffness of the rib cage significantly affected the predicted number of fractured ribs and rib fractures in both frontal and lateral chest impacts, whereas the stiffness of the internal organs and superficial muscles did not affect the number of fractured ribs and rib fractures.   Another interesting correlation that is not very significant but is nevertheless noteworthy was that a heavier chest was likely to have more rib fractures in frontal (R = 0.60 and $p < 0.001$) and lateral (R = 0.49 and $p < 0.05$) impacts.   Wong et al. (1983)[163] conducted *in-vitro* impact tests on tibiae obtained from human cadavers and found that the mass density of human tibiae correlated with the wave velocity based on the stiffness of the material.   Similarly, Bouxsein et al. (1999)[11] noted a significant correlation between the bone mineral density (BMD) and the strength of the proximal femur under dynamic impact loading conditions.   Although no literature has explained the correlations between the BMD and the impact responses of the chest to the best of the author's knowledge, it can be assumed that the BMD plays an important role in high-speed impacts.   The current study aims to partially verify this assumption by exaggerating the effect of mass density using numerical simulations.   As expected, the effect of mass density is minimal based on the impact scenarios selected.   Therefore, we believe that the current study makes certain contributions to the existing literature because our findings are more intuitive and contrast those previously reported in the literature.   In addition, a change in the mass density of superficial muscles correlated with the number of rib fractures in frontal impacts, and that of internal organs corresponded to the number of rib fractures in lateral impacts.

No statistical significance was observed between the model-predicted numbers of rib fractures and fractured ribs and the global response variables K_a, F_{max}, and D_{max}.   Additionally, when only rib cage bony fractures were considered as the injury variable, the results of this study did not indicate any correlation with the weight or height of the human body.

Figure 5.10 shows the correlations of C_{max} with the numbers of rib fractures (RFxs) and fractured ribs (FxdR). C_{max} could predict the numbers of RFxs and FxdR accurately with an R value of 0.93 and 0.94, respectively.   This finding agreed with another series of experimental studies (Kent et al., 2003a[64]).   In cadaveric studies, the Abbreviated Injury Scale (AIS) for the chest injury severity was derived from the number of fractured ribs.   Therefore, the results from this study suggest that the C_{max} would be a better predictor when estimating the risk of chest injury.
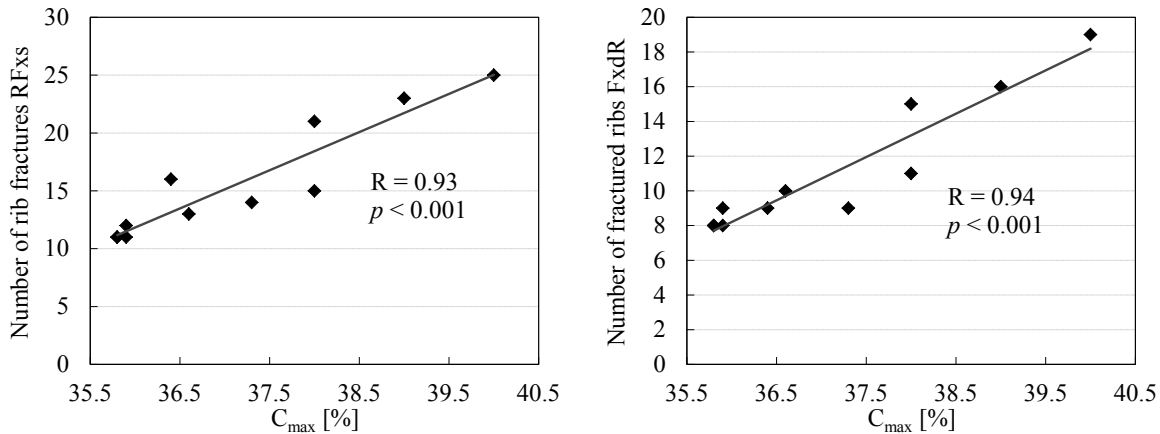
Figure 5.10: Linear correlations of the number of rib fractures and fractured ribs with the maximum chest compression ratio

The finding of a linear relationship between D_{max} and height agrees in part with the scaling method proposed by Eppinger et al. (2000)[28] that stated that an increase in size results in an increase in the chest deflection.   If the scaling method was correct, C_{max} should not be influenced by body size effects because it is already normalized by the initial chest depth.   However, this study revealed the negative correlation of C_{max} with the height.   In addition, C_{max} showed a more significant correlation with I_{Rc}.   Our results showed that the height and cross-sectional properties of the rib cage both affect C_{max}.

5.5.4. Effects of area moment of inertia of the rib cage or rib alone

I_{Rc} and I_{rib} are better predictors when calculating C_{max}, which correlated significantly with the numbers of rib fractures (R = 0.93) and fractured ribs (R = 0.94).   Furthermore, C_{max} correlated significantly with I_{Rc} (R = −0.86) and I_{rib} (R = −0.85).   Additionally, the coefficients of correlation are all greater than 0.72 when correlating I_{Rc} and I_{rib} with the numbers of rib fractures and fractured ribs (Table 5.8). Consequently, it can be concluded that I_{Rc} and I_{rib} affects the chest response and bony injury variables. However, the area moment of inertia of the ribs (I_{rib}) has not been routinely reported to be significant in the field of impact biomechanics, and therefore, the geometric properties of the rib were not available in whole body impact tests.   It is recommended that future whole-body tests should include measurements of the rib area moment of inertia as an anthropometric parameter to normalize the biomechanical responses and tolerances of the human body.

5.5.5. Limitations

To consider the safety of occupants with various body sizes from 5th to 95th percentiles, it would be necessary to obtain experimental corridors for these two groups.   However, it is difficult to obtain cadaveric specimens of a specific size in experimental studies.   Therefore, only the baseline 3D human model was validated against the 50th percentile human cadaveric data.   The baseline model was scaled to represent different height and body weight combinations, without validation, to determine the effect of various biomechanical parameters on the overall impact responses.   Future studies need to address the validation of body size effects.

This study provides some critical data that explain the effect of body weight, height, and I_{Rc} on K_a, D_{max}, F_{max}, and C_{max} to better understand the blunt impact response of the chest.   However, this study considered only frontal pendulum impacts without a belt or distributed loading conditions, assumed no gender or age differences in terms of material properties, and did not consider other response variables such as the viscous criterion (VC).   Therefore, further studies using cadavers tested under other loading conditions are needed to improve our understanding of the chest injury biomechanics.

The LS-DYNA code has very sensitive ranges for the mesh size, and the assumed cortical bone failure strain of 3% exceeds the reported experimental value of 2% by 50%; therefore, the confidence in the results can be improved by performing sensitivity analyses.   Similarly, the assumed cancellous bone failure strain of 10.3% was arbitrarily chosen, and it is necessary to perform sensitivity analyses on this parameter by varying the failure strain from 3% to 23% (see section 5.2), as reported in experimental studies. Additionally, it may be necessary to refine the models with a more accurate moment of inertia, as the current model used a value of 131.4 mm^4 that is somewhat lower than the experimentally obtained value of 209.6 mm^4 (Chapter 4).   These refinements will add to the confidence in the results and conclusions of the present study.

In this chapter, the study assumed that all body types have a similar body structure to mid-sized males even though the subjects were small females or large males.   However, there is a wide variety in human body proportions (Friess and Corner, 2004[34]).   Other parameters that may affect the overall chest response should be considered.   Instead of anthropometric data of the body weight, height, and area moment of inertia in this study, the subject's body mass index (BMI) must be considered in future studies.   Arbabi et al. (2003)[3] reported that BMI affects the maximum AIS of automotive crash injuries.   In their study, overweight occupants had a significantly low injury severity score and MAIS in the abdomen owing to the cushioning effect provided by their bodies.   A future model on impact biomechanics would need to consider obesity and its role in impacts.

5.6. Conclusions

The predictions of the numerical simulations depend on the assumptions and parameters used in modeling the physical system.   Characterizing the sensitivity of the model to the assumed values of the parameters is an essential step in evaluating the usefulness of the model.   In this case, we have shown how

the predicted values of rib fractures depend on specific assumptions regarding material parameters (stiffness and density).   The effects of variations in other parameters such as the location and duration of impact should be characterized similarly and be used to evaluate this numerical injury model.

The following specific conclusions are drawn from this study based on two series of parametric studies; a total of 106 numerical simulations of frontal and lateral pendulum impacts and 11 numerical simulations of frontal pendulum impacts using the AM50 THUMS model were performed toward this end:

1.   The K_a was significantly affected by changing the mass density of the entire chest, especially of the superficial muscles, and the stiffness of the superficial muscles.   This finding was associated with the effects of the weight of the human body, which somewhat correlated with the K_a and F_{max}.

2.   The stiffness and mass density of the internal organs noticeably affected the F_{max} and deflection in frontal impacts.   However, this effect was not observed in lateral impacts.

3.   The height of the human body has a significant positive correlation with the D_{max} and a negative correlation with the C_{max}.   All existing scaling methods assumed that the C_{max} is constant, whereas the current study shows that it varied according to the body parameters.

4.   The weight of the whole chest had some effect on the number of rib fractures in both frontal and lateral impacts.   On the other hand, the weight and height of the whole human body did not show any correlation with any injury variable considered in the second series of parametric studies.

5.   The stiffness of the rib cage significantly affected the number of rib fractures in both frontal and lateral impacts.   More importantly, I_{Rc} and I_{rib} significantly correlated with the C_{max} and the number of rib fractures and fractured ribs.   Based on these findings, it can be concluded that I_{Rc} or I_{rib} affects the response and injury variables.

Chapter 6   Development of a 5th Percentile Female Chest Model

6.1. Introduction

Several key findings obtained from previous chapters suggested that the chest responses and injuries were influenced by the specimens' anthropometry, such as body weight and height. However, scaling methods cannot be applied to the development of a small female chest model, because the maximum chest compression ratio (C_{max}), which all existing scaling methods assumed as a constant variable, varied according to the height of the human body or area moment of inertia of the rib cage. In addition, the chest depth and cross-sectional geometry of the ribs did not associate with any anthropometric data of the human body. According to Chapter 4, the cross-sectional geometry of the ribs indicated significant gender differences, whereas the chest depth showed no gender differences.

Moreover, Chapter 5 indicated that the cross-sectional geometry affects C_{max} and the numbers of rib fractures and fractured ribs. As C_{max} was a good indicator of gender difference in terms of the impact response of the chest, it is important to consider the cross-sectional properties of the rib cage. In addition, owing to the inhomogeneous and complex nature of the impact responses of the chest, validation test data must be selected from female subject data.

A small-sized female driver has a greater risk of automotive-related injuries than a mid-sized male driver (see Chapter 1). American Female 5th percentile (AF05) was designed to be representative of a small-sized female. Therefore, this chapter aims to develop a new 5th percentile female chest model based on the knowledge obtained from previous chapters. Only the female subject data reported by Nahum et al. (1970)[98], Kroell et al. (1971[76] and 1974[77]), Viano (1989)[154], Talantikite et al. (1998)[141], Chung et al. (1999)[17], and Wilhelm (2003)[161] were used for validating the AF05 model developed in this study.

6.2. Methods

A 5th percentile small female chest model (FEM-5F) was developed based on a small female finite element (FE) model, Total HUman Model for Safety (THUMS)-AF05 occupant version 1.0β (Kimpara et al. 2002[67]) integrated with internal organ models available in the Wayne State University Human Thoracic Model (WSUHTM: Wang, 1995[158]; Shah et al., 2001[134]).

6.2.1. Anthropometry and mesh geometry

(a) Anthropometrical data

Cerney and Adams (2004)[14] reported significant overall differences in terms of the body shape between males and females as well as differences in the manner in which the body shape changes with respect to body size based on landmark-based geometric morphometric methods and North American data

from the Civilian American and European Surface Anthropometry Resource (CAESAR).   According to their conclusions, gender differences have not been carefully managed in the field of biomechanics.   It is essential that any new anthropomorphic test devices (ATDs) and computational models of the human body should consider gender differences not only in terms of the body size but also the body shape.   Figure 6.1 shows skeletal gender differences, especially in the thoracic and pelvic regions (Sato, 1990[129]; Yokochi, 1996[167]). According to Gray's Anatomy (Clemente, 1985[19]), the female chest has less volume and a shorter sternum in comparison with that of a male, whereas the female pelvis is more open than that of a male to facilitate parturition.   Furthermore, the upper margin of the sternum for a female is located at a level of around the third thoracic vertebra, whereas that of a male is located near the second thoracic vertebra.   Lastly, the upper ribs are more movable in females to permit greater enlargement of the upper thorax.   Thus, it is very important to include female-specific parameters in the FEM-5F.
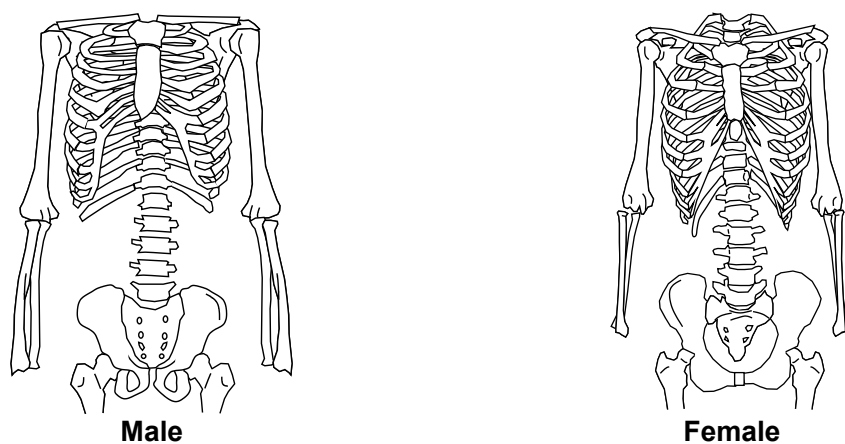
Male   **Female**

Figure 6.1:   Geometric comparison of male and female skeleton (Sato, 1990; Yokochi, 1996)

The anthropometry and posture of FEM-5F were taken from Schneider et al. (1983)[132] and Robbins (1983)[124] to simulate a seated 5th percentile female occupant.   The other dimensions were based on the scaling of a commercially available 3D FE model of the whole human body THUMS-AM50 (Version 1.52) reported by Iwamoto et al. (2002)[60] with modifications to reflect gender differences in the thoracic and pelvic regions.   However, gender differences were not considered for other regions such as the head, neck, and extremities in this study.   A preprocessor, HyperMesh Version 6.0 (Altair Engineering, Inc., Troy, MI), was used for mesh generation.

The skeletal geometry of the female chest, obtained from the View Point database, was not the same as that of a 5th percentile female.   Using the distances between landmark points (for example, the upper sternum, 10th rib edge point, etc.) reported by Robbins et al. (1983)[124], interconnected bones were individually scaled to fit the 5th percentile female anthropometry before meshing was performed.

Figure 6.2 shows frontal and lateral views of the skeleton of the FEM-5F used in this study.   The segmental lengths in the sagittal plane reported by Robbins (1983)[124] were used in the current model; these are listed in Table 6.1.
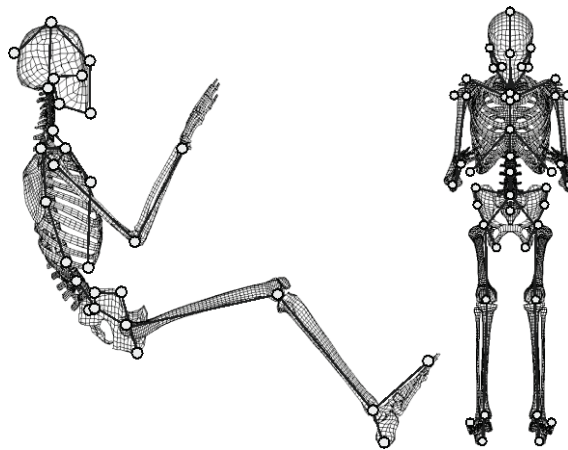
Figure 6.2:   Frontal and lateral views of the skeleton of the FEM-5F

Table 6.1:   Summary of the segment length of FEM-5F

Segment	Length [m]
Head	0.148
Neck	0.090
Thorax	0.302
Lumber	0.209
Leg	0.771
Arm	0.486
Total height	1.520

In Table 6.2, the masses of the thorax, abdomen, and pelvis of the FE model were combined into one lumped torso mass because natural boundaries do not exist among these segments.   Figure 6.3 shows the enlarged view of the thoracic and pelvic regions of the FEM-5F.

Table 6.2:   Mass distribution reported by Robbins (1983) and used in the FEM-5F

Segment	Robbins (1983) [kg]	FEM-5F [kg]
Head	3.697	3.751
Neck	0.601	0.509
Thorax	11.944	
Abdomen	1.610	20.890
Pelvis	6.976	
R Upper Arm	1.124	1.102
R Lower Arm	1.138	1.008
R Upper Leg	5.914	5.896
R Lower Leg	2.360	2.366
R Foot	0.638	0.637
Total	47.176	47.168
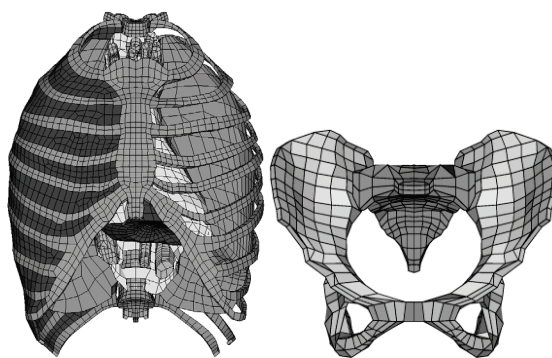
Figure 6.3:   Mesh geometries of FEM-5F for the chest and pelvis portions of the 5th percentile female

(b) Thoracic internal organs

      The geometry of the internal organs in the thoracic cavity, such as that of the heart, lungs, aorta, and veins, was scaled from the WSUHTM to fit the skeleton of the FEM-5F.   When needed, the mesh was modified to improve its quality in order to avoid any potential problems during the numerical simulation. Figure 6.4 shows a frontal view of the model with internal organs integrated.
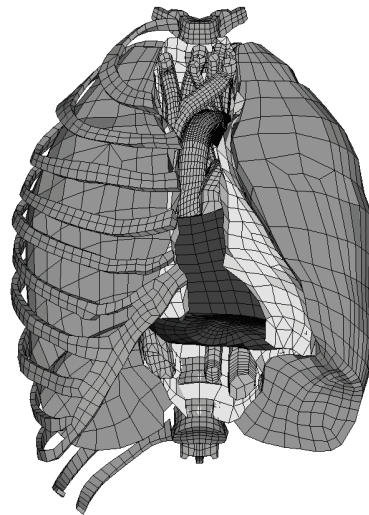
Figure 6.4:   A frontal view of rib bones and internal organs in the thoracic cavity of the FEM-5F

(c) Superficial geometry

      Figure 6.5 shows an oblique view of the superficial geometry obtained by Schneider et al. 1983[132]. Superficial geometrical data were obtained from the computer-aided engineering (CAE) data of a small female.   This superficial geometry coincided with the key anthropometric information of the FEM-5F and provided a smooth superficial surface for the skin and superficial muscles.
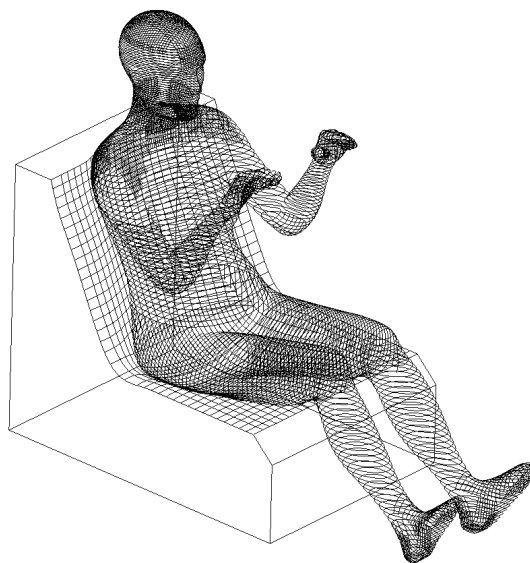
Figure 6.5:   An oblique view of superficial geometry obtained by Schneider et al. (1983)

6.2.2. Structure

Figure 6.6 shows an oblique view of the entire small female model.   The skin on the right part was removed to reveal the skeleton of the model.   The entire model consists of 85,499 nodes and 116,733 elements, including 47,348 solid, 66,685 shell, 588 bar, and 2,112 seatbelt as tension only bar elements.
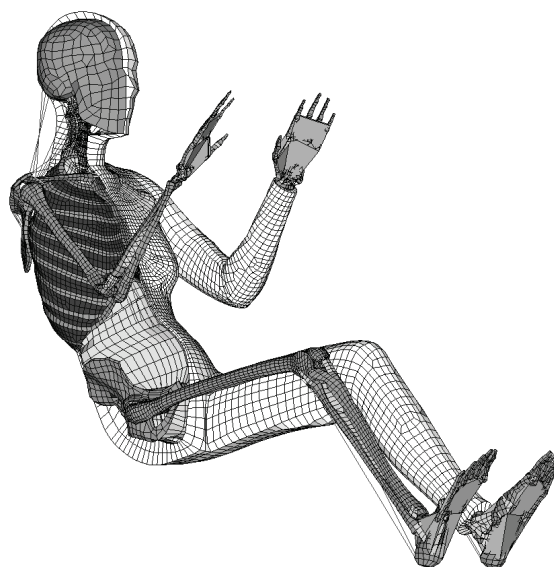
Figure 6.6:   An oblique view of the complete FEM-5F

(a)   Rib cage

The rib cage consists of the spine, sternum, costal cartilage, and 12 pairs of ribs.   The ribs were modeled using one layer of shell elements and one layer of solid elements corresponding to cortical and cancellous bones, respectively.   The length of each elastic-plastic shell element representing the cortical bone of the ribs has a minimum dimension of 2.5 mm to ensure a reasonable time step, while a uniform thickness of 0.7 mm was assumed.

When using explicit FE methods, the minimum time step for each element is governed by its size and material properties.   The smallest element with the stiffest property controls the initial time step of the entire model.   To achieve the same minimum time step of 1 μs for the entire model, the number of elements was proportionally reduced in the FEM-5F model, in comparison with the THUMS 50th percentile male model, so that the critical size of all elements remained 2.5 mm or larger.   According to the findings from Chapter 4, the cross-sectional area and area moment of inertia of the 6th and 7th ribs at the mostly straight portion of the FEM-5F were 18.3 ± 1.8 mm^2 and 76.9 ± 33.5 mm^4, respectively.   The articulations of the rib cage, which included the sternocostal joints and interchondral articulations, were treated as if they were directly connected, similar to those reported by Lee and Yang (2001)[80].   However, the costovertebral joints, which are the costotransverse joints between the ribs and the vertebral body, were modeled as junctura fibrosa that is tightly bounded by the ligaments.   Diarthrodial joints were modeled by defining a contact interface layer between opposing bones with a coefficient of friction of zero to simulate joint articulations without cartilage modeling.   Joint motions were controlled by associated ligaments.   All ligaments were modeled

using tension-only elastic membrane or bar elements.   The vertebrae were modeled as rigid bodies, and intervertebral discs and intercostal muscles were modeled using linear elastic solid elements because vertebral injuries were seldom reported during chest impact tests.

(b) Internal organs

The structures of the internal organs in the thoracic cavity, including the heart and lungs, were the same as those used in the WSUHTM.   The thorax and abdomen were separated by the diaphragm.   The pericardium, which restricts the horizontal motion of the heart, was combined with the pleural reflection on the mediastinum and was attached to the diaphragm directly.   The pleural reflection on the mediastinum was modeled as a single layer of membrane elements.   The ligamentum arteriosum, which is a fibrous connection between the aorta and the pulmonary trunk, was modeled using one layer of membrane elements. The pulmonary trunk bifurcates into the right and left pulmonary arteries and conveys deoxygenated blood to the lungs.   The aortic wall was considered to be single layered and isotropic, and the descending aorta was assumed to be of constant diameter.   The abdominal internal organs were represented by two simplified lumped solid elements, as reported by Huang et al. (1994a)[53].

(c) Skin and superficial muscles

Skin and superficial muscles were modeled using 1–3 layers of solid and membrane elements.   In this study, superficial muscles were directly connected to the rib cage.   In the abdominal area, contact interfaces were defined between the superficial muscles and the lumped solid elements representing abdominal organs.

6.2.3. Material modeling

Material models of FEM-5 were usually comparable with the THUMS-AM50 model (Chapter 5).

(a) Bones

LS-DYNA material type MAT_123, an elastic-plastic fully integrated shell element (shell element type 16) with a failure material model, was used to simulate the cortical bone of the ribs and sternum. Young's modulus of 9.86 GPa, yield stress of 66.66 MPa, and Poisson's ratio of 0.3 were assumed for the cortical bone of ribs (Kimpara et al., 2004[69]).

LS-DYNA material type MAT_024, an elastic-plastic fully integrated selectively reduced (S/R) solid element (solid element type 2) with damage, was used to model the cancellous bone of the ribs and sternum.   Young's modulus of 40 MPa, yield stress of 1.8 MPa, and Poisson's ratio of 0.45 were assumed. The material properties used for all other bones (scapular, clavicle, pelvis, etc.) in the FEM-5F model were based on previous modeling studies mentioned above.

(b) Cartilage

The costal cartilage was modeled using the same material law as the cancellous bones with Young's modulus of 49 MPa, yield stress of 4.9 MPa, and Poisson's ratio of 0.4.

(c) Soft tissues

        LS-DYNA material type MAT_057, a low-density foam material with a constant stress solid element (solid element type 1), was used to model the lungs and fat/muscle; this was the same material as that used by Wang (1995)[158] and Shah et al. (2001)[134].   Ruan et al. (2003)[128] used the linear viscoelastic material law to represent all internal organs whereas Lee and Yang (2001)[80] used the same law with nearly incompressible material property to model abdominal solid organs.   Because the lungs are not solid organs, MAT-057 was considered more suitable.   The properties of the lungs were taken from Wang (1995)[158].

        LS-DYNA material type MAT_006, a linear viscoelastic material model, was used to represent the heart and upper and lower lumped abdominal internal organs.   LS-DYNA material type MAT_001, a linear elastic shell element with a Belytschko-Tsay shell model (shell element type 2), was used to model the aorta, veins, diaphragm, and ligaments; material properties were taken from those reported by Shah et al. (2001)[134].   Fluid elements representing blood were incorporated inside the aorta to simulate pressure changes due to impact based on the method used by Shah et al. (2001)[134].   A summary of the material properties (Nishigaki et al., 2000[108]; Plank and Eppinger, 1991[120]) is shown in Table 6.3 and Table 6.4.

Table 6.3:   Material properties of the solid models

	Mass density (kg/m^3)	Young's modulus E (MPa)	Poisson ratio	Yield stress (MPa)	Reference
Rib's cancellous bone	1,000	40.0	0.45	1.8	Abe et al. (1996) Yamada (1970)
Sternum's cancellous bone	1,000	40.0	0.45	1.8	
Costal cartilage	1,000	49.0	0.4	4.9	
Intercostal muscle	1,000	1.0	0.3	-	
Vertebra bone	2,000	11,000.0	0.3	-	
Intervertebral disc	1,000	12.7	0.34	13.3	Nishigaki et al. (2000)
Lung	600	0.01			Wang (1995)
Fat/Muscle	900	0.50			Lee and Yang (2001)
		Bulk Modulus K (MPa)	Shear Modulus G_0 (MPa)	G_∞ (MPa)	
Heart	1,000	1.33	0.22	0.075	Ruan et al. (2003)
Upper Abdomen	1,100	0.65	0.067	0.022	Lee and Yang (2001)
Lower Abdomen	1,350	0.15	0.015	0.005	Plank and Eppinger (1991)

Table 6.4:   Material properties of the shell/membrane models

	Mass density (kg/m^3)	Young's modulus E (MPa)	Poisson ratio	Yield stress (MPa)	Thickness t (mm)	Reference
Rib's cortical bone	2,000	9,860.0	0.3	66.7	0.70	Rib test
Sternum's cortical bone	2,000	9,860.0	0.3	66.7	1.0	Rib test
Aorta	4,000	4.0	0.4		3.0	Shah et al. (2001)
Pulmonary Trunk	2,000	4.0	0.4		3.0	
Vena cave	2,000	20.0	0.4		3.0	
Pulmonary veins	2,000	20.0	0.4		3.0	
Trachea	2,000	10.0	0.4		3.0	
Esophagus	2,000	3.0	0.4		3.0	
Ligaments	2,000	20.0	0.4		10.0	
Diaphragm	1,000	2.0	0.4		2.0	
Pleural or Mediastinum membrane	1,000	13.0	0.4		1.0	
Cervical diaphragm	2,000	1.0	0.4		2.0	
Skin	900	31.5	0.45		0.1	

6.2.4. Experimental data set for model validation

Many blunt impact tests have been conducted to determine the force-deflection corridors of the human chest (Nahum et al., 1970[98]; Kroell et al., 1971[76]; Stalnaker et al., 1973[137]; Kroell et al., 1974[77]; Cesari et al., 1981; Viano, 1989[154]; Talantikite et al., 1998[141]; Chung et al., 1999[17]).   Blunt impacts have been suggested to be a better test method when assessing the stiffness of the chest compared to sled tests because in blunt impacts with a stationary subject, it is not necessary to account for the kinetic energy input of the test subject (Kimpara et al., 2002[67]).

(a)   Frontal pendulum impact

A total of 35 frontal chest pendulum impact tests have been conducted by Nahum et al. (1970)[98] and Kroell et al. (1971[76] and 1974[77]).   This data series was the same as that used for validating the FE model in Section 5.2.3 of this thesis.   However, the data reported by Stalnaker et al. (1973)[137] were not used for model validation because a mechanical stop was used in their study, making it difficult to assess the maximum chest deflection (Neathery, 1974[104]).   Of all 35 tests in the literatures, 9 were conducted using female unembalmed cadavers.   First, a Student's t-test was conducted to investigate gender differences in the obtained data.   It was found that female subjects were statistically shorter, lighter, and smaller in terms of chest depth than males ($p < 0.01$), whereas the subjects' ages were statistically comparable between males and females ($p > 0.05$).   The mass of the impactor used to strike these female subjects ranged from 1.59 to 23.6 kg, and the impact velocity ranged from 4.02 to 13.23 m/s.   It should be noted that the viscous criterion was not calculated in these tests because it was proposed only in the 1980s (Viano, 1989[154]), a long time after these papers were published.

According to Robbins (1983)[124], the 5th percentile small female had a height of 1.52 m and weight of 47.2 kg.   Thus, none of these nine subjects tested fits the 5th percentile female definition.   When a ±10%

difference in height and a ±15% difference in weight were considered, i.e., height of 1.37–1.67 m and weight of 40.1–54.3 kg, subject Nos. 10FF (Nahum et al., 1970[98]) and 30FF (Kroell et al., 1974[77]) have somewhat comparable anthropometry to a 5th percentile female. Table 6.5 lists the subject information, impact conditions, and chest responses of the two tests conducted using small female subjects referred from Nahum et al. (1970)[98] and Kroell et al. (1974)[77].

Table 6.5:   **Cadaver data, impact conditions, and test results from the frontal blunt impact test data (Nahum et al., 1970; Kroell et al., 1974)**

Cadaver data				Impact Conditions		Chest Responses			
No.	Sex	Age (y)	Height (m)	Weight (kg)	Mass (kg)	Velocity (m/s)	F_{max} (kN)	D_{max} (mm)	C_{max} (%)	NRF
Nahum et al. (1970)									
10FF	F	82	1.60	43.1	19.3	4.92	1.80	65.5	38.9	12
Kroell et al. (1974)									
30FF	F	52	1.56	40.8	1.59	13.23	4.57	55.9	31.1	3

(b)   Lateral pendulum impact

At least four series of lateral pendulum chest impacts have been reported by Cesari et al. (1981)[15], Viano (1989)[154], Talantikite et al. (1998)[141], and Chung et al. (1999)[17]. Data reported by Cesari et al. (1981)[15] were excluded because they did not report the method used to determine the chest deflection, and the pendulum was aimed directly at the arm when testing only female subjects. The pure lateral impact data reported by Viano (1989)[154] was also excluded because the detailed test results were not presented in his paper. Additionally, the data reported by Chung et al. (1999)[17] were not included in this study because none of the specimens fit the small female size defined by Robbins (1983)[124].

Talantikite et al. (1998)[141] conducted lateral chest pneumatic pendulum impact tests using a total of 11 unembalmed cadavers. The test specimens were seated on a Teflon sheet glued to a rigid table. The center of the impactor was aligned to the right side of the chest at the same vertical height as the xiphoid process. The impactor had a mass of either 12.0 or 16.0 kg, diameter of 150 mm, and average velocity of 10.9 m/s with a range of 8–12 m/s. The tests were filmed at 1,000 fps (frames per second) from behind the subject. The displacement of the impactor with respect to the spine at the eighth vertebra body was measured to calculate the half chest deflection. When a ±10% difference in the height and weight of the 5th percentile female was considered, test subject No. LCT04 reported by Talantikite et al. (1998)[141] was somewhat comparable to the 5th percentile female. Table 6.6 lists the relevant information of the cadaver, impact conditions, and chest responses for lateral chest impacts obtained from one female test subject reported by Talantikite et al. (1998)[141].

(c) Oblique pendulum impact

A series of 15 oblique pendulum chest impact tests was reported by Viano (1989)[154].   The cadavers used in this series did not show any statistical gender difference in terms of height or weight.   Among the 15 cadaveric pendulum impact tests, 3 were conducted using two female test specimens.   One female specimen was used in Test No. 11 and two tests, No. 29 and No. 33, were conducted on the second specimen.   Because the author did not find any bony injuries after Test No. 29, Test No. 33 was conducted using the same specimen.   In these oblique impact tests, the impactor was rotated 30° anteriorly so that the axis of the applied force passed through the center of gravity of the torso.   The center of the impactor was aligned at the same vertical height as the xiphoid process.   The pendulum had a mass of 23.4 kg and diameter of 150 mm.   The impact velocities were categorized into three distinct groups—4.5, 6.7, and 9.4 m/s—for determining the corridor at each velocity.   Test No. 29 (5.2 m/s) was conducted at low speed; Test No. 11 (6.71 m/s), at medium speed; and Test No. 33 (9.7 m/s), at high speed.   These test setups resulted in compression without any rib cage rotation being applied to the chest.   Multiple rib fractures were frequently observed.

When a ±10% difference in height and ±15% difference in weight was considered, the subject used for Test No. 29 and No. 33 (Viano 1989[154]) had somewhat comparable anthropometry to the 5th percentile female.   It should be noted that the first female subject (Test No. 11) was much larger than the 5th percentile female.   The relevant information for oblique chest impacts obtained from the two female tests reported by Viano (1989)[154] are presented in Table 6.6.

Table 6.6:   Cadaver data, impact conditions, and test results from lateral (Talantikite et al., 1998) and oblique (Viano, 1989) blunt impact tests

No.	Sex	Age (y)	Height (m)	Weight (kg)	Mass (kg)	Velocity (m/s)	F_{max}[†1] (kN)	D_{max}[†2] (mm)	C_{max}[†3] (%)	VC_{max}[†4] (m/s)	NRF[†5]
Cadaver data					Impact Conditions		Chest Responses				
Lateral impact, Talantikite et al. (1998)											
LCT04	F	93	1.57	43	12.0	6.00	1.76	72.6	28.8	1.36	16
Oblique impact, Viano (1989)											
29	F	52	1.57	53.1	23.4	5.20	2.67	91	31.9	0.89	0
33	F	52	1.57	53.1	23.4	9.70	5.67	151	53.0	2.66	12

[†1] F_{max}: Maximum chest force,   [†2] D_{max}: Maximum chest deflection,

[†3] C_{max}: Maximum chest compression ratio,   [†4] VC_{max}: Maximum viscous criterion,

[†5] NRF: Number of rib fracture

(d) Ballistic breast impact

Wilhelm (2003)[161] conducted a series of six breast impact tests using four unembalmed female test specimens.   The cadaver was seated in an erect position on the flat surface of a rigid table, held upright with a harness around the upper chest and shoulders, and allowed to swing freely in the direction of impact.   The ballistic impact test was conducted using a 140-g stiff baton with a diameter of 37 mm and length of 100 mm

fired at an average velocity of 40 m/s.   The total mass of the baton ranged from 150 to 152 g, including the mass of the accelerometer and cable.   The impact was aimed at the transition region of the breast, i.e., above the peak of the breast in the slope of the breast, at an approximate angle of 30°.   A Kodak HG100K video camera recorded the event at 20,000 fps.   Backlighting was used to illuminate the bobbers on the rib mounts as well as those on the impactor.   Chest deflection was calculated from the distance between markers on the impactor and rib mounts from video analysis using the Sensors Application Inc. (SAI) Image Express motion analysis software (Motion Engineering Company, Inc., Indianapolis, IN).   The force was obtained from the product of the instantaneous acceleration of the impactor and the impactor mass.   Breast chest impact corridors were generated from the force-time, deflection-time, and force-deflection curves.   Table 6.7 lists the relevant information of the cadaver, impact conditions, and the chest responses for ballistic breast impacts obtained from Wilhelm (2003)[161].

Table 6.7:   Cadaver data, impact conditions, and test results from ballistic impact tests (Wilhelm 2003)

| No. | Sex | Cadaver data | | | Impact Conditions | | Chest Responses | | NRF |
		Age (y)	Height (m)	Weight (kg)	Mass (g)	Velocity (m/s)	F_{max} (kN)	D_{max} (mm)	
30670R	F	74	1.56	72.5	152	39.63	3.72	65	0
30750R	F	66	1.68	73.4	152	39.54	-	94	3
30750L	F	66	1.68	73.4	152	40.35	6.32	73	3
304R	F	82	1.58	48.6	152	38.43	4.82	86	5
432R	F	85	1.56	52.5	152	42.98	-	84	5
432L	F	85	1.56	52.5	150	43.49	4.64	101	5

6.2.5.   Simulation conditions

A total of six simulations were prepared for the validation of FEM-5F.   The impact force and chest deflection time histories were calculated using a commercially available FE solver, double precision LS-DYNA 970 revision 5434a (LSTC, Livermore, CA), using an Advanced Micro Devices (AMD) Opteron 64-bit-based computer running Linux operating system.   Post-processing of the simulation results was performed using the LS-PREPOST post-processor (LSTC, Livermore, CA.).   For pendulum chest impact simulations, the model-predicted results were sampled at 10 kHz and filtered using an Society of Automotive Engineers (SAE) digital low-pass filter at a channel frequency class (CFC) of 1,000 Hz (SAE J211, 1994). For the breast ballistic chest impact, a sampling rate of 100 kHz and low-pass filter of 6 kHz were used (Wilhelm, 2003[161]).

6.3. Results

6.3.1. Frontal pendulum impact

For the frontal pendulum impact validation of the model, test No. 10FF (Nahum et al., 1970[98]) and No. 30FF (Kroell et al., 1974[77]) were simulated. These two experiments were selected because the basic anthropometry of the test subjects was similar to that of a 5th percentile female.

Figure 6.7 shows the model-predicted overall kinematics from 0 to 40 ms at an interval of 10 ms for simulating a frontal pendulum chest impact at 4.92 m/s (Nahum et al., 1970[98]). In this simulation, the pendulum reached its maximum penetration and started to rebound at 21 ms. Figure 6.8 illustrates the distortion of the chest internal organs in a transverse section through the mid sternum. It can be observed that the energy delivered by the pendulum passed through the skin, superficial muscle layer, and rib cage and then transferred to the heart and lungs. Figure 6.9 shows the maximum principal stress contours of the rib cage and the locations of rib fracture at 21 ms, when the chest compression reached its maximum. In this figure, darker contours represent higher stresses.

Figure 6.10 and Figure 6.11 show comparisons of the chest force-deflection curves between those obtained experimentally (dotted lines) and those predicted by the FEM-5F (solid lines) when simulating the test conducted using subject No. 10FF reported by Nahum et al. (1970)[98] and subject No. 30FF reported by Kroell et al. (1974)[77], respectively. The model predictions matched the experimental results reasonably well. Additionally, the numbers of model-predicted rib fractures, eight for No. 10FF and five for No. 30FF, were also close to the numbers observed experimentally, 12 and 3, respectively.

t = 0 ms

t = 10 ms

t = 20 ms

t = 30 ms

t = 40 ms
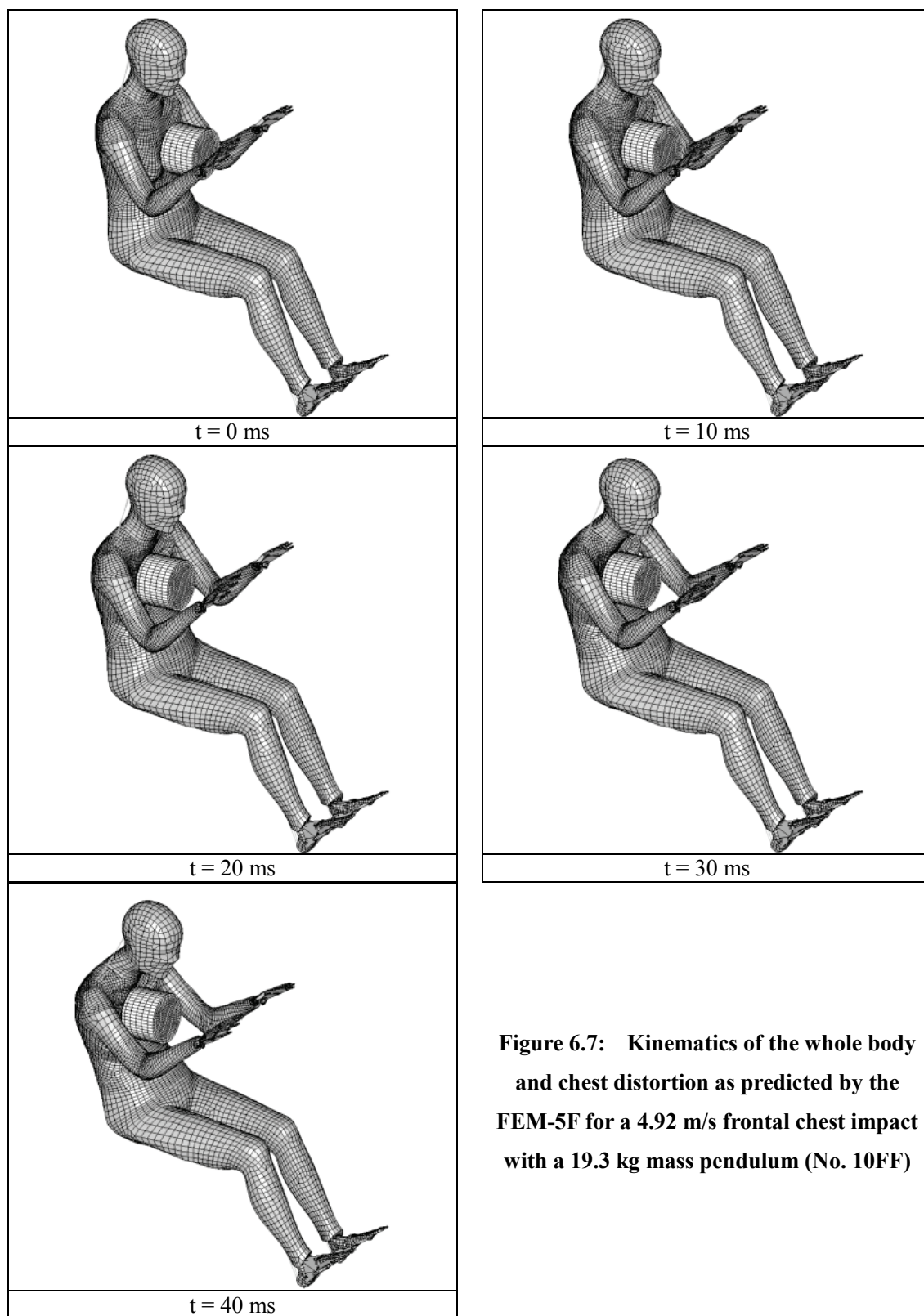
Figure 6.7:   Kinematics of the whole body and chest distortion as predicted by the FEM-5F for a 4.92 m/s frontal chest impact with a 19.3 kg mass pendulum (No. 10FF)

t = 0 ms

t = 10 ms

t = 20 ms

t = 30 ms

t = 40 ms
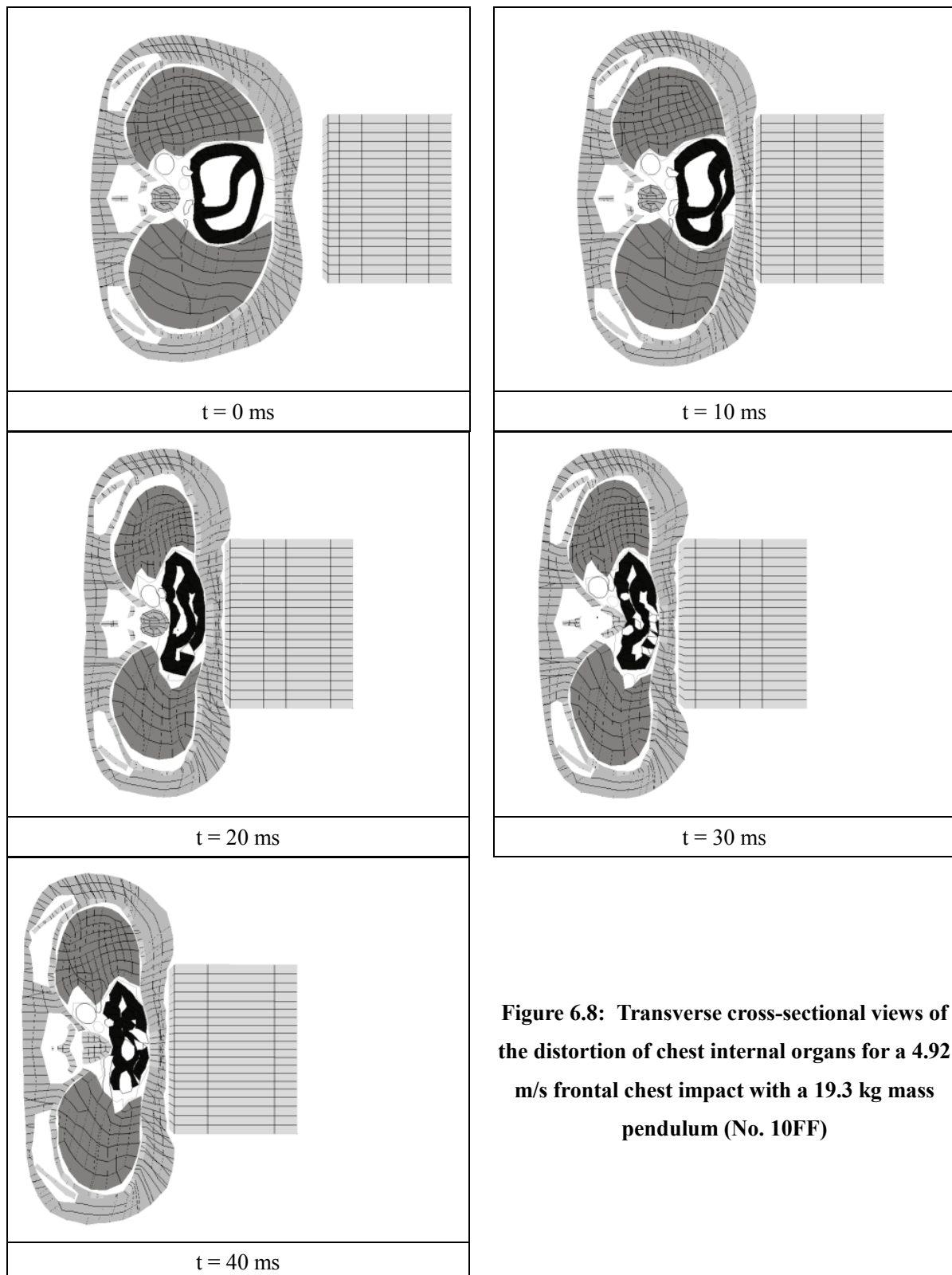
Figure 6.8: Transverse cross-sectional views of the distortion of chest internal organs for a 4.92 m/s frontal chest impact with a 19.3 kg mass pendulum (No. 10FF)
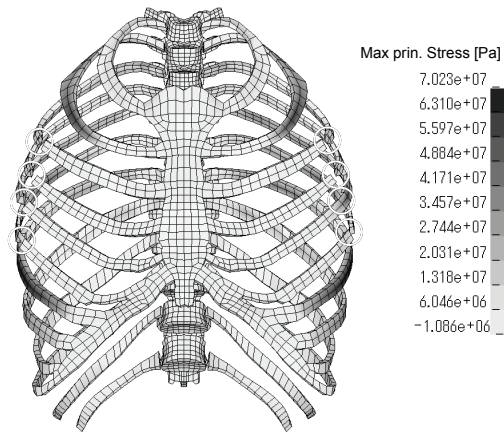
Figure 6.9:   A frontal view of the rib cage distortion showing the maximum principal stress contours and the locations of rib fracture at 21 ms for a 4.92 m/s frontal chest impact with a 19.3 kg mass pendulum (No. 10FF, Nahum et al. 1970)

Figure 6.10: Comparison of the force-deflection response of a frontal chest impact.   The solid line indicates the FEM-5F output and the dotted line, the cadaver test result for subject No. 10FF by Nahum et al. (1970).

Figure 6.11: Comparison of the force-deflection response of the chest to a frontal impact.   The solid line indicates the FEM-5F output and the dotted line, the cadaver test result for subject No. 30FF by Kroell et al. (1974).

6.3.2. Lateral pendulum impact

One test subject (No. LCT04) in an impact test conducted by Talantikite et al. (1998)[141] had a basic anthropometry similar to that of a 5th percentile female.   Figure 6.12 shows the chest force-deflection curve predicted by the model (solid line) compared to that obtained experimentally (dotted line).   FEM-5F predicted 16 rib fractures.   This number agreed perfectly with that reported by Talantikite et al. (1998)[141]. However, the peak force predicted by the model was 47% higher than that obtained experimentally.
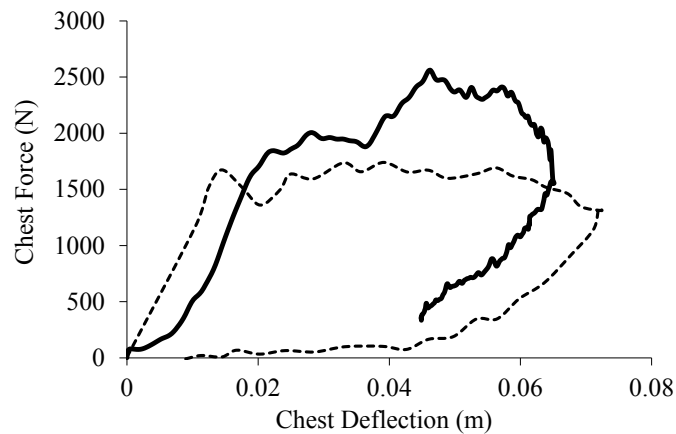
Figure 6.12: Comparison of the force-deflection response of a lateral chest impact.   The solid line indicates the FEM-5F output and the dotted line, the female cadaver test result for subject No. LCT04 by Talantikite et al. (1998).

6.3.3. Oblique pendulum impact

One subject used for two oblique impact tests (Test No. 29 and No. 33) had a basic anthropometry similar to that of a 5th percentile female.   Figure 6.13 and Figure 6.14 show the chest force-deflection curves predicted by the model (solid lines) for Test No. 29 and No. 33, respectively, compared to experimentally obtained curves (dotted lines) for the same tests as reported by Viano (1989)[154].   The numbers of rib fractures predicted by the model was 17 and 33, respectively, for Test No. 29 and No. 33, whereas the numbers reported in the experiments were 0 and 12.   Although the number of rib fractures predicted for oblique pendulum impact tests was quite different from that observed experimentally, the contact force-deflection characteristics predicted by the model seemed to fit the experimental data quite well.
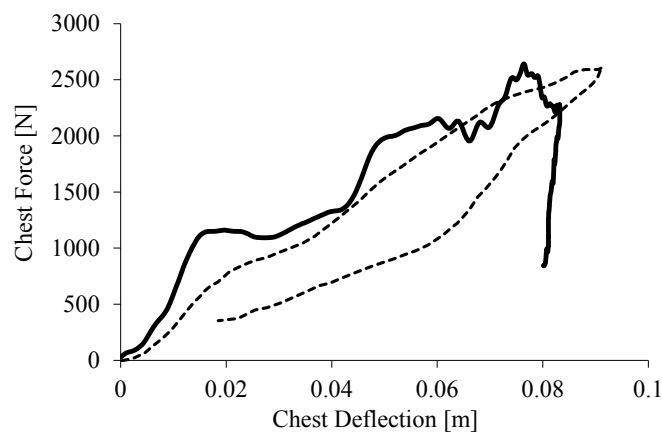
Figure 6.13: Comparison of the force-deflection response of an oblique chest impact.   The solid line indicates the FEM-5F output and the dotted line, the result from Test No. 29 reported by Viano (1989).
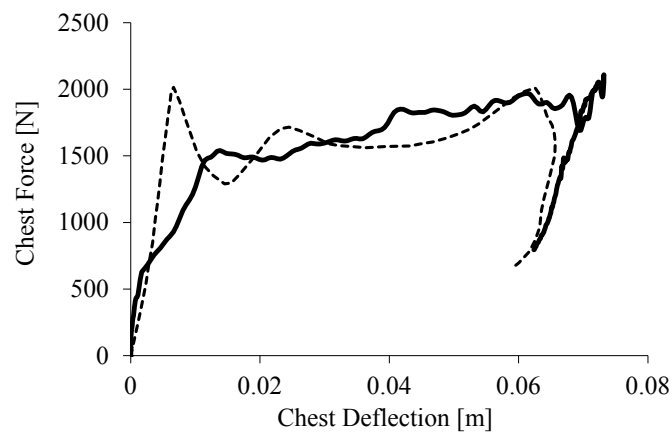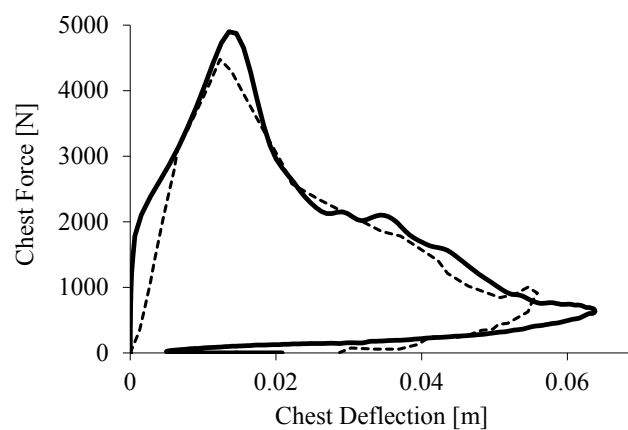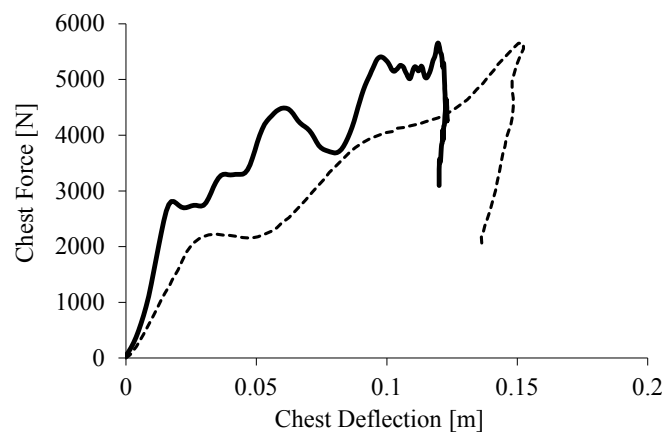

Figure 6.14: Comparison of the force-deflection response of an oblique chest impact.   The solid line indicates the FEM-5F output and the dotted line, the result from Test No. 33 reported by Viano (1989).

6.3.4. Ballistic breast impact

Figure 6.15 shows comparisons of the chest force-time, deflection-time, and force-deflection curves for ballistic impact. The results predicted by the FEM-5F are indicated by solid lines and those obtained experimentally, by dotted-gray lines. The experimental corridors are indicated by dashed-black lines (Wilhelm, 2003[161]). Even though the force magnitude was higher than the upper corridor at 0.6 ms, the model-predicted results compared favorably with the experimental data. The number of rib fractures predicted by the FEM-5F was three, which compared favorably with the average reported number of rib fractures of 3.5 ± 2.0.

(a) Force-time history

(b) Deflection-time history
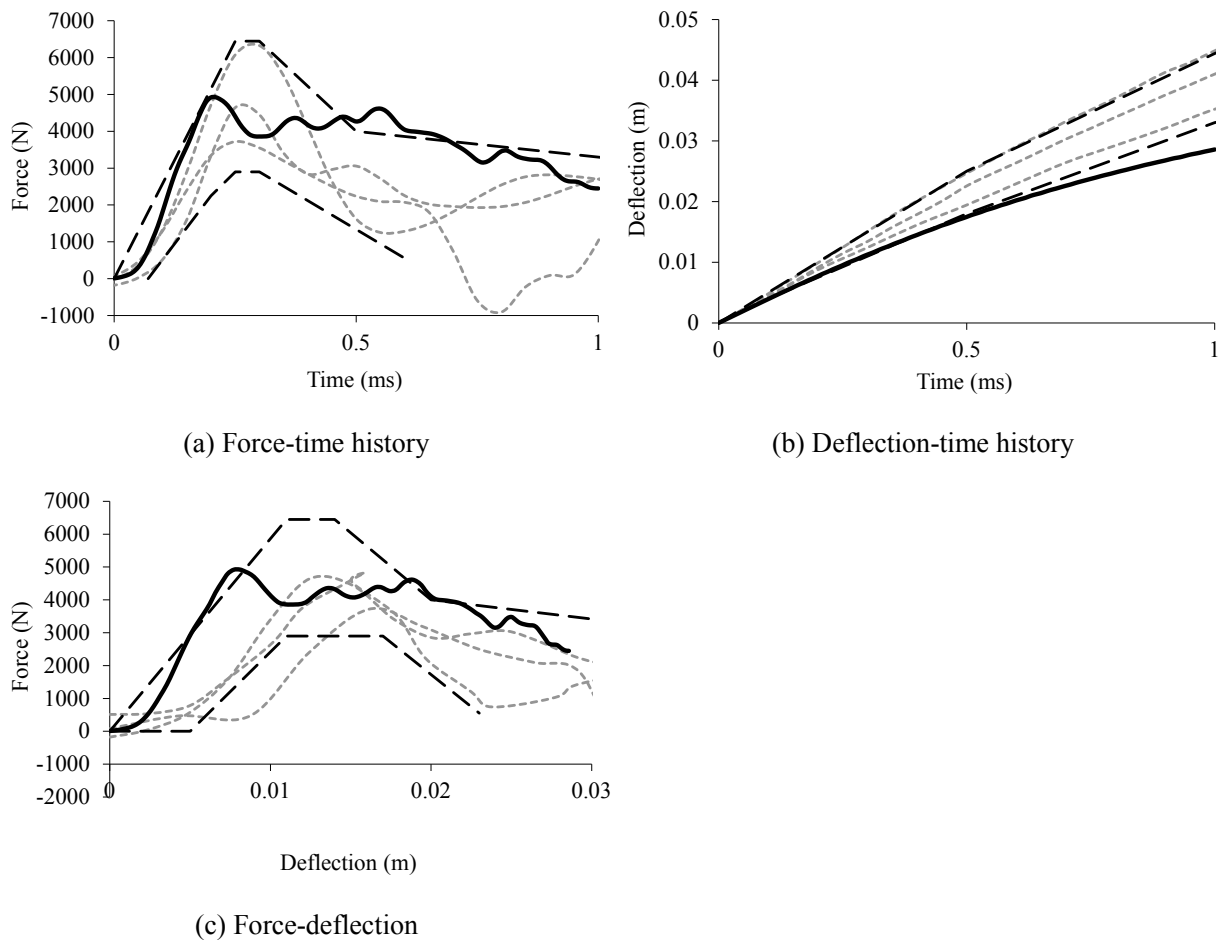
(c) Force-deflection

Figure 6.15: Comparisons of the force-time, deflection-time, and force-deflection responses due to ballistic breast impacts. The solid, dotted-gray, and dashed-black lines respectively indicate the model predictions, experimental data, and corridors generated by Wilhelm (2003).

6.4.   Discussion

A 3D FE model of the 5th percentile female (FEM-5F) has been developed to study its responses to frontal, lateral, and oblique blunt impacts and high-speed ballistic breast impacts.   This model includes a detailed description of the bony skeleton, chest internal organs, and superficial muscles.   The overall responses predicted by FEM-5F agreed reasonably well with the experimental data obtained from cadavers with anthropometry similar to that of a 5th percentile female.

Gender differences could be observed in terms of anatomical features and biomechanical properties.   This study takes into consideration gender differences in the shape of the rib cage and the locations of internal organs based on the report by Clemente (1985)[19].   Additionally, the biomechanical characteristics of the rib cortical bone due to gender differences (Kimpara et al., 2004[69]) were implemented when modeling the ribs.   The area moment of inertia and cross-sectional area of female ribs are smaller than those of males; these factors could contribute significantly to differences in the chest deformation and number of rib fractures (Kimpara et al. 2004[69]).   As the predicted impact responses showed reasonably good agreement with the experimental data, the assumptions proposed in previous chapters were verified by the validation results of FEM-5F.   Further study is needed to determine the existence of dominant parameters that influence the impact response due to gender.

On the other hand, the material constitutive laws and material properties chosen in this study were usually consistent with previous studies designed to develop the 50th percentile male models, because Yamada (1970)[164] and Kimpara et al. (2004)[69] have reported that no significant gender difference was found in the material properties.

However, there is a lack of information regarding the material properties of internal organs under high-speed loading.   While considerable information is available on the properties of the bony skeleton, little information is available about the properties of the soft tissues subjected to dynamic loading.   In this study, some of the material properties have been taken from experimental data such as those reported by Abe et al. (1996)[1], Fung (1993)[35], Granik and Stein (1973)[40], Hayes (1991)[49], Shah et al. (1978)[133], Tamura et al. (2002)[145], Viano (1983)[153], and Yamada (1970)[164].   Properties that were not available experimentally were taken from previous modeling studies such as those reported by Iwamoto et al. (2000[59] and 2002[60]), Lee and Yang (2001)[80], Lee (2002)[81], Lizee et al. (1998)[83], Shah et al. (2001)[134], Plank et al. (1998)[121], Ruan et al. (2003)[128], Wang (1995)[158], and Yang and King (1984).

The number of female cadaveric subjects tested and reported in literatures is very limited.   Of these, only a handful of small female subjects have been tested.   Therefore, various scaling methods based on body weight and height have been developed (Eppinger et al., 1984[27]; Mertz et al., 1989[94]; Eppinger et al., 2000[28]).   Owing to the uncertainty in the reliability of these scaling methods, this study focused on simulations of those experimental studies in which small female subjects were tested.   Additionally, is aimed to develop a generic 5th percentile female model.   Unfortunately, experiments have not been conducted on 5th percentile female specimens.   Consequently, a maximum difference of 10% in height and 15% in weight was allowed for selecting test subjects from which experimental data were used for model validation.   We believe that it is especially critical to select data obtained from small subjects when modeling a 5th percentile

female because the 20 kg mass impactor used in most experimental studies is approximately two times the mass of the chest of a small female.

In ballistic breast impact tests, a lightweight 150 g mass baton impactor was used. Thus, the impact response was localized only to the breast area. Therefore, the force-time history, deflection-time history, and force-deflection curve corridors of female breast impact were used for validating FEM-5F regardless of the anthropometry. The model predictions for ballistic breast impact compared favorably with the experimental data. Based on the ballistic impact simulation, the maximum force occurred at 0.2 ms with a penetration of 8.1 mm. As there was no rib deformation until 0.5 ms, which corresponded to a penetration of 17 mm, the initial response of the ballistic breast impact was due solely to the property of breast tissues, which were modeled as a low-density foam material with Young's modulus of 500 kPa and mass density of 900 kg/m^3. The selection of these material properties appeared to be appropriate.

For lateral pendulum impact simulations, the maximum contact force predicted by FEM-5F was 47% higher whereas the maximum predicted deflection was 10% lower than that obtained experimentally. The test subject used in this case was a 93-year-old specimen, and it is suspected that the material properties of this subject were more compliant than those of the younger specimens. Based on a study reported by Kimpara et al. (2004b)[69] to investigate the effect of changing material properties, it is not unexpected that the model predicted higher responses in this case.

For the oblique pendulum impact simulation, the chest contact force predicted by the model was comparable with the experimental data, whereas the maximum deflection was slightly lower than that obtained experimentally. The number of rib fractures predicted by the model for frontal and lateral impact was reasonably close to that obtained from experimental data, whereas for oblique pendulum impact, the model predicted a higher number of rib fractures. Even though the number of rib fractures in frontal and lateral impacts agreed well with the experimental data, the same was not the case for oblique impacts. Future studies are needed to consider other bone injury mechanisms to better predict rib fractures.

Age has a significant effect on the biomechanical properties of the bone. For example, the 93-year-old test subject used in the lateral pendulum impact test showed greater chest deflection and lower chest force compared to the chest responses predicted by our FE model (Figure 6.12). It is expected that using lower material properties in the model for the rib cage and/or internal organs would induce more compliant chest responses to frontal and lateral impacts. Unfortunately, large variations exist in terms of the relationship between age and biomechanical properties. As a result, scaling methods that are based on height and weight, as reported in literatures, may yield unreliable results as they do not include age effects. Similarly, our modeling study did not include such effects. More research is needed to study the effect of age in FE modeling so that the model can cover a wide age range.

The model failed to predict an initial inertial spike seen in some experimental data. Because the peak force observed experimentally at this initial period was lower than the maximum force of the entire impact and the model-predicted rib fracture occurred much later than the time of the initial spike, it was determined that the model-predicted results are good enough for the current model. Nevertheless, this observed discrepancy warrants future studies to, perhaps, numerically detect the contact interface.

It should be noted that the FEM-5F model was designed to balance the degree of anatomical detail against the expenditure of CPU time for explicit FE codes.   If the minimum mesh size is 0.5 mm with Young's modulus of 11 GPa, the minimum time step would be ~0.1 μs.   This would increase the number of elements by more than five times and the corresponding CPU time, by more than 50 times.   Thus, it is impractical to execute a model with such detail within a reasonable turnaround time.   The FEM-5F model developed in this study should be treated as the first step in understanding the injury biomechanics related to a small female.

6.5. Conclusions

A 3D FE model of a 5th percentile female (FEM-5F) has been developed and validated against cadaveric experimental test data.   In addition to the use of the basic anthropometry of a 5th percentile female, the model incorporated a female-specific skeleton with detailed descriptions of the internal organs in the thorax and geometrical properties of female ribs.   This study attempted to simultaneously achieve two contradictory goals: greater complexity to include gender- and size-specific geometric properties while maintaining simplicity so that the minimum time-step can be greater than 1 μs.   Consequently, the number of elements was reduced, relative to the THUMS 50th percentile male model, to maintain the same critical mesh size of 2.5 mm for the same minimum time step.

The model results correlated relatively well with five sets of pendulum experimental data and a series of ballistic breast impacts.   Consequently, some of these results proved the proposed assumptions of size effect and gender difference for the rib cage cross-sectional area.   More research is needed to increase the prediction accuracy of rib fractures so that the mechanisms responsible for injury to the chest of a small female can be better understood.   Additionally, almost all new vehicles sold worldwide are equipped with airbags, and a high percentage of vehicular occupants are restrained by seatbelts.   Unfortunately, human response data mimicking real world distributed loading conditions are still largely lacking.   Thus, the model developed in this study needs to be further validated when these data become available.

Chapter 7   Conclusions and Future Works

7.1. Conclusions

Predicting the risks and determining the mechanisms of sustaining serious–fatal injuries due to impact loadings are challenging themes in the field of impact biomechanics.   For gaining a better understanding of the injury mechanisms, human body surrogating technologies are necessary.   Although anthropomorphic test devices (ATDs) and multibody-based models were good at predicting the whole body kinematics during impacts, the various biological properties were simply considered by employing scaling methods in these designs.   However, the human body is too complex to be represented by a simple system.   The composition of the materials and structures of internal organs could affect the biomechanical responses and injuries of the human body.   Therefore, this doctoral thesis aimed to apply finite element (FE) modeling techniques for the human head, neck, and chest regions to analyze serious–fatal injurious impact scenarios and investigate the injury mechanisms of serious–fatal injuries using human body FE models.

The main results of each chapter can be summarized as follows:

In Chapter 1, a quantitative metric for injury severities in the Abbreviated Injury Scale (AIS) rating system was found to associate better for gaining an understanding of traffic injuries and their mechanism. Injury analysis using the AIS score suggested that the head and chest were the two most frequent body regions that suffered from serious or more severe injuries (AIS 3+ injuries).   Considering AIS 3 or more injuries and severe residuals, spinal cord injury could also be remarkable along with head and chest injuries. The results of traffic accident analyses also showed increasing numbers of female drivers on the road and suggested the vulnerability of female occupants in automotive crashes.   Consequently, the investigation of head, neck, and chest injuries could contribute effectively to reduce the number of serious–fatal injury cases.

In Chapter 2, a series of parametric studies was conducted using a human head-neck complex FE model.   According to the predicted results of the anteroposterior head-neck responses during severe frontal impacts, the following key findings were observed:

1.   Soft head contact or no head contact could reduce the numerical values of injury predictors for diffuse axonal injury (DAI).

2.   For neck responses, the inertial effect of the human body plays an important role in the relative displacement between the head and the torso.

3.   Backward neck extension would increase the strain of the spinal cord.   In both forward and backward extension, the large relative displacement between the head and the torso stretched the cervical ligaments.

4.   A better configuration for the head-neck complex would be an arrangement of soft restraints for the head with some forward offset and hard restraints for the torso.

In Chapter 3, the brain FE model was used for developing two criteria based on the angular accelerations in traumatic brain injuries (TBIs).   Nonconcussive and concussive football head impacts were analyzed using the human brain FE model.   Although the impact energies of football head impacts would be less than those during automotive crashes, the predicted head and brain impact responses would reflect the phenomena of real-world human head injuries because the data used could be assumed to represent the actual head kinematics.   According to correlation analyses with brain strain variables, we found two new brain injury criteria based on the rotational head motion—Rotational Injury Criterion (RIC) and Power Rotational Head Injury Criterion ($PRHIC$).   As the maximum integral time duration for RIC and $PRHIC$ was set to 36 ms, this study specified the variables RIC_{36} and $PRHIC_{36}$, respectively.   The following four specific conclusions can be drawn for RIC_{36} and $PRHIC_{36}$.

1.   Based on hypotheses of the brain injury severity with axonal stretch, Cumulative Strain Damage Measure (CSDM) with a greater strain threshold of 30% may predict severe TBI, whereas CSDM 10% may predict milder brain injuries such as concussion due to football head impacts.

2. RIC_{36} showed a significant correlation with CSDM 10% (R > 0.92), whereas $PRHIC_{36}$ was strongly correlated with CSDM 30% (R > 0.90).

3.   The present study determined the thresholds for 50% probabilities of sustaining mild traumatic brain injury (MTBI) as RIC_{36} of 1030 and $PRHIC_{36}$ of 870 based on concussive National Football League (NFL) head impact data.   However, as $PRHIC_{36}$ could be considered an injury predictor for severe TBI, the injury threshold of $PRHIC_{36}$ should be verified with further case data of severe TBI head impacts.

4.   All criteria—Head Injury Criterion (HIC_{15}), RIC_{36}, and $PRHIC_{36}$—are necessary for head injury analyses because injury criteria based on translational and rotational head kinetics would predict various types of head injuries such as skull fracture, brain contusion, and mild or severe TBI.

In Chapter 4, a retrospective analysis using published literature data of 83 frontal and lateral blunt cadaveric impacts was conducted to find correlations among biological variables such as cadaveric anthropometric data, chest impact responses, and resulting chest injuries.   In addition, 87 isolated 6th and 7th ribs were obtained from 11 male and 13 female cadavers to characterize the biomechanical properties of human ribs.   The results obtained in this chapter are summarized as follows:

1.   The maximum chest deflection, compression ratio, and maximum force somehow correlated linearly with the impact energy for both males and females for frontal impacts.

2.   The maximum deflection and compression ratio for females are considerably higher than those for males when subjected to the same impact energy.

3.   The material properties were not significantly different between males and females. There was no significant gender difference in Young's modulus and BMD based on isolated rib bending tests.

4.   However, significant gender differences were observed in their geometric properties such as the cross-sectional area and moment of inertia. The cross-sectional area and area moment of inertia of female ribs were ~22% and 50.3% lower than those of male ribs, respectively.

5.   The anthropometric properties of the utilized test subjects showed that the chest depth and rib geometry did not associate with the height or weight of the human body. This finding may imply the inhomogeneous and complex nature of the human body.

6.   Even at a loading rate that is 40,000 times the lowest loading rate, the ultimate stress increased by only 33% and 10% in males and females, respectively. It can be concluded that the human rib is not highly rate sensitive.

In Chapter 5, two series of parametric studies, with a total of 106 numerical simulations of frontal and lateral pendulum impacts, and another 11 numerical simulations of frontal pendulum impacts using the American Male 50th percentile (AM50) Total HUman Model for Safety (THUMS) were conducted to elucidate how the predicted values of rib fractures depend on specific assumptions regarding body size, material parameters (stiffness and density), and skeletal geometry. The following specific conclusions were drawn:

1.   The stiffness of the rib cage significantly affected the number of rib fractures in both frontal and lateral impacts.

2.   The stiffness and mass density of the internal organs affected the maximum chest force and deflection in frontal impacts as well. However, this effect was not observed in lateral impacts.

3.   The initial chest apparent stiffness somewhat correlates with the body weight.

4.   The maximum chest compression ratio (C_{max}), which correlates with the area moment of inertia of the rib cage and the ribs, is a good predictor for the numbers of rib fractures and fractured ribs.

In Chapter 6, a 3D FE model of the 5th percentile female (FEM-5F) was developed by modeling several features of previous conclusions reported in literatures in terms of anatomical features and biomechanical properties. The model results correlated relatively well with five sets of pendulum experimental data and a series of ballistic breast impacts. Consequently, some of the obtained results proved the proposed assumptions of size effect and gender difference of the rib cage cross-sectional area.

The studies conducted in this thesis were based on FE analysis in consideration of human anthropometric data and bony structure. This study succeeded in demonstrating the role of body size and geometrical effects on the impact responses of the human body. The head-neck complex model could suggest the probabilities of TBI based on the strain values of the intracranial elements. New injury criteria

for mild or severe TBI and their thresholds were also proposed using this model.   Additionally, skeletal injuries of the chest could be demonstrated, and this study suggested that the maximum compression ratio was a good injury predictor for the chest.   Therefore, it can be concluded that biomechanical FE modeling techniques are effective for investigating injury mechanisms and designing safety devices.

7.2.   Recommendation for Future Research

Future research works should focus on three issues: (1) spinal cord injury, (2) injury criteria and their thresholds for TBI, and (3) chest injury mechanisms for small females.

The head-neck model has a detailed central nervous system (CNS) structure and material properties including the brain and spinal cord.   In this study, this model was applied to investigate anteroposterior responses and injuries to the head-neck for only severe frontal impacts.   However, it is possible to employ this model for further investigations or application studies.   For example, there is a discussion about the mechanisms of whiplash injury: one of the major theories is based on the mechanical strain of the cervical facet joint capsule[135], and another is based on the pressure change in the spinal canal[140].   Although the pressure change in the spinal canal needs other techniques for expressing the relationships between the pressure and the volume inside the spinal canal, this model can be useful for assessing the effectiveness or sensitivities of strain on the cervical facet joint and spinal canal due to relative motion of cervical vertebra.

This study proposed RIC_{36} and $PRHIC_{36}$ as the TBI predictors based on rotational head kinematics. However, the correlations between these predictors and FE-based injury predictors using the THUMS brain model are limited to helmeted football head impacts.   In the last few decades, the injury probabilities for TBI have been determined by the relationships of maximum angular acceleration vs. angular velocity (see Figure 3.5 in page 43 of this thesis) [29], [85], [88], [110].   One of the evaluation methods would be describing the threshold curves generated by RIC_{36} and $PRHIC_{36}$ on the same graph of maximum angular acceleration vs. angular velocity.   On the other hand, it is important for understanding and agreement to introduce RIC_{36} and $PRHIC_{36}$ as TBI predictors to researchers in this field.   Encouraging a comparison of TBI predictors with human brain FE models other than THUMS would be another way of evaluating RIC_{36} and $PRHIC_{36}$.

In this research, the human chest FE model for a 5th percentile small female was developed with the whole structure of the human body.   This model has female-specific characteristics for the rib's cross section, rib cage shape, and anthropometry.   The utilized blunt chest impact test data were taken from old literatures published between 1970 and 1998.   However, in 2014, new experimental data using a 5th percentile small female Post Mortem Human Subject (PMHS) has been published in the Stapp Car Crash Journal[6].   Additional validations would contribute toward improving the model and developing new injury criteria and thresholds for female chest.   On the other hand, a comparison between the responses of female-specific FE models and a scaled one from an AM50 model could provide a better understanding of the gender differences in the injury mechanisms.

REFERENCES

[1]   Abe, H., Hayashi, K., and Sato, M. (Eds.), (1996): Data Book on Mechanical Properties of Living Cells, Tissues, and Organs. Springer, New York.

[2]   Anderson T.E. and Viano D.C., (1986): Estimated united states incidence of disabling and fatal central nervous system traumas: a need to re-evaluate priorities? Proc. of 1986 International Research Council on the Biomechanics of Impact (IRCOBI), Zurich (Switzerland), pp.41-51.

[3]   Arbabi, S., Wahl, W., Hemmila, M., Kohoyda-Inglis, C., Taheri, P., and Wang, S., (2003): The Cushion Effect. J. Trauma, Vol. 54, pp. 1090–1093.

[4]   Association for the Advancement of Automotive Medicine (AAAM), (1998): The Abbreviated Injury Scale 1990 revision update-98. Gennarelli, T.A., and Wodzin E. ed; Barrington, IL.

[5]   Association for the Advancement of Automotive Medicine (AAAM), (2005): The Abbreviated Injury Scale 2005. Gennarelli, T.A., and Wodzin E. ed; Barrington, IL.

[6]   Baudrit, P., Petitjean, A., Potier, P., Trosseille, X., and Vallencien, G., (2014): Comparison of the Thorax Dynamic Responses of Small Female and Midsize Male Post Mortem Human Subjects in Side and Forward Oblique Impact Tests. Stapp Car Crash Journal, Vol. 58, pp. 103-121.

[7]   Begeman, P.C., Kopacz, J.M. and King, A.I., (1990): Steering assembly impacts using cadavers and dummies. Proc. 34th Annual Stapp Car Crash Conference, SAE 902316.

[8]   Bilston, L.E., and Thibault, L.E., (1996): The mechanical properties of the hunan cervical spinal cord in vitro. Annals of Biomedical Engineering, Vol.24, pp.67-74.

[9]   Bilston, L.E., (1998): Finite element analysis of some cervical spinal cord injury modes. Proc. of 1988 International Research Council on the Biomechanics of Impact (IRCOBI), Goeteborg (Sweden).

[10] Bouquet, R., Ramet, M., Bermond, F. and Cesari, D., (1994): Thoracic and Pelvis Human Response to Impact. Proc 14th ESV, pp. 100-109.

[11] Bouxsein, M.L., Coan, B.S., and Lee, S.C., (1999): Prediction of the strength of the elderly proximal femur by bone mineral density and quantitative ultrasound measurements of the heel and tibia. Bone, Jul; 25 (1), pp.49-54.

[12] Broglio, S.P., Schnebel, B., Sosnoff, J.J., Shin, S., Fend, X., He, X., and Zimmerman, J., (2010): Biomechanical properties of concussions in high school football. Med Sci Sports Exerc., 42:2064-71.

[13] Carr, A.M., Bailes, J.E., Helmkamp, J.C., Rosen, C.L., and Miele, V.J., (2004), Neurological injury and death in all-terrain vehicle crashes in west virginia: a 10-year retrospective review, Neurosurgery, Vol.54, No.4, pp.861-867.

[14] Cerney, M.M., and Adams, D.C., (2004): Sequestering Size: The Role of Allometry and Gender in Digital Human Modelling. SAE 2004-01-2182, Society of Automotive Engineers, Warrendale, PA.

[15] Cesari, D., Ramet, M., and Bloch, J., (1981): Influence of arm position on thoracic injuries in side impact. Proc. 25th Stapp Car Crash Conference, SAE 811007.

[16] Cheng, R., Yang, K.H., Levine, R.S., King, A.I., and Morgan, R., (1982): Injuries to the cervical spine caused by a distributed frontal load to the chest.   Proc. of 26th Stapp Car Crash Conference, SAE Paper No. 821155, Society of Automotive Engineers, Warrendale, PA.

[17] Chung, J., Cavanaugh, J.M., King, A.I., Koh, S.W., and Deng, Y.C., (1999): Thoracic injury mechanisms and biomechanical responses in lateral velocity pulse impacts.   Stapp Car Crash Journal, Vol.43, 99SC04.

[18] Clarke, T.D., Gragg, C.D., Sprouffske, J.F., Trout, E.M., Zimmerman, R.M., and Muzzy, W.H., (1971): Human head linear and angular accelerations during impact.   Proc. of 15th Stapp Car Crash Conference, SAE Paper No. 710857, Society of Automotive Engineers, Warrendale, PA.

[19] Clemente, C.D.; ed. (1985): Gray's Anatomy, 30th American Edition of the Anatomy of the Human Body by Henry Gray, 1825-1861.   Lea & Febiger, PA.

[20] Cobb, J.D., Maclennan, P.A., McGwin, G.Jr., Metzger, J.S., and Rue L.W.III, (2005):   Original contribution: motor vehicle mismatch-related spinal injury.   The journal of spinal cord medicine, Vol.28, No.4, pp.314-319.

[21] Deng, Y.C., (1995): How airbags and seat belts work together in frontal crashes.   Proc. of 39th Stapp Car Crash Conference, SAE Paper No. 952702, Society of Automotive Engineers, Warrendale, PA.

[22] Deng, Y.C., Li, X., and Liu, Y., (1999): Modeling of the human cervical spine using finite element techniques.   SAE 1999-01-1310, Society of Automotive Engineers, Warrendale, PA.

[23] Dokko, Y., Anderson, R., Manavis, J., Blumburgs, P., McLean, J., Zhang, L., Yang, K.H., and King, A.I., (2003):   Validation of the human head FE model against pedestrian accident and its tentative application to the examination of the existing tolerance curve.   Proc. of 18th International Technical Conference on the Enhanced Safety of Vehicles (ESV), Paper No. 322.

[24] Donnelly, B.R., Morgan, R.M., and Eppinger, R.H., (1983):   Durability, repeatability and reproducibility of the NHTSA side impact dummy.   Proc. 27th Stapp Car Crash Conf., SAE 831624.

[25] Dryden, D.M., Saunders, L.D., Jacobs, P., Schopflocher, D.P., Rowe, B.H., May, L.A., Yiannakoulias, N., Svenson, L.W., Voaklander, D.C., (2005):   Related Articles, Links Direct health care costs after traumatic spinal cord injury.   J. Trauma. Aug;59(2):443-9.

[26] Dvorak, M.F., Fisher, C.G., Hoekema, J., Boyd, M., Noonan, V., Wing P.C., and Kwon, B., (2005): Factors predicting motor recovery and functional outcome after traumatic central cord syndrome. Spine, Vol.30, No.20, pp.2303-2311.

[27] Eppinger, R.H., Marcus, J.H., and Morgan, R.M., (1984): Development of dummy and injury index for NHTSA's thoracic side impact protection research program.   SAE 840885, Society of Automotive Engineers, Warrendale, PA.

[28] Eppinger, R., Sun, E., Kuppa, S., and Saul, R., (2000): Supplement: Development of Improved Injury Criteria for the Assessment of Advanced Automotive Restraint Systems – II.   National Highway Traffic Safety Administration, U.S. Department of Transportation, Washington, D.C.

[29] Ewing, C., Thomas, D., Lustic, L., Becker, E., Willems, G., and Muzzy, W., (1975):   The effect of the initial position of the head and neck on the dynamic response of the human head and neck to –Gx impact acceleration.   Proc. 19th Stapp Car Crash Conf., SAE 751157.

[30] Fayon, A., Tarriere, C., Walfisch, G., Got, C., Patel, A. (1975): Thorax of 3-point belt wearers during a crash (experiments with cadavers).   Proc. 19th Stapp Car Crash Conference, SAE 751148.

[31] Feist, F., Gugler, J., Arregui-Dalmases, C., del Pozo de Dios, E., Lopez-Valdèz, F., Deck, C., and Willinger, R., (2009):   Pedestrian collisions with flat fronted vehicles: Injury patterns and importance of rotational accelerations as a predictor for traumatic brain injury (TBI).   Proc. of 21st International Technical Conference on the Enhanced Safety of Vehicles (ESV), pp.15-18.

[32] Franklyn, M., Fildes, B., Zhang, L., Yang, K., and Sparke, L., (2005): Analysis of finite element models for head injury investigation: Reconstruction of four real-world impacts.   Stapp Car Crash Journal, vol.49, 2005-22-0001, pp.1-32.

[33] Freeman, R., and Haslegrave, C.M., (2004): The Determination of Optimal Pedal Positioning for Automobiles Using Jack.   SAE 2004-01-2149, Society of Automotive Engineers, Warrendale, PA.

[34] Friess, M. and Corner, B.D. (2004): From XS to XL: Statistical Modeling of Human Body Shape Change using 3D Surface Scans.   SAE 2004 Transactions, Journal of Aerospace, Vol.1, pp.215-220.

[35] Fung, Y.C. (1993): Biomechanics: Mechanical Properties of Living Tissues.   Second Edition, Springer-Verlag New York, Inc.

[36] Gadd, C.W., (1966):   Use of a weighted-impulse criterion for estimating injury hazard.   Proc. of 10th Stapp Car Crash Conf., SAE 660793.

[37] General Insurance Association of Japan, (2005): Actual Trend of Traffic Accidents based on Automotive Accident data, (in Japanese).

[38] Gennarelli, T.A., Ommaya A.K., Thibault, L.E., (1971): Comparison of translational and rotational head motions in experimental cerebral concussion.   Proc. 15th Stapp Car Crash Conference, SAE P-39: pp.797-803.

[39] Got, C., Walfisch, G., Fayon, A. and Faverjon, G., (1975): Les caractéristiques morphologiques, chimiques et physiques des côtes et leurs relations avec la déflexion provoquée du thorax.   Proc. of 1975 International Research Council on the Biomechanics of Impact (IRCOBI), Birmingham (UK), pp.220-228 (in French).

[40] Granik, G. and Stein, I., (1973): Human ribs: static testing as a promising medical application,   J. Biomechanics,Vol. 6, pp.237-240.

[41] Guskiewicz, K.M., Mihalik, J.P., Shankar, V., Marshall, S.W., Crowell, D.H., Oliaro, S.M., Ciocca, M.F., and Hooker, D.N., (2007): Measurement of head impacts in collegiate football players: Relationship between head impact biomechanics and acute clinical outcome after concussion. Neurosurgery, Vol.61, pp.1244-1253.

[42] Halldin, P.H., Brolin, K., Kleiven, S., von Holst, H., Jakobsson, L., and Palmertz, C., (2000), Investigation of conditions that affect neck compression – flexion injuries using numerical techniques. Stapp Car Crash Journal, Vol.44, 2000-01-SC10, The Stapp Association, Ann Arbor, MI.

[43] Hanks, S.E., Vogt, M., and Donaldson, W.F., (2003): The effect of the airbag on preventing injury to the cervical spine in motor vehicle accidents, Proc. of thirty first annual meeting Cervical spine research society, pp.20-21

[44] Happee, R., Ridella, S., Nayef, A., Morsink, P., de Lange, R., Bours, R., van Hoof, J., (2000): Mathematical Human Body Models Representing a Mid Size Male and a Small Female for Frontal, Lateral and Rearward Impact Loading. Proc. of 2000 International Research Council on the Biomechanics of Impact (IRCOBI), Montpellier (France).

[45] Hardy, W.N., Foster, C.D., Mason, M.J., Yang, K.H., King, A.I., and Tashman, S., (2001): Investigation of head injury mechanisms using neutral density technology and high-speed biplanar X-ray. Stapp Car Crash J., 45:337-368.

[46] Hart, R.A., Mayberry, J.C., and Herzberg, A.M., (2000): Acute cervical spinal cord injury secondary to air bag deployment without proper use of lap or shoulder harnesses. Journal of Spinal Disorders, Vol.13, No.1, pp.36-38.

[47] Hasegawa J., and Shiomi, A., (2003): A Study of Whiplash Injury Occurrence Mechanisms Using Human Finite Element Model. Proc. of the 18th International Technical Conference on the Enhanced Safety of Vehicles (ESV), Paper No# 195.

[48] Hayes, W.C., and Gerhart, T.N., (1985): Biomechanics of bone: Applications for assessment of bone strength. Bone and Mineral Research, edited by Peck, W.A., pp. 259-294, Elsevier Science Publishers, Amsterdam.

[49] Hayes, W.C., (1991): Biomechanics of cortical and trabecular bone: implications for assessment of fracture risk. ed. Mow, V.C. and Hayes, W.C., Basic Orthopaedic Biomechanics, Raven Press. Ltd., New York, pp.93-142.

[50] Hedenstierna, S., Halldin, P., Brolin, K., and von Holst, H., (2006): Development and evaluation of a continuum neck muscle model. Abstracts of the 5th World Congress of Biomechanics, (Journal of Biomechanics, Vol.39, Supplement 1), Munich, Germany, 29 Jul – 4 Aug.

[51] Hertz, E, (1993): A note on the head injury criterion (HIC) as a predictor of the risk of skull fracture. 37th Annual Proc. 37th the Association for the Advancement of Automotive Medicine, Association for the Advancement of Automotive Medicine, 303–312.

[52] Holly, L.T., Kelly, D.F., Counelis, G.J., Blinman, T., and McArthur, D.L., (2002): Cervical spine trauma associated with moderate and severe head injury: incidence, risk factors, and injury characteristics. J. Neurosurg, (Spine 3), Vol.96, pp.285-291.

[53] Huang, Y., King, A.I., and Cavanaugh, J.M., (1994a): Finite Element Modeling of Gross Motion of Human Cadavers in Side Impact. Proc. 38th Stapp Car Crash Conference, SAE 942207, SAE, Warrendale, PA.

[54]   Huang, Y., King, A.I., and Cavanaugh, J.M., (1994b): A MADYMO Model of Near-Side Human Occupants in Side Impacts.   J. Biomechanical Engineering, Vol. 116, pp.228-235.

[55]   Ichihara, K., Taguchi, T., Shimada, Y., Sakuramoto, I., Kawano, S., and Kawai, S., (2001): Gray matter of the bovine cervical spinal cord is mechanically more rigid and fragile than the white matter.   J. Neurotrauma, vol.18, No.3, pp.361-367.

[56]   Ichihara, K., Taguchi, T., Sakuramoto, I., Kawano, S., and Kawai, S., (2003): Mechanism of the spinal cord injury and the cervical spondylotic myelopathy: new approach based on the mechanical features of the spinal cord white and gray matter.   J. Neurosurgery, vol.99 (3 Suppl), pp.278-285.

[57]   Institute for Traffic Accident Research and Data Analysis (ITARDA), (2006): "Kotsu Tokei, 2005" (Annual Report on Automotive Traffic in 2005) (in Japanese).

[58]   Irwin, A.L., Mertz, H.J., Elhagediab, A.M. and Moss S., (2002): Guidelines for assessing the biofidelity of side impact dummies of various sizes and ages.   Stapp Car Crash Journal, Vol.46, 2002-22-0016, pp.297-319.

[59]   Iwamoto, M., Miki, K., Mohammad, M., Nayef, A., Yang, K.H., Begeman, P.C., and King, A.I., (2000): Development of a Finite Element Model of the Human Shoulder.   Stapp Car Crash Journal, Vol.44, pp. 281-297.

[60]   Iwamoto, M., Kisanuki, Y., Watanabe, I., Furusu, K., Miki, K., and Hasegawa, J., (2002): Development of a finite element model of the total human body model for safety (THUMS) and application to injury reconstruction.   Proc. of 2002 International Research Council on the Biomechanics of Impact (IRCOBI), Munich (Germany), pp. 31-42.

[61]   Kahle, W., Leonhardt, H., and Platzer, W., (1986): Taschenatlas der Anatomie für Studium und Praxis: Band3: Nervensystem und Sinnesorgane.   Georg Thieme Verlag Stuttgart, New York.

[62]   Kent, R., Bolton, J., Crandall, J., Prasad, P., Nusholtz, G., Mertz, H. and Kallieris, D., (2001): Restrained Hybrid III dummy-based criteria for thoracic hard-tissue injury prediction.   Proc. of 2001 International Research Council on the Biomechanics of Impact (IRCOBI), Isle of Man (UK), October.

[63]   Kent, R. W., Crandall, J., Patrie, J., Fertile, J., (2002):   Radiographic Detection of Rib Fractures: A Restraint-Based Study of Occupants in Car Crashes.   Traffic Injury Prevention 3, pp. 49–57.

[64]   Kent, R, Sherwood, C, Lessley, D, Overby, B, and Matsuoka, F., (2003a): Age-related changes in the effective stiffness of the human thorax using four loading conditions.   Proc. of 2003 International Research Council on the Biomechanics of Impact (IRCOBI), Lisbon (Portugal).

[65]   Kent, R., Bass, C.R., Woods, W., Sherwood, C., Madeley, N.J., Salzar, R. and Kitagawa, Y., (2003b): Muscle Tetanus and Loading Condition Effects on the Elastic and Viscous Characteristics of the Thorax.   Traffic Injury Prevention, Vol. 4, pp.1–18.

[66]   Kent, R, Lessley, D, and Sherwood, C., (2004): Thoracic response corridors for diagonal belt, distributed, four-point belt, and hub loading.   Stapp Car Crash Journal, Vol.48 pp.495-519.

[67]   Kimpara, H., Iwamoto, M., and Miki, K. (2002): Development of a small female FEM model.   JSAE, Paper No. 20025242.

[68]   Kimpara, H., Iwamoto, M., Miki, K., Lee, J.B., Begeman, P.C., Yang, K.H., and King, A.I., (2003): Biomechanical properties of the male and female chest subjected to frontal and lateral impacts.   Proc. of 2003 International Research Council on the Biomechanics of Impact (IRCOBI), Lisbon (Portugal).

[69]   Kimpara, H., Iwamoto, M., Watanabe, I., Miki, K., Lee, J.B., Yang, K.H. and King, A.I., (2004): Numerical analysis of the biomechanical characteristics and impact response of the human chest. 2004 ASME International Mechanical Engineering Congress and RD&D EXPO, November 2004, Anaheim, CA.

[70]   Kimpara, H., Nakahira, Y., Iwamoto, M., Miki, K., Ichihara, K., Kawano, S., and Taguchi, T., (2006): Investigation of Anteroposterior Head-Neck Responses during Severe Frontal Impacts Using a Brain-Spinal Cord Complex FE Model.   Stapp Car Crash Journal, 50, pp.509-544.

[71]   King, A.I., Yang, K.H., Zhang, L., Hardy, W., and Viano D.C., (2003):   Is head injury caused by linear or angular acceleration?   Proc. of the 2003 International Research Conference on the Biomechanics of Impact (IRCOBI).

[72]   Kleinberger, M., (1993): Application of finite element techniques to the study of cervical spine mechanics.   Proc. 37th Stapp Car Crash Conference, SAE Paper No. 933131, Society of Automotive Engineers, Warrendale, PA

[73]   Kleiven, S., and von Holst, H., (2001):   Consequences of Brain Size following Impact in Prediction of Subdural Hematoma evaluated with Numerical Techniques.   Proc. IRCOBI Conference, pp. 161-172, Isle of Man (UK). International Research Council on the Biomechanics of Impact, Bron, France.

[74]   Kleiven, S, (2007):   Predictors for traumatic brain injuries evaluated through accident reconstructions.   Stapp Car Crash J., 51: 81-114.

[75]   Koh, S., (2000): Effect of rib strength on injury tolerance in side impact.   Master's Thesis, Department of Mechanical Engineering, Wayne State University, Detroit, MI.

[76]   Kroell, C.K., Schneider, D.C., and Nahum, A.M., (1971): Impact tolerance and response of the human thorax.   Proc. 15th Stapp Car Crash Conference, SAE 710851.

[77]   Kroell, C.K., Schneider, D.C., and Nahum, A.M., (1974): Impact tolerance and response of the human thorax II.   Proc. of 18th Stapp Car Crash Conference, SAE 741187.

[78]   Kuppa, S.M. and Eppinger, R.H., (1998): Development of an improved thoracic injury criterion. Proc. of 42nd Annual Stapp Car Crash Conference, SAE 983153.

[79]   Lange, R.de, Rooij, L.van, Mooi, H., and Wismans J., (2005): Objective biofidelity rating of a numerical human occupant model in frontal to lateral impact.   Stapp Car Crash Journal, vol.49, 2005-22-0020, pp.457-479.

[80]   Lee, J.B. and Yang, K.H., (2001): Development of a finite element model of the human abdomen. Stapp Car Crash Journal, Vol.45, 2001-22-0004, pp. 79-100.

[81]   Lee, J.B., (2002): Development of a Finite Element Model of the Human Abdomen (WSUHAM). Ph.D. Dissertation, Bioengineering Center, Wayne State University, Detroit, MI.

[82] Lenard, J. and Welsh, R., (2001): A comparison of injury risk and pattern of injury between male and female occupants of modern European passenger cars. Proc. of 2001 International Research Council on the Biomechanics of Impact (IRCOBI), Isle of Man (UK), October, pp.15-26.

[83] Lizee, E., Robin, S., Song, E., Bertholon, N., Le Coz, J.Y., Besnault, B., and Lavaste, F., (1998): Development of a 3D Finite Element Model of the Human Body. SAE Paper No. 983152, SAE International Congress and Exposition, Warrendale, PA.

[84] Lobdell, T.E., Kroell, C.K., Schneider, D.C., Hering, W.E. and Nahum, A.M., (1973): Impact Response of the Human Thorax, Human Impact Response Measurement and Simulation. W.F. King, H.J. Mertz, eds., Plenum Press, London, pp.201-45.

[85] Lowenhielm, P., (1974): Strain tolerance of the Vv. Cerebri sup. (Bridging Veins) calculated from head-on collision tests with cadavers. Z.Rechtsmedizin, 75:131-144.

[86] Mackay, M. and Hassan, A.M., (2000): Age and gender effects on injury outcome for restrained occupants in frontal crashes: a comparison of UK and US databases. Proc. 44th Annual Scientific Conference of the Association for the Advancement of Automotive Medicine, Chicago, IL, October, pp.75-91.

[87] Manary, M.A., Reed, M.P., Flannagan, C.A.C. and Schneider, L.W., (1998): ATD positioning based on driver posture and position. Proc. of 42nd Annual Stapp Car Crash Conference, SAE 983163, Society of Automotive Engineers, Warrendale, PA.

[88] Margulies, S.S. and Thibault, L.E., (1992): A proposed tolerance criterion for diffuse axonal injury in man. J Biomech., 25(8): 917-923.

[89] Martini, F.H., Timmons, M.J., and McKinley M.P., (2000): Human Anatomy, Third Edition, ISBN: 0-13-010011-0, Pearson Education, Inc.

[90] Maxwell, W.L., Povlishock, J.T., and Graham. D.L., (1997): A mechanistic analysis of nondisruptive axonal injury: A review. J. Neurotrauma 14(7): 419-440.

[91] Melvin, J.W., Horsch, J.D., McCleary, J.D., Wideman, L.C., Jensen, J. L., and Wolanin, M. J., (1993): Assessment of Air BagDeployment Loads with the Small Female Hybrid IIIDummy. Proc. 37th Stapp Car Crash Conference SAE 933119, Society of Automotive Engineers, Warrendale, PA.

[92] Menard, S.W., (1995): Applied logistic regression analysis, Thousand Oaks. Calif. Sage Publications, Inc., CA.

[93] Mertz, H.J., (1984): A procedure for normalizing impact response data. SAE 840884, Society of Automotive Engineers, Warrendale, PA.

[94] Mertz, H.J., Irwin, A.L., Melvin, J.W., Stalnaker R.L. and Beebe, M.S., (1989): Size, weight and biomechanical impact response requirements for adult size small female and large male dummies. SAE 890756, Society of Automotive Engineers, Warrendale, PA.

[95] Mertz, H.J., Irwin, A.L. and Prasad, P., (2003): Biomechanical and scaling bases for frontal and side impact injury assessment reference values. Stapp Car Crash Journal, Vol. 47, pp. 155-188.

[96]   Meyer, F., Bourdent, N., Deck, C., Willinger, R., and Raul, J.S., (2004): Human Neck Finite Element Model Development and Validation against Original Experimental Data.   Stapp Car Crash Journal, Vol.48, 2004-22-0008, The Stapp Association, Ann Arbor, MI.

[97]   Moinerean D, Frund JM, Brochard J, Valeta MP, Marini B, Joly P, Guichard D, Bhandari S, Sherry A, France C, Sanderson DJ. (1999):   The Use of Local Approach to Fracture in Reactor Pressure Vessel Structural Integrity Assessment: Synthesis of a Cooperative Research Program Between EDF, CEA, Framatome and AEA Technology.   In Fatigue and Fracture Mechanics: Twenty-Ninth Volume, ASTM STP 1332, Ed. T.L. Panontin, S.D. Sheppard, American Society for Testing and Materials,West Conshohocken, PA, pp. 284–314.

[98]   Nahum, A.M., Gadd, C.W., Schneider, D.C., and Kroell C.K., (1970): Deflection of the human thorax under sternal impact.   SAE 700400, Society of Automotive Engineers, Warrendale, PA.

[99]   Nahum, A. M., Smith, R., and Ward, C.C., (1977):   Intracranial pressure dynamics during head impact.   Proc of the 21st Stapp Car Crash Conf., SAE 770922: 339-366.

[100] Nakahira, Y., Furukawa, K., Niimi, H., Ishihara, T., Miki, K., and Matsuoka, F., (2000):   A combined evaluation method and modified maximum likelihood method for injury risk curves.   Proc. of the IRCOBI Conf., pp.147-156.

[101] National agency for Automotive Safety & Victims' Aid in Japan, (2006): Report of senior counselor pro-reform promotion meeting for government-affiliated corporations, (in Japanese)

[102] The National Highway Traffic Safety Administration (NHTSA), (2001): Traffic Safety Facts 2001, older population, National Center for Statistics & Analysis.   DOT HS 809 475, Washington, D.C.

[103] The National SCI Statistical Center, (2005): Spinal Cord Injury, Facts and Figures at a Glance. Birmingham, AL
       Available at: http://images.main.uab.edu/spinalcord/pdffiles/factsfig.pdf Accessed May 2006.

[104] Neathery, R.F., (1974): Analysis of chest impact response data and scaled performance recommendations.   Proc. of 18th Stapp Car Crash Conference, SAE Paper No. 741188.

[105] Neathery, R.F., (1975): Prediction of thoracic injury from dummy responses.   Proc. 19th Stapp Car Crash Conference, San Diego, California, SAE 751151, pp.295-316, Warrendale, PA.

[106] Newman, J.A., Barr, C., Beusenberg, M.C., Fournier, E., Shewchenko, N., Welbourne, E., and Withnall, C., (2000a):   A new biomechanical assessment of mild traumatic brain injury. Part 2: results and conclusions.   Proc. of 2000 IRCOBI, pp. 223–233.

[107] Newman J.A., Shewchenko, N., and Welbourne, E., (2000b):   A proposal new biomechanical head injury assessment function – the maximum power index.   Stapp Car Crash J., 44: 215-247.

[108] Nishigaki, H., Amago, T., Miki, K., Ishiyama, S., Tanaka, E., Yamamoto, S., (2000): Fundamental Study of Dynamic Analysis of Lumbar Vertebrae.   Human Biomechanics and Injury Prevention, Edited by Kajzer J., Tanaka, E., Yamada, H., Springer, pp.243-248.

[109] Ommaya, A.K., Yarnell, P., Hirsch, A., and Harris, D., (1967): Scaling of experimental data on cerebral concussion in sub-human primates to concussive thresholds in man. Proc. 11th Stapp Car Crash Conf., SAE 670906.

[110] Ommaya, A.K. and Hirsch, A.E., (1971): Tolerances for cerebral concussion from head impact and whiplash in primates. J. Biomech., 4:13-21.

[111] Ono, K., Kaneoka, K., Wittek, A., and Kajzer, J., (1997): Cervical injury mechanism based on the analysis of human cervical vertebral motion and head-neck-torso kinematics during low-speed rear impacts. Proc. of 41st Stapp Car Crash Conference, SAE Paper No. 973340, Society of Automotive Engineers, Warrendale, PA.

[112] Patrick, L.M., Lissner, H.R., and Gurdjian, E.S., (1963): Survival by design – head protection. Proc. 7th Stapp Car Crash Conf., SAE 1963-12-0036: 483-499.

[113] Patrick, L.M., Kroell, C.K., Mertz, H.J., (1965): Forces on the human body in simulated crashes. Proc. 9th Stapp Car Crash Conference, Minnesota, Minneapolis, pp.237-259, Warrendale, PA.

[114] Patrick, L.M., Nyquist, G.W., and Trosien, K.L., (1972): Safety performance of shaped steering assembly airbag. Proc. of 16th Stapp Car Crash Conference, SAE Paper No. 720976, Society of Automotive Engineers, Warrendale, PA.

[115] Patrick, L.M. and Andersson, A., (1974): Three-Point Harness Accident and Laboratory Data Comparison. Proc. of 18th Stapp Car Crash Conference, SAE 741181, pp.201-282.

[116] Pellman, E.J., Viano, D.C., Tucker, A.M., Casson, I.R., and Waeckerle, J.F., (2003): Concussion in professional football: Reconstruction of game impacts and injuries. Neurosurgery. 53:799-812; discussion 812-814.

[117] Perese, D.M., (1960): Relationship of the spinothalamic tract to the dentate ligament in the thoracic and the cervical cord. Surg Forum, 11, pp.398-400.

[118] Pintar F.A., Yoganandan, N., Voo, L., Cusick, J.F., Maiman, D.J., and Sances, A.Jr., (1995): Dynamic characteristics of the human cervical spine. Proc. of 39th Stapp Car Crash Conference, SAE Paper No. 952722, Society of Automotive Engineers, Warrendale, PA.

[119] Plank, G.R., and Eppinger, R.H., (1989): Computer dynamic response of the human thorax from a finite element model. Proc. 12th International Technical Conference on the Enhanced Safety of Vehicles (ESV), pp. 665-672.

[120] Plank, G.R., and Eppinger, R.H., (1991): An improved finite element model of the human thorax. Proc. 13th International Technical Conference on the Enhanced Safety of Vehicles (ESV), pp.902-907.

[121] Plank, G.R., Kleinberger, M., and Eppinger, R.H., (1998): Analytical Investigation of Driver Thoracic Response to Out of Position Airbag Deployment. Proc. 42nd Stapp Car Crash Conference, SAE Paper No. 983165, SAE, Warrendale, PA.

[122] Pope, A.M. and Tarlov, A.R. (1991): Disability in america: toward a national agenda for prevention. National academic Press, Washington D.C., pp.147-183.

[123] Prasad, P. and Mertz, H.J., (1985):   The position of the United States delegation to the ISO Working Group 6 on the use of HIC in the automotive environment.   SAE Paper #851246, Society of Automotive Engineers, Warrendale, PA.

[124] Robbins, D.H., (1983): Anthropometric specifications for small female and large male dummies, Volume 3.   UMTRI-83-53-3, NHTSA.

[125] Roberts, V.L. and Compton, C.P., (1993): The relationship between delta v and injury.   Proc. of 37th Stapp Car Crash Conference, SAE 933111, pp.35-41.

[126] Rowson, S., Brolinson, G., Goforth, M., Dietter, D., and Duma, S., (2009):   Linear and angular head acceleration measurements in collegiate football.   J. of Biomech. Eng., 131(6):061016.

[127] Rowson, S., Beckwith, J.G., Chu, J.J., Leonard, D.S., Greenwald, R.M., and Duma, S.M., (2011):   A six degree of freedom head acceleration measurement device for use in football.   J Appl Biomech. 27:8-14.

[128] Ruan, J., El-Jawahri, R., Chai, L., Barbat, S., and Prasad, P., (2003): Prediction and Analysis of Human Thoracic Impact Responses and Injuries in Cadaver Impacts Using a Full Human Body Finite Element Model.   Stapp Car Crash Journal, Vol. 47 (October 2003), pp. 299-321.

[129] Sato, T., McMinn, R.M.H., and Hutchings, R.T., (1990): A colour atlas of human anatomy.   Nankodo, Tokyo.

[130] Schmitt, K.U., Niederer, P., and Walz, F., (2009):   Trauma Biomechanics: Introduction to Accidental Injury, Berlin, Germany: Springer, pp.39-56.

[131] Schnebel, B., Gwin, J.T., Anderson, S., and Gatlin, R., (2007):   In vivo study of head impacts in football: A comparison of National Collegiate Athletic Association Division I versus high school impacts.   Neurosurgery, 60:490-495; discussion 5-6.

[132] Schneider, L.W., Robbins, D.H., Pflug, M.A. and Snyder, R.G., (1983): Anthropometry of Motor Vehicle Occupants.   Vol. 2.   UMTRI-83-53-2, NHTSA.

[133] Shah, J.S., Hampson, W.G.J., and Jayson, M.I.V., (1978): The distribution of surface strain in the cadaveric lumbar spine.   Journal of Bone and Joint Surgery 60B, pp. 246 – 251.

[134] Shah, C.S., Yang, K.H., Hardy, W.N., Wang, H.K., and King, A.I. (2001): Development of a computer model to predict aortic rupture due to impact loading.   Stapp Car Crash Journal, Vol. 45 (November 2001), pp.161-182.

[135] Siegmund, G.P., Myers, B.S., Davis, M.B., Bohnet, H.F., Winkelstein, B.A., (2001): Mechanical evidence of cervical facet capsule injury during whiplash: a cadaveric study using combined shear, compression, and extension loading.   Spine, 26(19), pp.2095-2101.

[136] Smith, J.A., Siegel, J.H., and Siddigi, S.Q., (2005): Spine and spinal cord injury in motor vehicle crashes: a function of change in velocity and energy dissipation on impact with respect to the direction of crash.   The journal of trauma injury, infection, and critical care, Vol.59, No.1, pp.117-131.

[137] Stalnaker, R.L., McElhaney, J.H., Roberts, V.L., and Trollope, M.L., (1973): Human torso response to blunt trauma. ed. King, W.F., and Mertz H.J., Human impact response, New York, Plenum Press, pp.181-199.

[138] Stein, I.D. and Granik, G., (1976): Rib structure and bending strength: an autopsy study. Calcified tissue research, Vol. 20, pp.61-73.

[139] Suzuki, M., and Shimamura, T., (1994): Morphological study of the axial view of the cervical spinal cord by MR images. J. Japan, Orthop. Assoc., vol.68, No.1, pp.1-13. (in Japanese)

[140] Svensson, M.Y., Aldman, B., Hansson, H.A., Loevsund, P., Seeman, T., Suneson, A., and Oertengren, T., (1993): Pressure effects in the spinal canal during whiplash extension motion: a possible cause of injury to the cervical spinal ganglia. Proc. IRCOBI, 21, pp.189-200.

[141] Talantikite, Y., Bouquet, R., Ramet, M., Guillemot, H., Robin, S., and Voiglio, E., (1998): Human thorax behaviour for side impact. influence of impact masses and velocities. Paper number 98-S7-O-03, Proc. of 16th International Technical Conference on the Enhanced Safety of Vehicles (ESV), Windsor, Canada, pp.1542-1549.

[142] Takhounts E.G., Crandall, J.R. and Darvish, K., (2003): On the development of the SIMon finite element head model. Stapp Car Crash J., 47:107-133.

[143] Takhounts E.G., Ridella, S.A., Hasija, V., Tannous, R.E., Campbell, J.Q., Malone, D., Danelson, K., Stitzel, J., Rowson, S., and Duma, S., (2008): Investigation of traumatic brain injuries using the next generation of simulated injury monitor (SIMon) finite element head model. Stapp Car Crash J., 52:1-31.

[144] Takhounts E.G., Hasija, V., Ridella, S.A., Rowson, S., and Duma, S.M., (2011): Kinematic rotational brain injury criterion (BRIC). The 22nd International Technical Conference on the Enhanced Safety of Vehicles (ESV), Paper No. 11-0263.

[145] Tamura, A., Omori, K., Miki, K., Lee, J.B., Yang, K.H., and King, A.I., (2002): Mechanical Characterization of Porcine Abdominal Organs. Stapp Car Crash Journal 46 (November 2002).

[146] Tamura A., Nagayama, K., Matsumoto, T., and Hayashi, S., (2007): Variation in nerve fiber strain in brain tissue subjected to uniaxial stretch. Stapp Car Crash J., 51: 139-154.

[147] Tanaka, Y., (1984): Morphological changes of the cervical spinal canal and cord due to aging, J. Japan, Orthop. Assoc., vol.58, No.9, pp.873-886. (in Japanese).

[148] Thibault, L.E., and Gennarelli, T.A., (1985): Biomechanics of diffuse brain injuries. Tenth International Technical Conference on Experimental Safety Vehicles, SAE 856022.

[149] Thunnissen, J.G.M., Wismans, J.S.H.M., Ewing, C.L., and Thomas, D.J., (1995): Human volunteer head-neck response in frontal flexion: a new analysis. Proc. of 39th Stapp Car Crash Conference, SAE Paper No. 952721, Society of Automotive Engineers, Warrendale, PA.

[150] Trosseille, X., Tarriere, C., Lavaste, F., Guillon, F., and Domont, A., (1992): Development of a F.E.M. of the human head according to a specific test protocol. Proc. of 36th Stapp Car Crash Conf., SAE 922527.

[151] Unterharnscheidt, F.J., (1971): Translational versus rotational acceleration: animal experiments with measured input. Proc. 15th Stapp Car Crash Conference, SAE Paper No. 710880.

[152] Versace, J, (1971): A review of the severity index. Proc. of 15th Stapp Car Crash Conf., SAE 710881.

[153] Viano D.C., (1983): Biomechanics of Nonpenetrating Aortic Trauma: A Review. Proc. of 27th Stapp Car Crash Conference, SAE Paper No. 831608, SAE, Warrendale, PA.

[154] Viano, D.C., (1989): Biomechanical responses and injuries in blunt lateral impact. Proc. 33rd Stapp Car Crash Conference, SAE 892432.

[155] Viano, D.C., Lau, I.V., Asbury, C., King, A.I., and Begeman, P., (1989): Biomechanics of the human chest, abdomen, and pelvis in lateral impact. Proc. 33rd Annual Scientific Conference of the Association for the Advancement of Automotive Medicine, Baltimore, Maryland, pp.367-382, Des Plaines, IL.

[156] Viano, D.C., and Lövsund, P., (1999): Biomechanics of brain and spinal cord injury: Analysis of neurophysiological experiments. J. Crash Prevention and Injury Control, 1:35-43.

[157] Walsh, M.J. and Kelleher, B.J., (1978): Evaluation of air cushion and belt restraint systems in identical crash situations using dummies and cadavera. Proc. of 22nd Stapp Car Crash Conference, SAE Paper No. 780893, Society of Automotive Engineers, Warrendale, PA.

[158] Wang, H-C.K., (1995): Development of a Side Impact Finite Element Human Thoracic Model. Ph.D. dissertation, College of Engineering, Wayne State University, Detroit, MI.

[159] Wang L, Brust FW, Atluri SN. (1997): The Elastic-Plastic Finite Element Alternating Methods (EPFEAM) and the Prediction of Fracture Under WFD Conditions in Aircract Structures. Part II: Fracture and the 7th Integral Parameter. Comput. Mech., Vol. 19, pp. 370–379.

[160] Welsh, R. and Lenard, J., (2001): Male and Female car drivers – differences in collision and injury risks. Proc. 45th Annual Scientific Conference of the Association for the Advancement of Automotive Medicine, San Antonio, TX, September, pp.73-91.

[161] Wilhelm, M.R., (2003): A biomechanical assessment of female body armor. Ph.D. dissertation, College of Engineering, Wayne State University, Detroit, MI.

[162] Willinger, R., and Baumgartner, D., (2003): Human head tolerance limits to specific injury mechanisms. International J. of Crashworthiness, 8(6): 605-617.

[163] Wong, F.Y., Pal, S., and Saha, S., (1983): The assessment of in vivo bone condition in humans by impact response measurement. J. Biomech, 16(10), pp.849-856.

[164] Yamada, H., (1970): Strength of Biological Materials, ed. Evans FG, The Williams and Wilkins Company, Baltimore, MD.

[165] Yang, K.H., Zhu, F., Luan, F., Zhao, L., and Begeman, P.C., (1998): Development of a finite element model of the human neck. Proc. of 42nd Stapp Car Crash Conference, SAE Paper No. 983157, Society of Automotive Engineers, Warrendale, PA.

[166] Yoganandan, N., Pintar, F.A., Haffner, M., Jentzen, J., Malman, D.J., Weinshel, S.S., Larson, S.J., Nichols, H., and Sances, A.Jr, (1989): Epidemiology and injury biomechanics of motor vehicle related trauma to the human spine.   Proc. 33rd Stapp Car Crash Conference, SAE Paper No. 892438, Society of Automotive Engineers, Warrendale, PA.

[167] Yokochi, C., Rohen, J.W., and Weinreb, E.L., (1996): Photographic anatomy of the human body. Igaku-Shoin, Tokyo.

[168] Zar, J.H., (1984): Biostatistical analysis, 2nd Ed., Prentice Hall, Englewood Cliffs, NJ.

[169] Zhang, L., Yang, K., Dwarampudi, R., Omori, K., Li, T., Kun, C., Hardy, W.N., Khalil, T.B., and King, A.I., (2001): Recent advances in brain injury research: A new human head model development and validation.   Stapp Car Crash Journal, vol.45, 2001-22-0017, pp.369-393, The Stapp Association, Ann Arbor, MI.

[170] Zioupos, P. and Currey, J.D., (1998): Changes in the stiffness, strength, and toughness of human cortical bone with age.   Bone, Vol. 22, No. 1, pp. 57-66.

PUBLICATIONS

Peer reviewed journal and conference papers

A1. **Kimpara, H.**, Iwamoto, M., Miki, K., Lee, J.B., Begeman, P.C., Yang, K.H., and King, A.I., (2003): Biomechanical properties of the male and female chest subjected to frontal and lateral impacts. Proc. of 2003 International Research Council on the Biomechanics of Impact (IRCOBI), Lisbon (Portugal), pp.235-247

A2. **Kimpara, H.**, Lee, J.B., Yang, K.H., King, A.I., Iwamoto, M., Watanabe, I., Miki, K., (2005): Development of a Three-Dimensional Finite Element Chest Model for the 5th Percentile Female. Stapp Car Crash Journal, 49, pp.251-269

A3. **Kimpara, H.**, Nakahira, Y., Iwamoto, M., Miki, K., Ichihara, K., Kawano, S., and Taguchi, T., (2006A): Investigation of Anteroposterior Head-Neck Responses during Severe Frontal Impacts Using a Brain-Spinal Cord Complex FE Model. Stapp Car Crash Journal, 50, pp.509-544

A4. **Kimpara, H.**, Iwamoto, M., Watanabe, I., Miki, K., Lee, J.B., Yang, K.H. and King, A.I., (2006B): Effect of assumed stiffness and mass density on the impact response of the human chest using a three-dimensional FE model of the human body. J Biomech Eng. 128(5), pp.772-776

A5. **Kimpara, H.**, Lee, J.B., Yang, K.H., and King, A.I., (2010): Effects of Bodyweight, Height, and Ribcage Area Moment of Inertia on Blunt Chest Impact Response. Journal of Traffic Injury Prevention, Vol. 11, No. 2

A6. **Kimpara H.**, Nakahira Y., Iwamoto M., Rowson S., and Duma S., (2011A): Head Injury Prediction Methods Based on 6 Degree of Freedom Head Acceleration Measurements during Impact. International Journal of Automotive Engineering, Vol.2, No.2, pp.13-19.

A7. **Kimpara H.**, Nakahira Y., and Iwamoto M., (2011B): New Injury Predictors for Brain Injuries without Skull Fractures. Transactions of Society of Automotive Engineers of Japan (Transactions of JSAE), Vol.42, No.6, pp.1327-1333. (in Japanese)

A8. **Kimpara H.** and Iwamoto M., (2012): Mild Traumatic Brain Injury Predictors Based on Angular Accelerations during Impacts. Annals of Biomedical Engineering, Vol.40, No.1, pp.114-126.

Oral presentation

B1. **<u>Kimpara, H.</u>**, Iwamoto, M., Watanabe, I., Miki, K., Lee, J.B., Yang, K.H. and King, A.I., (2004): Numerical analysis of the biomechanical characteristics and impact response of the human chest.   2004 ASME International Mechanical Engineering Congress and RD&D EXPO, November 2004, Anaheim, CA., IMECE2004-60983, pp. 1-11.

B2. **<u>Kimpara, H.</u>**, Iwamoto, M., Watanabe, I., Miki, K., Lee, J.B., Yang, K.H. and King, A.I., (2004): Effects of strain rate and gender on properties of human ribs.   5th Combined Meeting of the Orthopaedic Research Societies of Canada, USA, Japan, and Europe, October 2004, Banff, Canada

AWARDS

C1. **<u>Kimpara, H.</u>**, (2011): Best presentation award from Society of Automotive Engineers of Japan (JSAE).

C2. **<u>Kimpara, H.</u>**, (2012): Asahara Academic Incentive Award from Society of Automotive Engineers of Japan (JSAE).

C3. **<u>Kimpara, H.</u>**, Nakahira, Y., and Iwamoto, M., (2013): Best Paper Award from Society of Automotive Engineers of Japan (JSAE).

ASSOCIATED PUBLICATIONS (peer reviewed journal or conference papers)

D1. **<u>Kimpara, H.</u>**, Iwamoto, M., Watanabe, I., Miki, K., Lee, J.B., Yang, K.H., and King, A.I., (2005); "Effects of Bodyweight, Height, and Ribcage Area Moment of Inertia on Blunt Chest Impact Response". Proc. of 2005 International Research Council on the Biomechanics of Impact (IRCOBI), Prague (Czech Republic), pp.175-185

D2. Iwamoto, M., Nakahira, Y., **<u>Kimpara, H.</u>**, and Sugiyama, T., (2009); Development of a Human FE Model with 3-D Geometry of Muscles and Lateral Impact Analysis for the Arm with Muscle Activity. SAE Technical Paper 2009-01-2266.

D3. Iwamoto, M., **<u>Kimpara, H.</u>**, and Sugiyama, T., (2010): Bracing Occupant Simulations for Frontal Impacts using a Human Whole Body FE Model with Muscular Bar Elements. Transactions of Society of Automotive Engneers of Japan, 20104688, Vol.41, No.6, pp.1249-1254, (in Japanese).

D4. Iwamoto, M., Min, K., and **<u>Kimpara, H.</u>**, (2012): Prediction of Occupant Posture in Pre-crash by a Muscle Control Method Using a Whole Body Musculo-skeletal FE Model and a Mathematical Model of Learning in Brain. Transactions of Society of Automotive Engneers of Japan, Vol.43, No.4, pp.905-910, (in Japanese).

D5. Iwamoto, M., Min, K., and **<u>Kimpara, H.</u>**, (2012): Prediction of Head-neck Motions during Rear-end Impacts Using a Human Body FE Model with Muscle Activity. Transactions of Society of Automotive Engneers of Japan, Vol.43, No.5, pp.1111-1116, (in Japanese).

D6. Iwamoto, M., Nakahira, Y., **<u>Kimpara, H.</u>**, Sugiyama, T., and Min, K., (2012); Development of a human body finite element model with multiple muscles and their controller for estimating occupant motions and impact responses in frontal crash situations. Stapp Car Crash Journal, 56, pp.231-268.

D7. Iwamoto, M., Nakahira, Y., **<u>Kimpara, H.</u>**, and Min, K., (2013); Development of a Finite Element Model of 5TH Percentile Female with Multiple Muscles and its Application to Investigation on Impact Responses of Elderly Females. Proceedings of the 23rd International Technical Conference on the Enhanced Safety of Vehicles (ESV), 13-0366.

D8. **<u>Kimpara, H.</u>**, and Iwamoto, M., (2013): Injury Predictors for Mild Traumatic Brain Injuries due to Head Impacts in Football. Biomechanisms, 22, pp.189-199, (in Japanese).